Global Atmospheric Water Vapor Flux Climatology in the NCEP/NCAR Reanalysis and the Oort Data Set

by

Karen S. Friedman

Submitted to the Department of Civil and Environmental Engineering

in partial fulfillment of the requirements for the degree of

Master of Science in Civil and Environmental Engineering

at the

MASSACHUSETTS INSTITUTE OF TECHNOLOGY

May 1997

Author.....

Department of Civil and Environmental Engineering

May 16, 1997

Certified by.....

Dara Entekhabi

Professor, Department of Civil and Environmental Engineering

Thesis Supervisor

Accepted by.....

Joseph M. Sussman

Chairman, Departments Committee on Graduate Students

Global Atmospheric Water Vapor Flux Climatology in the NCEP/NCAR Reanalysis and the Oort Data Set

by

Karen S. Friedman

Submitted to the Department of Civil and Environmental Engineering on May 16, 1997,

In partial fulfillment for the degree of

Master of Science in Civil and Environmental Engineering

Abstract

The integrated water vapor flux is calculated for the National Centers for Environmental Prediction/ National Center for Atmospheric Research (NCEP/NCAR) reanalysis and the Oort objective analysis data sets with the purpose of intercomparison. The period of study is 1979 to 1995 for the NCEP/NCAR data and 1964 to 1989 for the Oort. Such lengthy time-series allow the estimation of interannual variability in the atmospheric branch of the hydrologic cycle. Global fields and zonal averages are displayed for the annual, December/January/February, and June/July/August averages. As part of the analysis, the data sets are each separated into years with and without an El Nino occurrence. The difference and divergence are calculated to investigate if the data sets can resolve the anomalies known to exist during El Nino Southern Oscillation (ENSO). Power spectra analysis is also performed to look for events within certain frequency ranges. Both data sets appear to resolve the global water vapor flux and ENSO conditions reasonably, but the Oort data does not perform as well possibly due to regions with inherently poor data.

Thesis Supervisor: Dara Entekhabi

Title: Professor

Acknowledgments

This research has been supported by NSF Fellowship GER-9354923 and NASA Grant NAGW-4163 to MIT.

I wish to thank my advisor, Dr. Dara Entekhabi, for his continued guidance. Also, the help and advice of Dr. Richard Rosen at AER, Inc., is sincerely appreciated. I am indebted to "my postdocs", John Galantowicz, Rene Kim, Judah Cohen and Chris Forest, for graciously helping me throughout my entire stay at MIT. Thanks to Campe Goodman for editing this thesis. Most of all, thank you to my wonderful friend, Nicole Gasparini, whose support was paramount.

Table of Contents

I. Introduction

Water is present in all aspects of our environment. We most often think of it in oceans and streams, or as rain. In order to keep this balance of water around the globe, there must be a transport mechanism. In actuality, there are many. Evaporation and evapotranspiration take water from the planet's surface into the atmosphere. Once in the atmosphere, it does not merely condense and fall as rain. The journey of water vapor in the atmosphere depends on circulation patterns that vary with location. For instance, the Hadley cells provide an uplift mechanism on both sides of the equator. This uplift of air causes condensation and thus rain. As the air continues to circulate, it dries out and descends in the subtropics causing regions of aridity. Other transport mechanisms include mid-latitude wave activity and storm tracks. They carry moisture principally west to east in the mid-latitudes. These cells and jets interact with many other phenomena that occur on seasonal, yearly and decadal time scales, to maintain the circulation of water vapor in the atmosphere.

Water is not only a building block of life, but a large forcing in the entire earth system. It absorbs solar and longwave radiation which in turn can cause the release of latent and sensible heat. The transfer of latent heat in the atmosphere plays a large part in the global energy balance

Because of water vapor's importance to many aspects of the climatic system, this study attempts to compare the ability two data sets to capture the atmospheric water vapor flux. They consist of a reanalysis data set, which merges observations and an atmospheric model, and a data set made purely from in situ measurements and interpolation. These data sets are

potentially very useful to the scientific community, since only recently have global data sets become available. With the present availability of large computing resources and the ability to measure meteorological parameters remotely, more complete data sets can be assembled.

1.1 Relevant Literature

Due to the lack of data and computing power, the study of atmospheric water vapor has experienced its most significant advances only in the last thirty years. Benton and Estoque were pioneers in the subject with their research on the transfer of water vapor over North America, published in 1954. They stressed the importance of studying water vapor as "...an essential building block in the meteorologist's understanding of the physics of atmospheric processes." Working with a data set of only thirty radiosonde* stations in North America and surrounding bodies of water for the calendar year 1949, they calculated the monthly integrated water vapor transfer of the atmosphere. Of significance was the finding that a substantial percentage of water vapor enters the United States by eddy flux (the covariance of wind and vapor perturbations) as opposed to mean motion. The divergence of the water vapor transfer was also calculated, and found to be an accurate measure of runoff over North America.

Soon after this, Starr and Peixoto (1958) used the above methods to study the balance of water vapor in the Northern Hemisphere for the year 1950 with data from 90 radiosonde stations. Reasoning that the divergence of the vertically integrated water vapor flux must, with small exception, equal the excess of evaporation over precipitation, they found that areas of convergence and divergence balance in the Northern Hemisphere. This is necessary in order to have no net flow across the equator and achieve a global balance of water vapor.

---

* Radiosondes are instrumented balloons that measure air temperature, humidity and wind speed components at the following lower atmosphere standard pressure levels (1000, 950, 900, 850, 700, 500, 400, 300 mb)

Another significant study was the first in a subsequent series of papers by Rasmusson (1966) using a five year data set. His first investigation involved computing the vertically integrated water vapor flux and its divergence for three months. Even though this data was sampled on a much smaller grid than Benton and Estoque (1954), he found a general agreement with their results. By using the same three months of data, he investigated the effect diurnal variations have on the results of data sampled only once daily. Rasmusson found that the flux calculated at only 0000 GMT does not sufficiently represent the mean water vapor flux divergence over the United states. He suggests that at a minimum, a second measurement at 1200 GMT must be used, and additionally two more at 0600 and 1800 GMT would be optimal.

The second and third of Rasmusson's studies (1967, 1968) using this data look at water vapor flux and the divergence, respectively, over North America and the Gulf of Mexico. Both cover the period May 1961 to April 1963. One important finding highlighted the failure of Benton and Estoque's 1954 study to resolve the summertime northward flux along the southwestern border of the United States . These differences can be attributed to the smaller spatial resolution of Rasmusson's data. He also noticed a large diurnal variation in the transport of water vapor over the central United States, Mexico and the Gulf of Mexico, especially in the summer, which would later be identified as the Low Level Jet (LLJ). Even though Rasmusson's data afforded him increased accuracy, he acknowledged that a study over a longer time span was needed.

---

twice daily at 0000 and 1200 GMT. About 150 sampling locations are distributed over the U.S. Sampling is generally limited to land regions.

Salstein et al. (1980) looked at the streamfunctions and potential fields for the annual average flow of water vapor. Their study covered six years over 800 stations across the entire Northern Hemisphere. By looking at streamfunctions, they could recognize a cellular pattern of moisture circulation over the centers of the Pacific and Atlantic that had not been noticed in other types of analyses on water vapor flux. It was also discovered that little interannual variability existed in the annual streamfunction and potential fields general character, but some changes in intensity were noticed over the Pacific Ocean and Indian subcontinent.

The methods used to study atmospheric water vapor have not changed greatly over the last couple decades, but the information gained from them has increased as larger data sets have become available. Using a 10 year data set interpolated onto a global grid, Brubaker et al. (1994) looked at the total, mean and eddy components of vapor flux into the continental boundaries of the Americas. They found eddy flux from the Gulf of Mexico contributes half of the total influx of water vapor into North America through this region. Their results were then applied to calculate annual runoff from each continent. The runoff appeared to be underestimated, but within an order of magnitude of what others had calculated by river discharge measurements.

With increased computer power, data sets from merged data and General Circulation Models (GCM's) have become increasingly useful in the study of atmospheric water vapor (Rasmusson and Mo, 1996; Trenberth and Guillemot, 1995; Mo and Higgins, 1996). These assimilation data sets use available observations to initialize atmospheric models. The resulting short-term prediction fields are used for analysis of

the climatic system. The assimilation data sets are blends of interpolated observations constrained by modeled physical processes.

Some interesting applications of these data sets include the study of regional vapor transport. Hefland and Schubert (1995) used data assimilated by the Goddard Earth Observing System (GEOS-1) atmospheric GCM with data saved every three hours to observe the Low Level Jet (LLJ) over the Great Plains of the United States. Data is needed at this time resolution to investigate a phenomenon such as the LLJ which has a strong diurnal cycle. They found that the LLJ transports approximately one-third of the atmospheric moisture that enters the United States. Most of this transfer occurs during the night.

Recently, several papers have assessed the accuracy of using model assimilation data as measurements of water vapor. One such study, Trenberth and Guillemot (1995), looks at the European Centre for Medium-Range Weather Forecasts (ECMWF), the U.S. National Meteorological Center (NMC), and NASA/Goddard GEOS-1 data. Like Rasmusson, Trenberth and Guillemot (1995), they found that the diurnal cycle is not captured well by twice daily data. This is the case more so for measurements of evaporation minus precipitation (E-P) as opposed to precipitable water* . They also found that there is little difference in the measurement of E-P for scales larger than T31 when the fields are first truncated at T42.

Dodd and James (1996) estimate the time mean fields of E and P using ECMWF data with a technique involving probability distribution. They found in most cases, that precipitation is fueled by evaporation from

* Precipitable water is the vertically-integrated mass of atmospheric water vapor content per unit surface area.

elsewhere, showing the importance of the advection process. The problems from this technique include finding the eastern subtropical oceans overly moist, and the need for better temporal resolution.

Recently reanalysis* data sets have become an important source of data to study water vapor. Both Higgins et al. (1996) and Mo and Higgins (1996) look at atmospheric water vapor transport in the NCEP/NCAR, and NASA/GEOS-1 reanalyses data products. They found that reanalyses have a tendency to inaccurately measure low level flow and fail to always calculate a positive P-E over land. They did see many features that confirmed the validity of reanalysis data, such as a large source of moisture from the Gulf of Mexico into the United States and the basic temporal and structural characteristics of the LLJ.

* Reanalysis refers to assimilation data sets resulting from merging a consistent (in time) atmospheric model and observations.

1.2 Atmospheric Water Vapor

The exact quantity that is analyzed in this paper is the time averaged, vertically integrated horizontal vapor flux. This is done by taking measurements of the zonal and meridional wind, u and v respectively, along with specific humidity, q, at every data location. The average (overbar) monthly fluxes are composed of transport by mean motion ($\bar{u}\bar{q}$ and $\bar{v}\bar{q}$) as well as by transient eddies ($\overline{u'v'}$ and $\overline{v'q'}$). The expansion of $\overline{uq}$ and $\overline{vq}$ terms into monthly mean and perturbations yield components that may then be vertically integrated. According to equations 1 and 2, the measurements are used to calculate the vertically-integrated vapor flux in the zonal and meridional directions, respectively.

$$\bar{Q}_\lambda = \int_0^{ps} \overline{(qu)} \frac{dp}{g} = \int_0^{ps} \bar{q} \cdot \bar{u} \frac{dp}{g} + \int_0^{ps} \overline{q'u'} \frac{dp}{g} \qquad (1)$$

$$\bar{Q}_\phi = \int_0^{ps} \overline{(qv)} \frac{dp}{g} = \int_0^{ps} \bar{q} \cdot \bar{v} \frac{dp}{g} + \int_0^{ps} \overline{q'v'} \frac{dp}{g} \qquad (2)$$

These equations calculate Q_λ, the zonal flux, and Q_ϕ, the meridional flux. The specific humidity is the measure of the mass of water vapor per unit mass of air. These integrals are performed over pressure levels, p. The surface pressure is p_s and it is estimated using auxiliary data sets to the radiosondes. The units for the winds are [m/s], for q are [kgH_2O/kgAir], and for Q are [kgH_2O /ms]. Gravity is represented by g, and the overbars denote an average over a month. The zonal and meridional components of Q are related to the total flux by

$$\vec{Q}(\lambda,\phi,t) = \int_0^{po} q\vec{V} = Q_\lambda \vec{i} + Q_\phi \vec{j} \qquad (3)$$

where λ, ϕ, and t are longitude, latitude, and time, respectively.

Furthermore, it is useful in this thesis to look at the mean and eddy components of the vapor flux. The mean component is represented by the first integral on the right hand side of (1) or (2) and expresses the mean motions in the atmosphere. Whereas the eddy component, the second integral on the right hand side of (1) and (2), is calculated using the deviations from the mean.

The divergence of the flux is represented by (4). Equation (4) is time-averaged (denoted by the overbar) so that the changes in precipitable water storage are eliminated. As noted by Star and Peixoto (1958) this quantity approximately equals the excess of evaporation over precipitation, therefore representing the sources and sinks of water vapor across the globe.

$$\nabla \bullet \overline{Q} = \frac{\partial}{\partial x} Q_{\lambda} \vec{i} + \frac{\partial}{\partial y} Q_{\phi} \vec{j} = \overline{E} - \overline{P} \qquad (4)$$

1.3 El Nino Southern Oscillation

El Nino is an anomalous warming of the eastern Pacific waters off the coast of South America. It is the main mode of interannual variability in the global climatic system resulting from ocean-atmosphere interaction. While it originally referred to the warming that occurred off of the coasts of Ecuador and Peru at Christmas time (Peixoto and Oort, 1992), the term is now used to refer to the anomalously warm waters present across a portion of the eastern Pacific and their consequences. El Nino's recur approximately every 3 to 7 years (Peixoto and Oort, 1992).

El Nino is not isolated to the eastern Pacific, but rather has global repercussions. It is part of a system that includes the Southern Oscillation and the Indian Monsoons (Barnett 1994). The Southern Oscillation can be thought of as the atmospheric component of the entire phenomenon, and involves an east-west shift of mass in the atmosphere across the Indian and Pacific Oceans (Peixoto and Oort, 1992). This system is often termed El Nino Southern Oscillation, or ENSO.

The typical length of an ENSO episode is approximately 16 months (Wyrtki, 1975). It was once believed that all ENSO's followed the seasonal cycle by beginning and ending at the same time of the year (Rasmusson and Carpenter, 1982). But Wang (1995) documents that the 1986-87 episode did not follow the trend of many of its predecessors. He also claims that there is a difference between the onset of pre-1970 events and post-1970 events.

The effects of ENSO are far reaching. Rasmusson and Carpenter (1982) observed that the warm Sea-Surface Temperatures (SSTs) in the

central equatorial Pacific cause enhanced atmospheric convection, which leads to increased rainfall and weakened surface easterlies. Normal circulation over the Pacific includes the Walker Cell, which rises over the western equatorial ocean and falls over the east. When the eastern waters increase in temperature, as they do in El Nino, this circulation is weakened. This leads to reduced uplift in the western equatorial Pacific, therefore resulting in less precipitation in regions such as Indonesia, and more in the central and eastern equatorial Pacific (Pexioto and Oort, 1992).

Increased rainfall has been documented in the coastal zone off of Ecuador and Peru, south of India, and over eastern equatorial Africa (Pexioto and Oort, 1992). The occurrence of droughts from ENSO are more widespread and are seen in the South Pacific Convergence Zone (SPCZ), southeastern Africa, and northeastern South America (Peixoto and Oort, 1992). Also, ENSO may be the cause of weaker monsoon rains over India (Pexioto and Oort, 1992).

Ropelewski and Halpert (1987, 1996) provide an up-to-date overview of global ENSO-precipitation relationships. In this study the vapor flux climatology and anomaly patterns are analyzed in support of understanding the underlying reasons for ENSO-precipitation correlations.

1.4 Thesis Outline

This thesis contains the following major sections:

1) An intercomparison of a data assimilation, the NCEP/NCAR reanalysis product, and an objective analysis data set, from Oort. I will investigate the relative characterization of vapor flux climatology by these data sets.
2) Study of the interannual variability in the atmospheric branch of the hydrologic cycle through spectral analysis of the long records.
3) Investigation of the effect of ENSO on the atmospheric branch of the hydrologic cycle.

II. Data

2.1 Data Sets

2.1.1 NCEP/NCAR Reanalysis

The National Centers for Environmental Prediction/ National Center for Atmospheric Research (NCEP/NCAR) reanalysis project will ultimately produce a 40 year data set covering the period 1957-96 (Kalnay et al., 1996). For the present study, only the years 1979-95 were available. The fields we use are those of zonal and meridional winds, their transient quantities ($\overline{u'q'}$ and $\overline{v'q'}$), surface pressure, and specific humidity. These fields, excluding surface pressure, have measurements at 17 pressure levels from 1000 to 10 mb, though only data up to 300 mb is used since water is concentrated in the lower atmosphere. We received the data as monthly mean fields courtesy of Atmospheric and Environmental Research, Inc. of Cambridge, MA.

Reanalyses take in situ and remotely sensed data, and use atmospheric models to fill in the data at unobserved locations. This data set uses data collected from the land surface, ships, rawinsondes, pibal, aircrafts and satellites. The data assimilation technique employs a T62 model. This gives an approximate horizontal resolution of 210 km resulting in a 2.5 by 2.5 degrees longitude/latitude grid of data. The assimilation is performed over 28 vertical sigma levels. Details on the data and methods used can be found in Kalnay et al. (1996).

2.1.2 Oort Data

The Oort data was compiled by Abraham H. Oort at the Geophysical Fluid Dynamics Laboratory in Princeton, NJ. It includes data from 1958-89, but globally only from 1964-89. This study uses only the global data.

Continuous sources of data over the entire study period were not available. Therefore, the data set consists of separate data sources pieced together to cover the whole time period. The data was collected by rawinsondes, surface marine observations and pibal. The common data objective analysis technique consisted of discarding bad data and then using a scheme to interpolate the available data onto a regular grid. The exact data sources and methods not mentioned here can be found in NOAA Professional Paper 14 by A. H. Oort

The available data for use in this study includes monthly values of zonal and meridional wind, their transient quantities, and specific humidity. Data is reported on a grid of 5 by 2.5 degrees longitude/latitude for 11 pressure levels from 1000 to 50 mb. At the levels near the earth's surface (1000, 950 and 900 mb) and at levels above 100 mb, the data is known to be less accurate than those in between, due to many incomplete rawinsonde reports. Data over the oceans of the Southern Hemisphere oceans is also sparse and so relies more on interpolation.

2.2 Data Problems

The use of discrete data in the study of a continuous phenomenon is inherently inaccurate. Diurnal variability is hard to capture with data collected only once or twice daily. Higgins et al. (1996) found that the Low Level Jet (LLJ) was difficult to study using reanalysis data due to its diurnal nature and its small vertical extent. Rasmusson (1966) did a study to determine how many measurements were needed to study phenomena with diurnal variations. He concluded that once daily data is not sufficient to study the vapor flux divergence and that at least two observations, at 0000 and 1200 GMT, are needed, and additional observations at 0600 and 1800 GMT are highly desirable.

Rasmusson (1966) also conducted a test to determine whether the average divergence over a 3 month period was comparable to the divergence over 3 one month periods averaged together. He found slight differences, but concluded that these computational methods had similar results overall.

Trenberth and Guillemot (1995) found that twice-daily data does not adequately capture the diurnal cycle in calculations of evaporation minus precipitation (E-P). They also tested the effects of changing horizontal resolution and found that in the calculation of the vertically integrated moisture budget, resolution did not play a large role in the results except in areas of steep orography.

III. Integrated Water Vapor Flux

3.1 Global Analysis

This study calculates the time averaged, vertically integrated horizontal vapor flux for both the NCEP/NCAR reanalysis and Oort data. The purpose is intercomparison and comparison to known water vapor flux characteristics. This data is plotted in Figures 1 through 18. In each of these Figures, plot "a" contours the magnitude, $(Q_\lambda^2 + Q_\phi^2)^{1/2}$, of the zonal and meridional components, Q_λ and Q_ϕ . Plot "b" is the vector sum of Q_λ and Q_ϕ , with each arrow's length scaled to size by its magnitude. This is done for the total, mean and eddy flux of three averaged time periods. These periods include December/January/February (DJF), June/July/August (JJA), and an annual average.

In all cases, the most obvious feature about the total flux is how closely it resembles lower tropospheric flow. This is no coincidence since water vapor is mainly concentrated in the lowest 30% of the troposphere (Salstein et. al., 1980). As in the flow of the troposphere, westerlies are visible in mid-latitudes and easterlies in the low-latitudes. Also little transport is seen in regions above 60 degrees latitude in each hemisphere since water vapor decreases from the equator to the poles following the temperature (which limits the water holding capacity of air through the Clausius-Clapeyron relation).

The zonal component has been observed to be a magnitude greater than the meridional component (Brubaker et al., 1994) which results in flow that is largely parallel to latitude circles. Also, the magnitude of the

eddy flux is typically an order of magnitude less than the magnitude of the total flux. Because of this large difference, it is obvious that the mean flux will largely resemble the total flux. Their relationship, given by Equations (1) and (2), expresses that the addition of the mean and the eddy terms equals the total flux. This is indeed what is seen in Figures 1-18.

Figures 1a and 2a, showing total flux during DJF in each data set, share many common features. They both have maxima over the oceans on either side of 20N, with minima in high latitudes and mountainous regions such as the Rockies, Andes and Himalayas. Both highs located in the Pacific from the NCEP/NCAR data stretch across the entire Pacific with a fairly constant magnitude. The Oort data, on the other hand, has centers of high flux localized to the western Pacific. All of these maxima have a smaller value in the Oort data than the NCEP/NCAR data except for the one closest to the equatorial South Pacific.

The separation between the westerlies and the easterlies is seen around 20N and 30S in both Figures 1b and 2b. Rasmusson (1967) found in his study of water vapor over North America, that transient eddies are the dominant meridional transport mechanism over 20N. It is therefore informative to look at the eddy fluxes in Figures 5 and 6 to investigate the meridional flux differences.

As was seen for the total fluxes, the eddy flux maxima in the NCEP/NCAR data are also proportionally larger than those in the Oort data. The northern Pacific high for NCEP/NCAR also stretches across the entire ocean whereas the Oort high is again centered in the western Pacific. The largest difference between Figures 5a and 6a lies over the Gulf Coast of the United States. The eddy center over the western U.S./Atlantic has its

center of maximum over the Gulf states of the U.S. in the Oort data and decreases over the Atlantic. The high in the NCEP/NCAR data has a similar magnitude over the Gulf states, but increases in value as it crosses the Atlantic.

Both NCEP/NCAR and Oort show the necessary poleward flux in Figures 5b and 6b along the eastern boundary of continents (along storm tracks). As was similarly detected by Dodd and James (1996), the values are higher in the winter hemisphere than the summer hemisphere from a strengthening of flux due to the winter storm tracks. Certain fluxes in the meridional direction are almost entirely due to the contribution by transient eddies. One example is the low level jet (LLJ) that comes into the US from the Gulf of Mexico which has been well documented by Hefland and Schubert (1994). In Figure 2b it can be recognized that the flux comes easterly at about 20N and then turns northward and enters the U.S. before exiting westerly through the east coast. In Figure 4b, the northerly turn is not detected in the mean motion. Instead, the westerly and easterly flow appear less connected. As would be expected, a northerly eddy flux is seen in this area in Figure 5b and 6b.

A case where meridional transport is mainly from mean motion is over the tropics where no eddy flux exists. In this circumstance, Figures 3b and 4b display large meridional motions following the low-level zonal tropical easterlies. Figures 5b and 6b show that there is no appreciable transient eddy contribution to vapor transport in the tropics.

Figures 7 through 12 show the same fields as Figures 1-6 but for JJA. As in the DJF diagrams, the maxima existing over the ocean have consistently higher values in the NCEP/NCAR data. Large differences

between the DJF and JJA fields are seen over the Indian Ocean and southern India where magnitudes have increased (see Figures 7a and 8a) and a semi-circular flow pattern has developed (see Figures 7b and 8b). This pattern, the Indian summer monsoon, is also noted by Rasmusson (1967). The values of the maxima have increased by a smaller amount over the northern tip of South America. It can be recognized in Figures 9 through 12 that this phenomenon is due to mean motion and not transient eddies.

In the case of total flux for the Oort data (Figure 8a), the northern Pacific maxima is barely distinguishable as a separate entity from the maxima to its south. Both data sets exhibit a seasonal northward shift of the division between the westerlies and the easterlies, which is observed by comparing Figures 1b and 7b in NCEP/NCAR, and also 2b and 8b for the Oort data.

In JJA, the eddy flux maxima have increased in the Southern Hemisphere (during the season of strong baroclinic instability) and now have values greater than those in the Northern Hemisphere (Figures 11a and 12a). The same was seen in Figures 5a and 6a with the winter hemisphere having larger transient eddies. Again, the eddy maxima in the Pacific are centered more towards the western Pacific in the Oort data compared to NCEP/NCAR. Also, the eddy flux over eastern South America has a maximum over the land in both data sets for JJA; however, it is only visible in the Oort data and absent in the NCEP/NCAR for DJF. The storm tracks are also evident these Figures.

Figures 13 through 18 display all three components of the vapor flux for the data averaged annually. Many of the features apparent in the JJA

and DJF data recur here. Included, is the tendency for the NCEP/NCAR data to have values larger than the Oort data, and to have high values of flux across the entire Pacific, not just over the western half. It can also be observed that the centers of maximum flux near the equator in the Pacific and Atlantic are consistently larger than those to their north and south. The equatorial region, known to be an area of much convection, no doubt affects this value. The flux maxima found to the north and the south are most likely fueled by the mid-latitude jet streams.

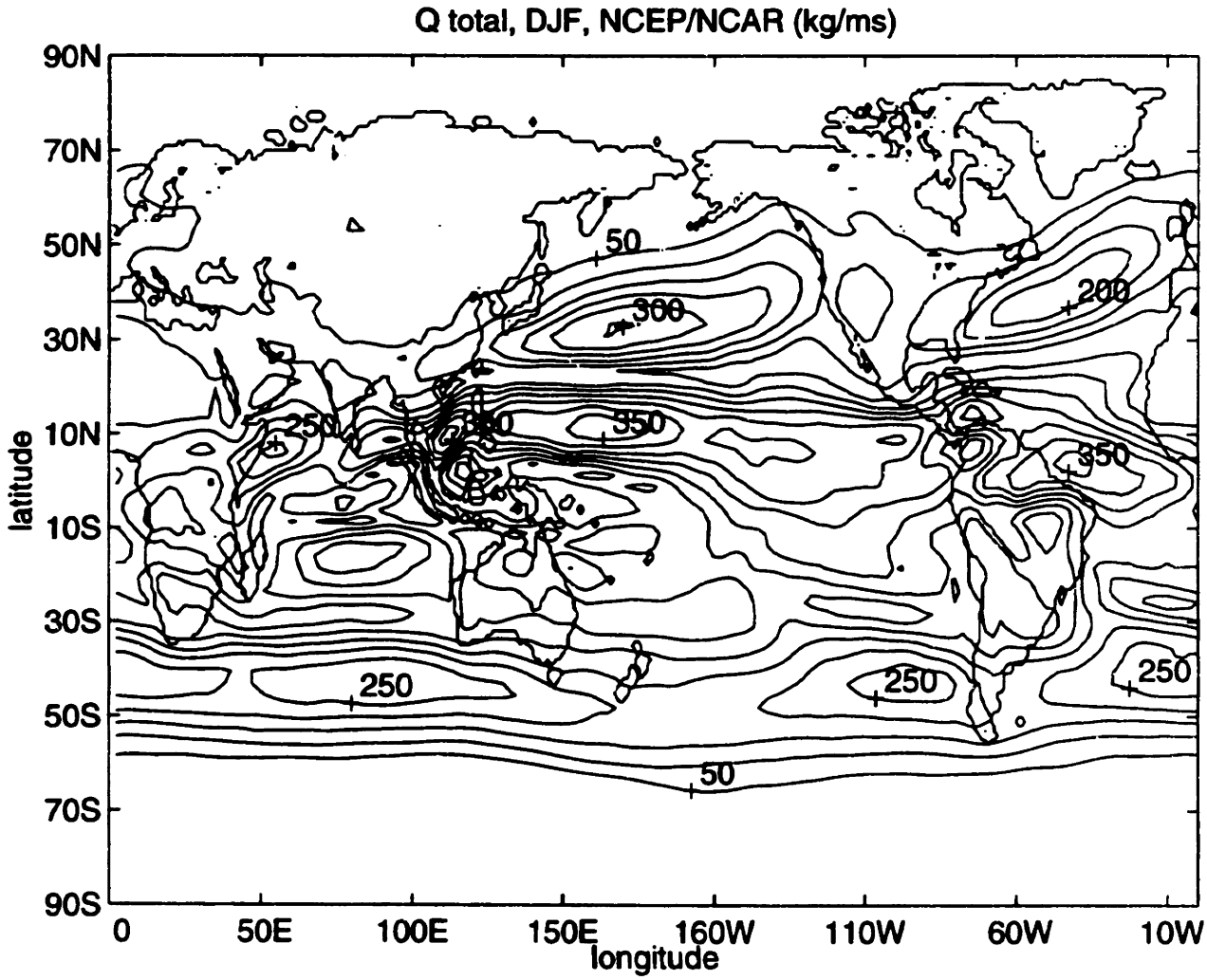

Fig 1a. The NCEP/NCAR total vapor flux for DJF. Contoured on 50 kg/ms intervals.

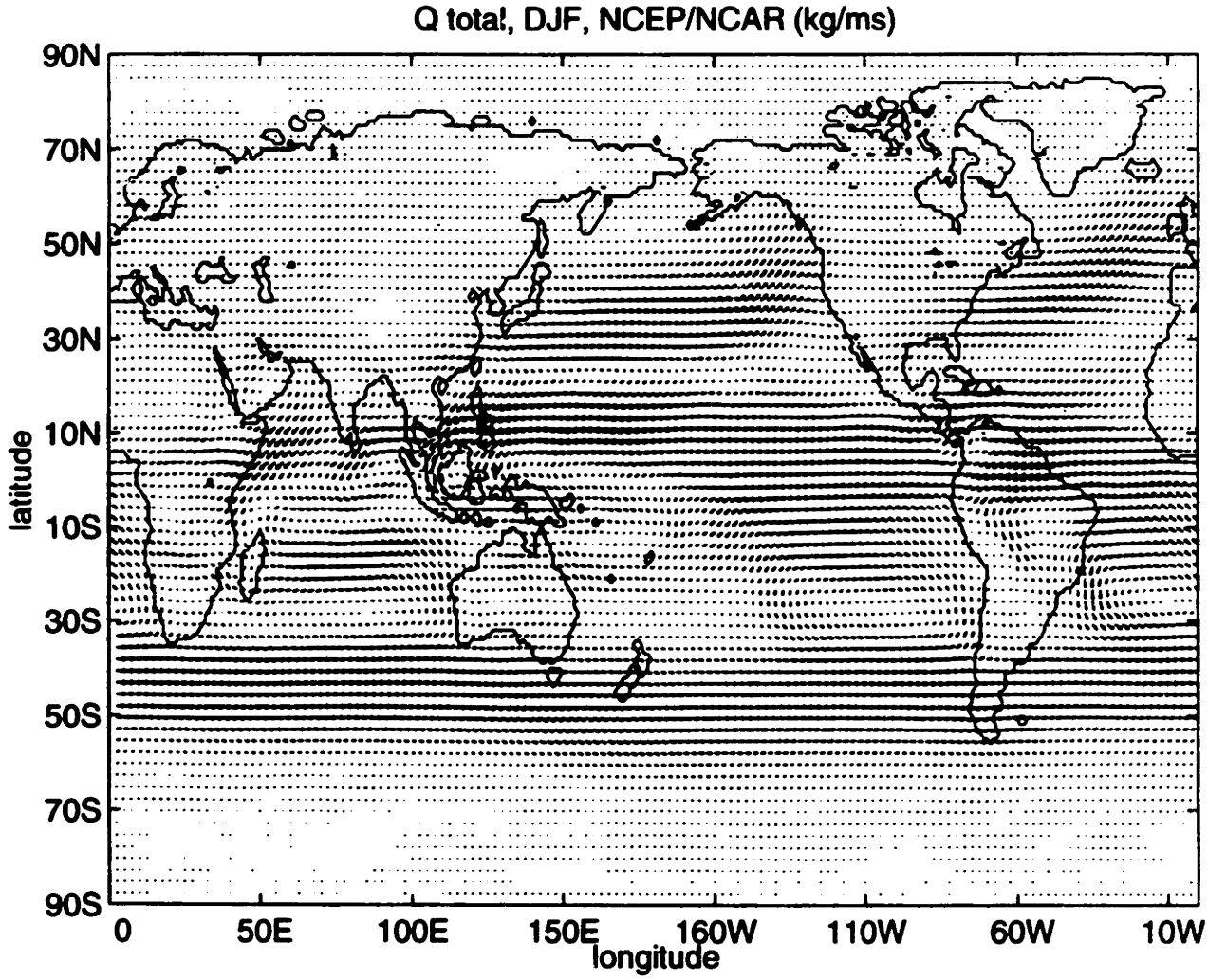

Fig 1b. The NCEP/ NCAR total vapor flux for DJF plotted as flux vectors.

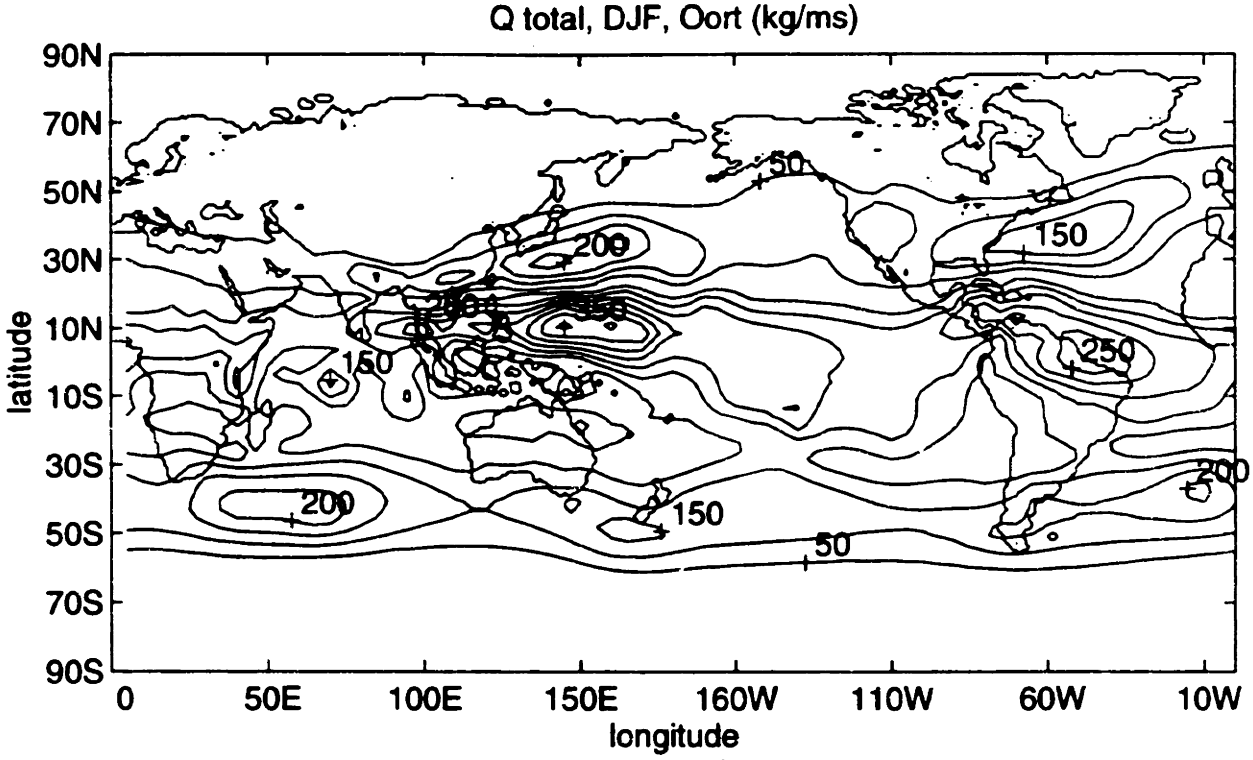

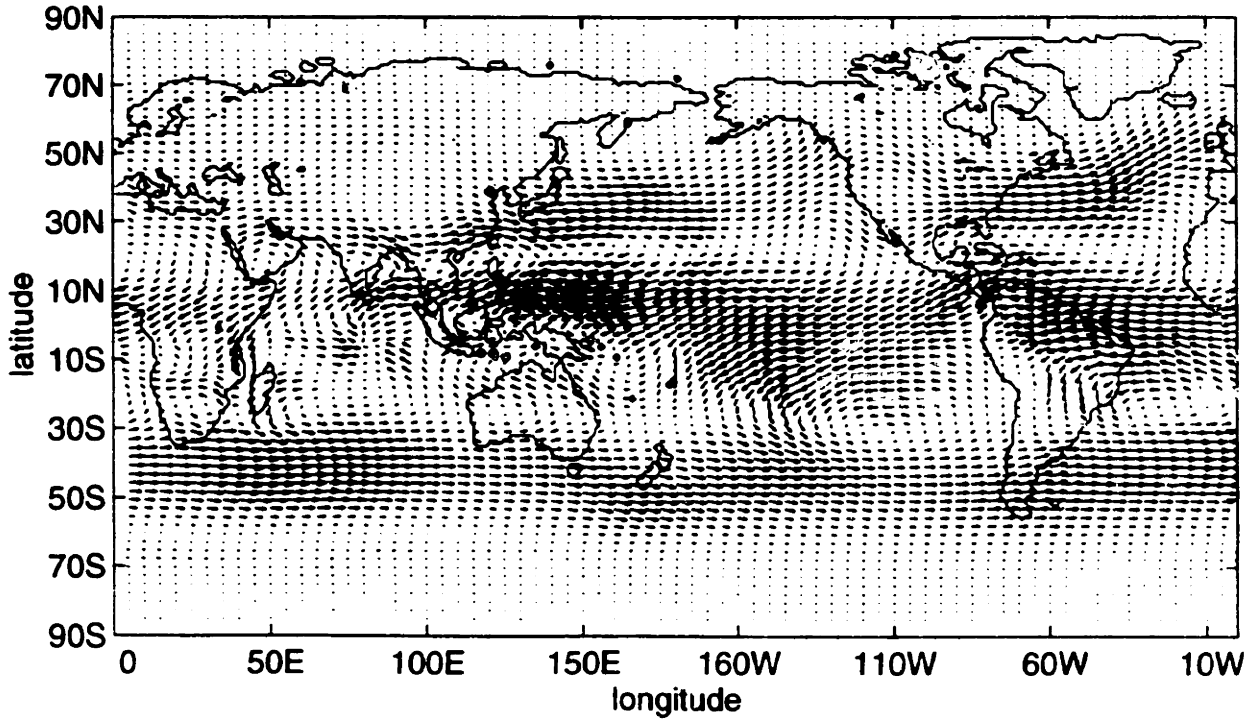

Fig 2a. (upper) The Oort total vapor flux for DJF. Contoured on 50 kg/ms intervals. 2b (lower) Above plotted as flux vectors.

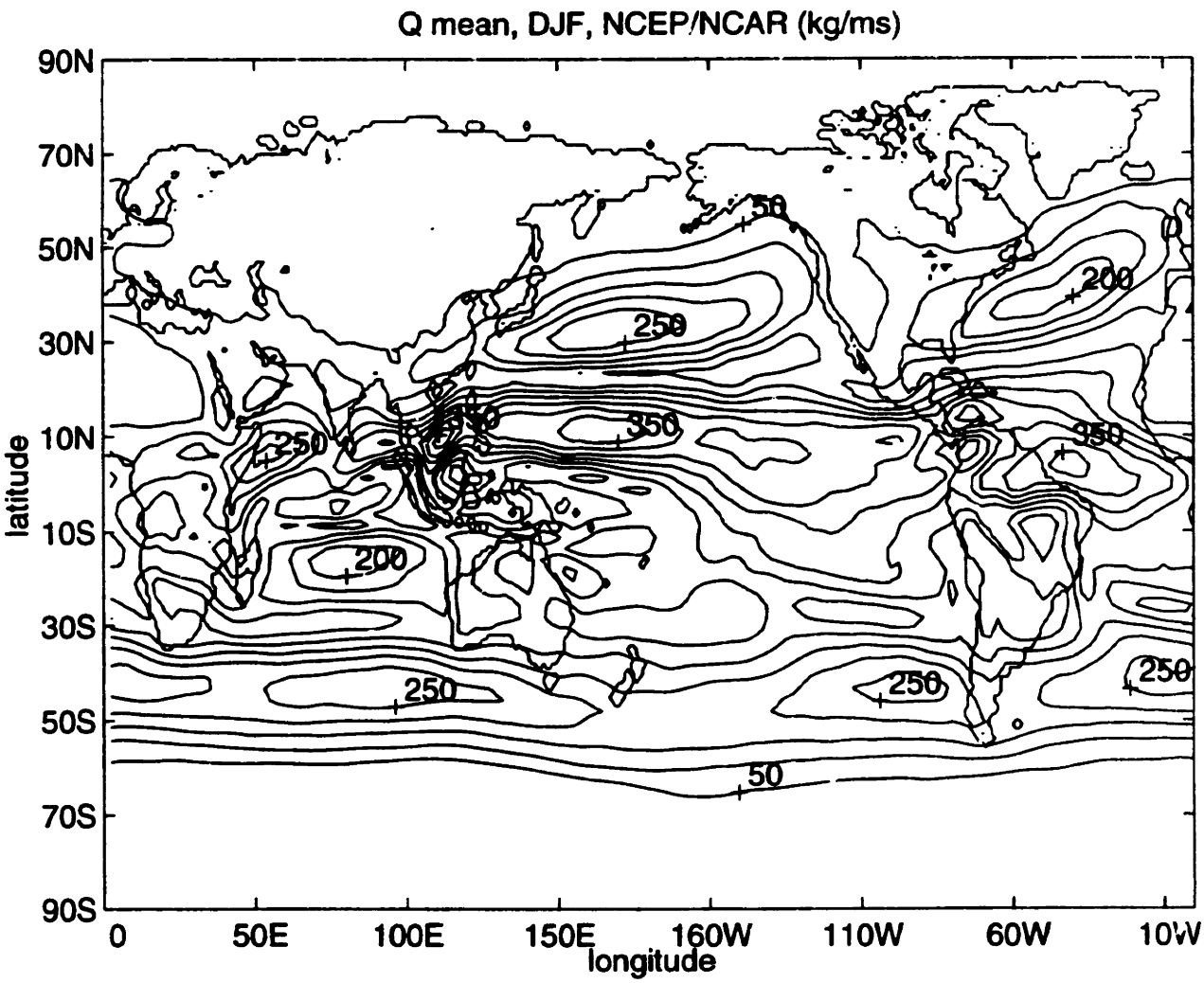

Fig 3a. The NCEP/NCAR mean vapor flux for DJF. Contoured on 50 kg/ms intervals.

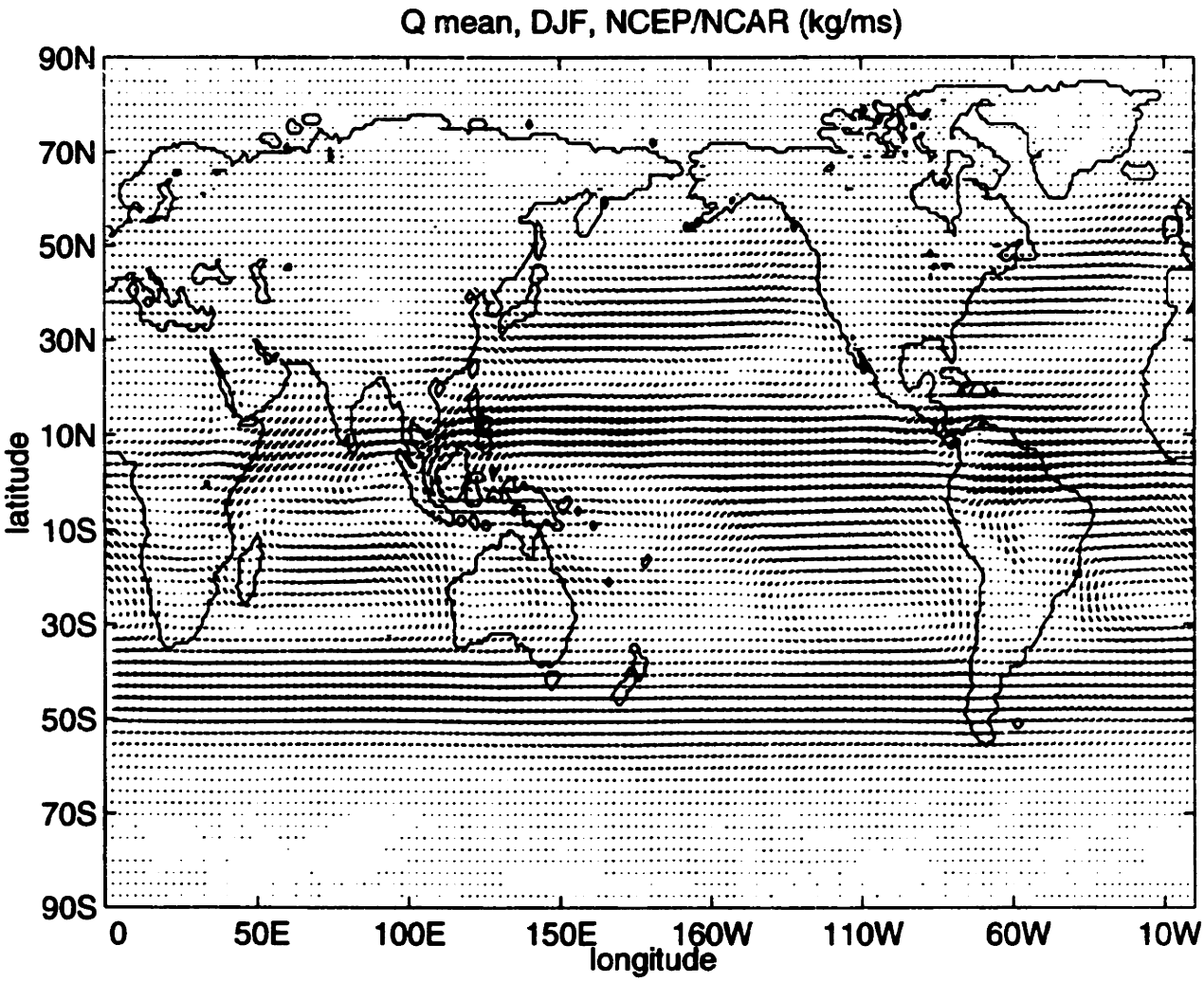

Fig 3b. The NCEP/NCAR mean vapor flux for DJF plotted as flux vectors.

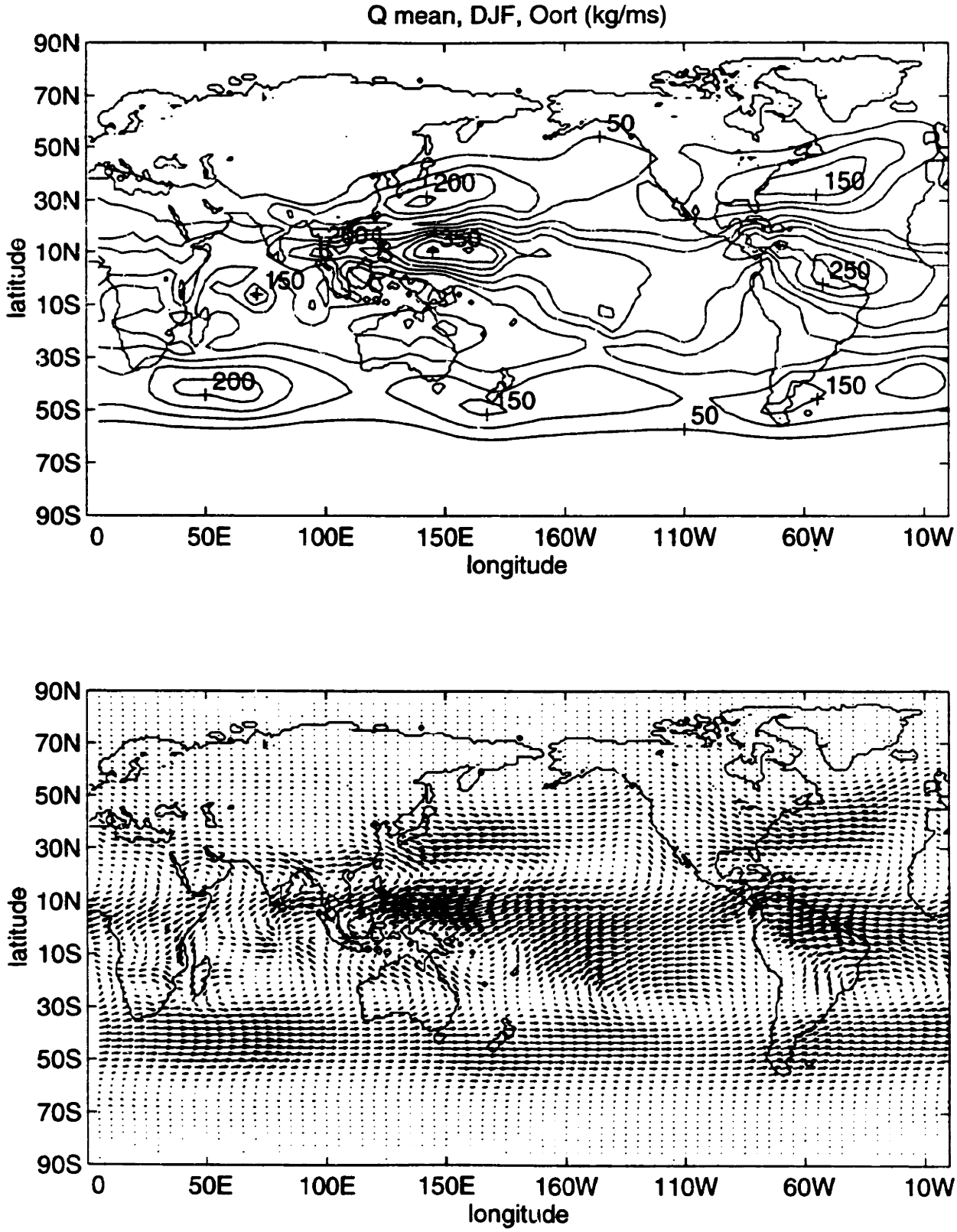

Fig 4a. (upper) The Oort mean vapor flux for DJF. Contoured on 50 kg/ms intervals. 4b (lower) Above plotted as flux vectors.

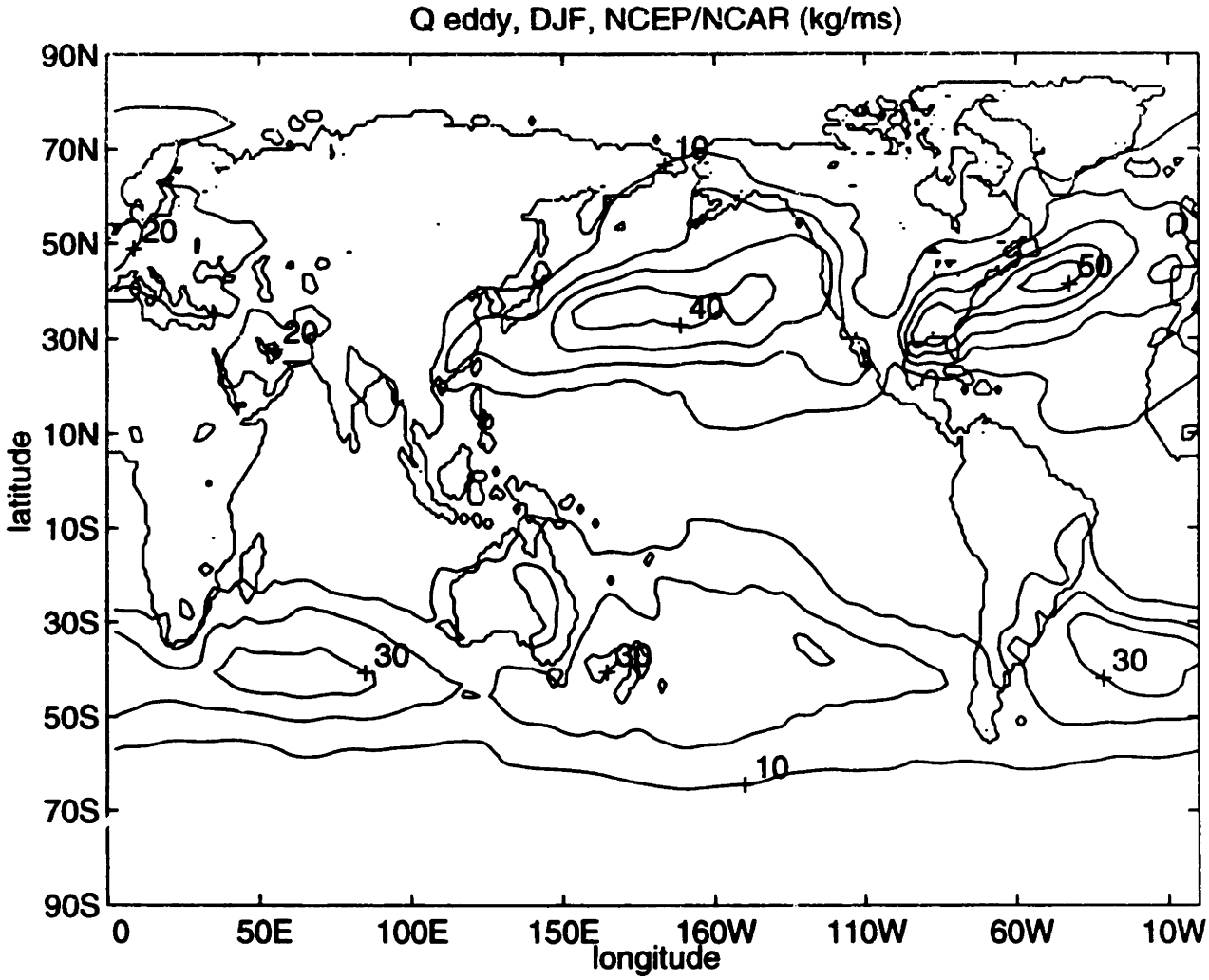

Fig 5a. The NCEP/NCAR eddy vapor flux for DJF. Contoured on 10 kg/ms intervals.

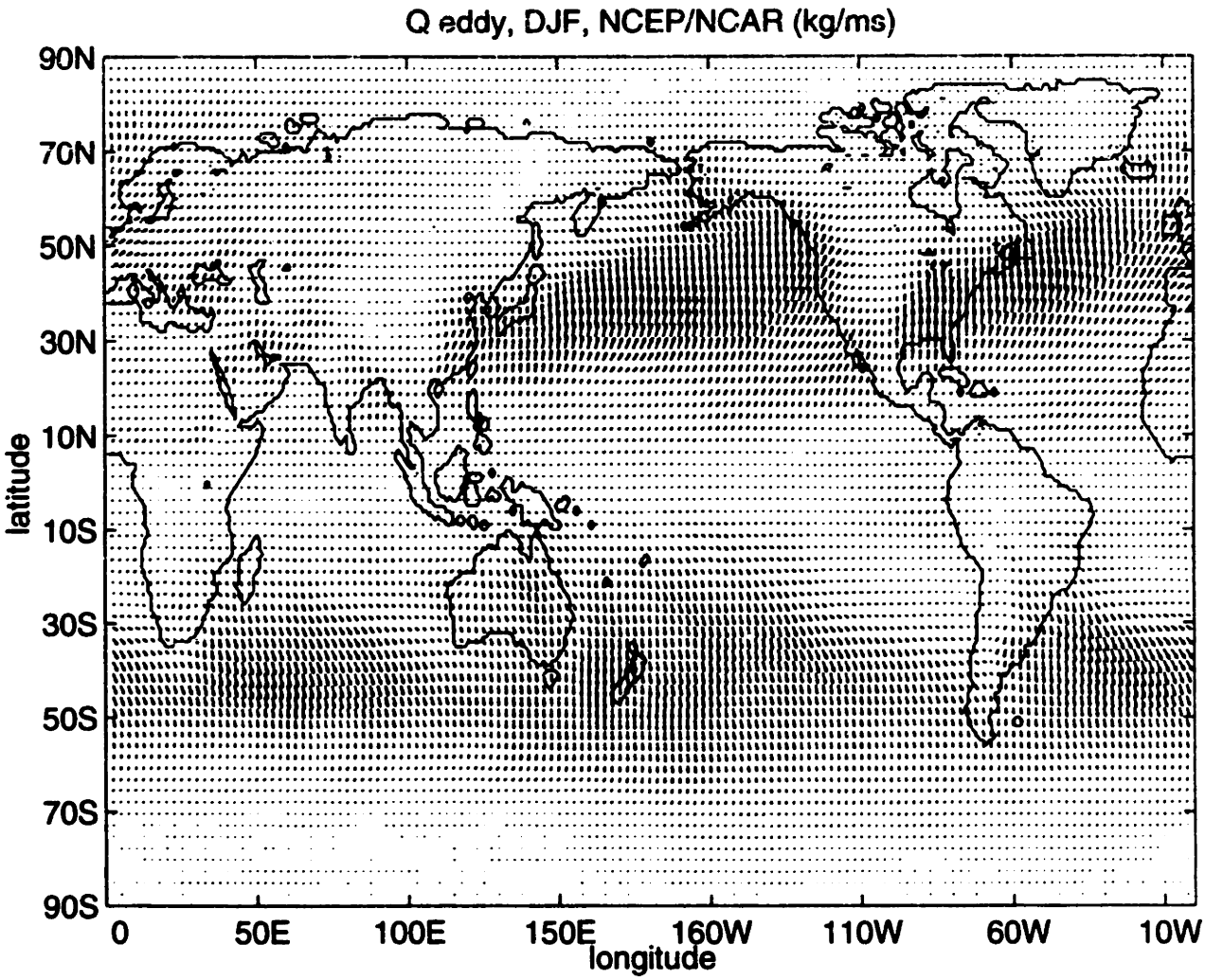

Fig 5b. The NCEP/NCAR eddy vapor flux for DJF plotted as flux vectors.

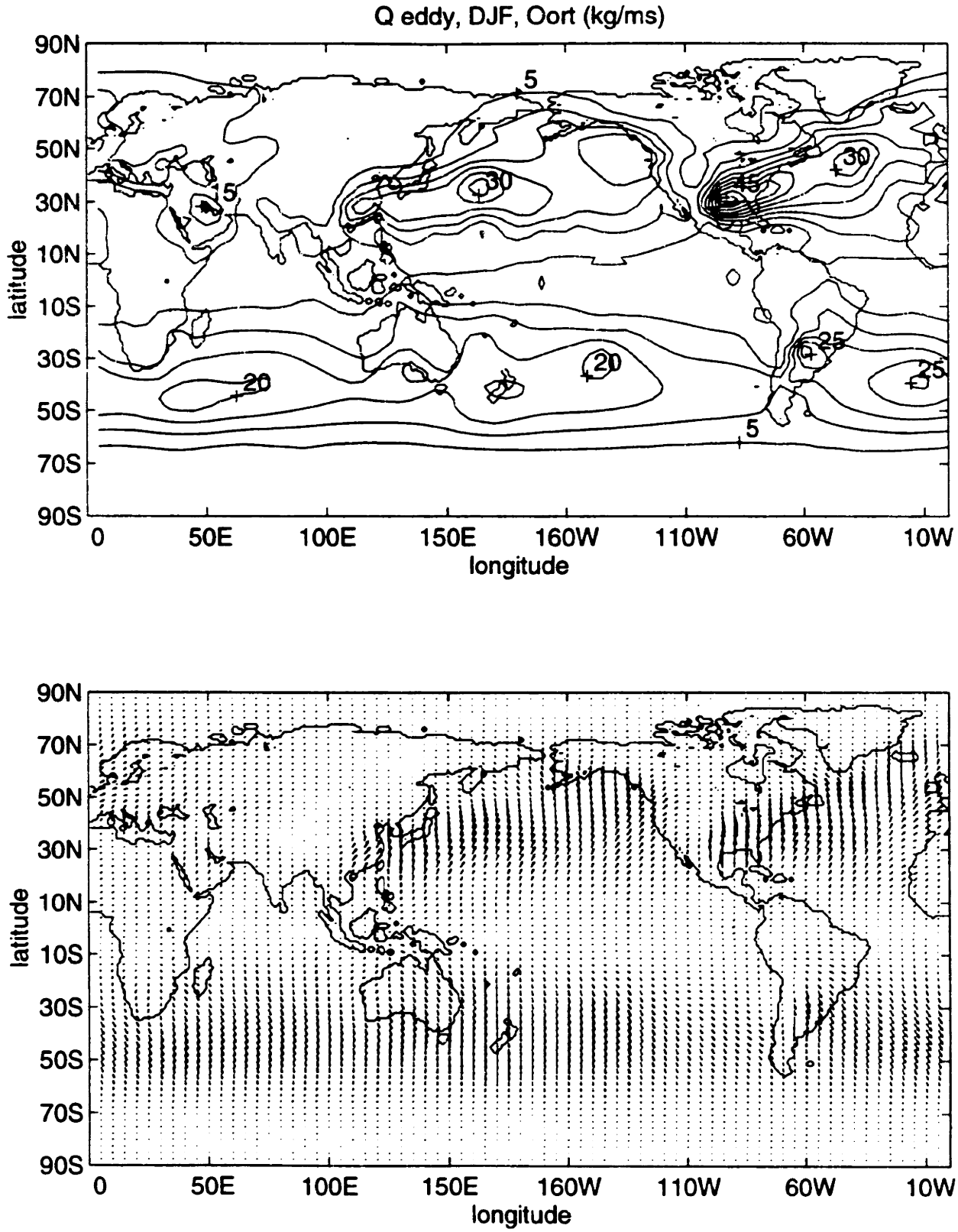

Fig 6a. (upper) The Oort eddy vapor flux for DJF. Contoured on 5 kg/ms intervals. 6b (lower) Above plotted as flux vectors.

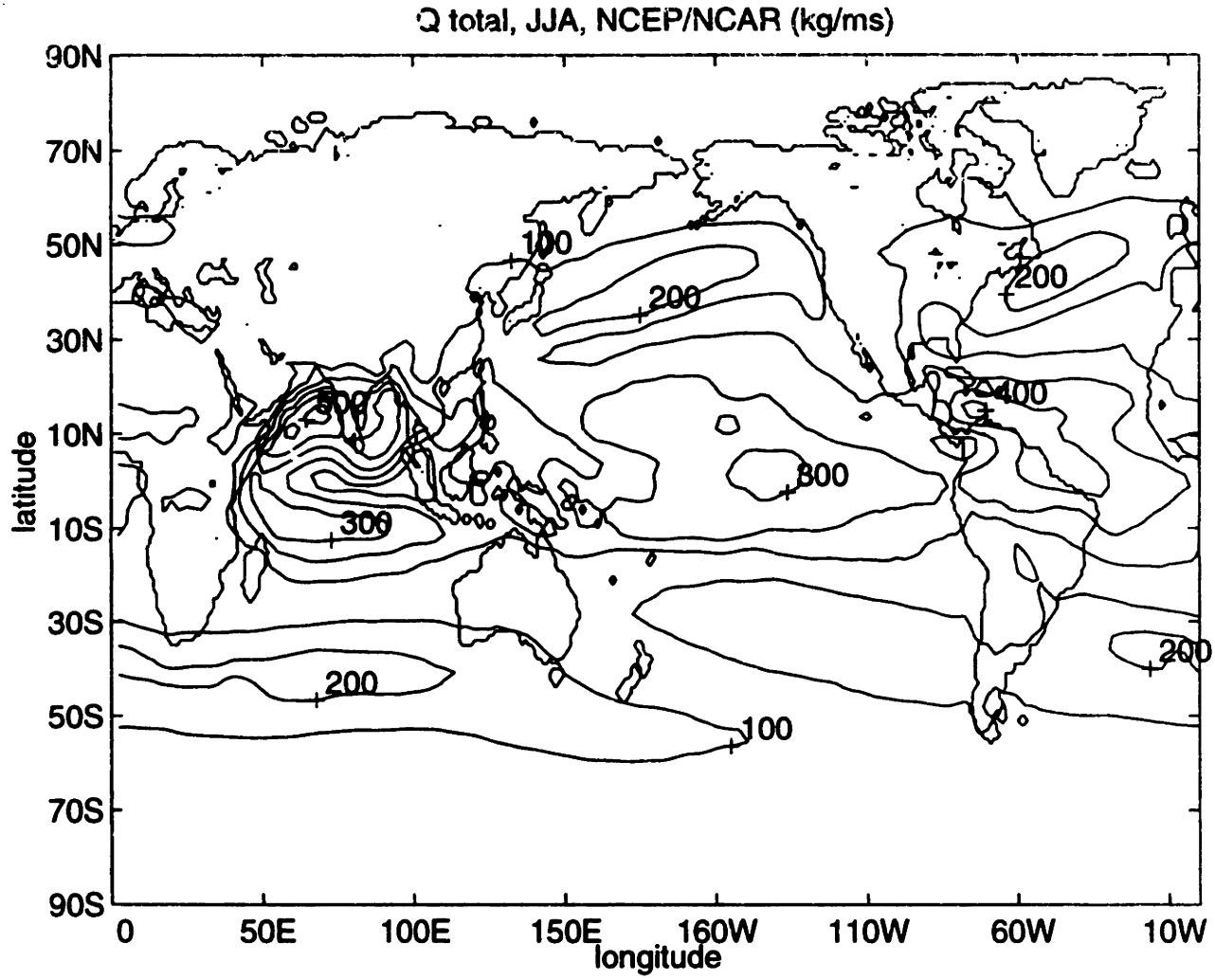

Fig 7a. The NCEP/NCAR total vapor flux for JJA. Contoured on 100 kg/ms intervals.

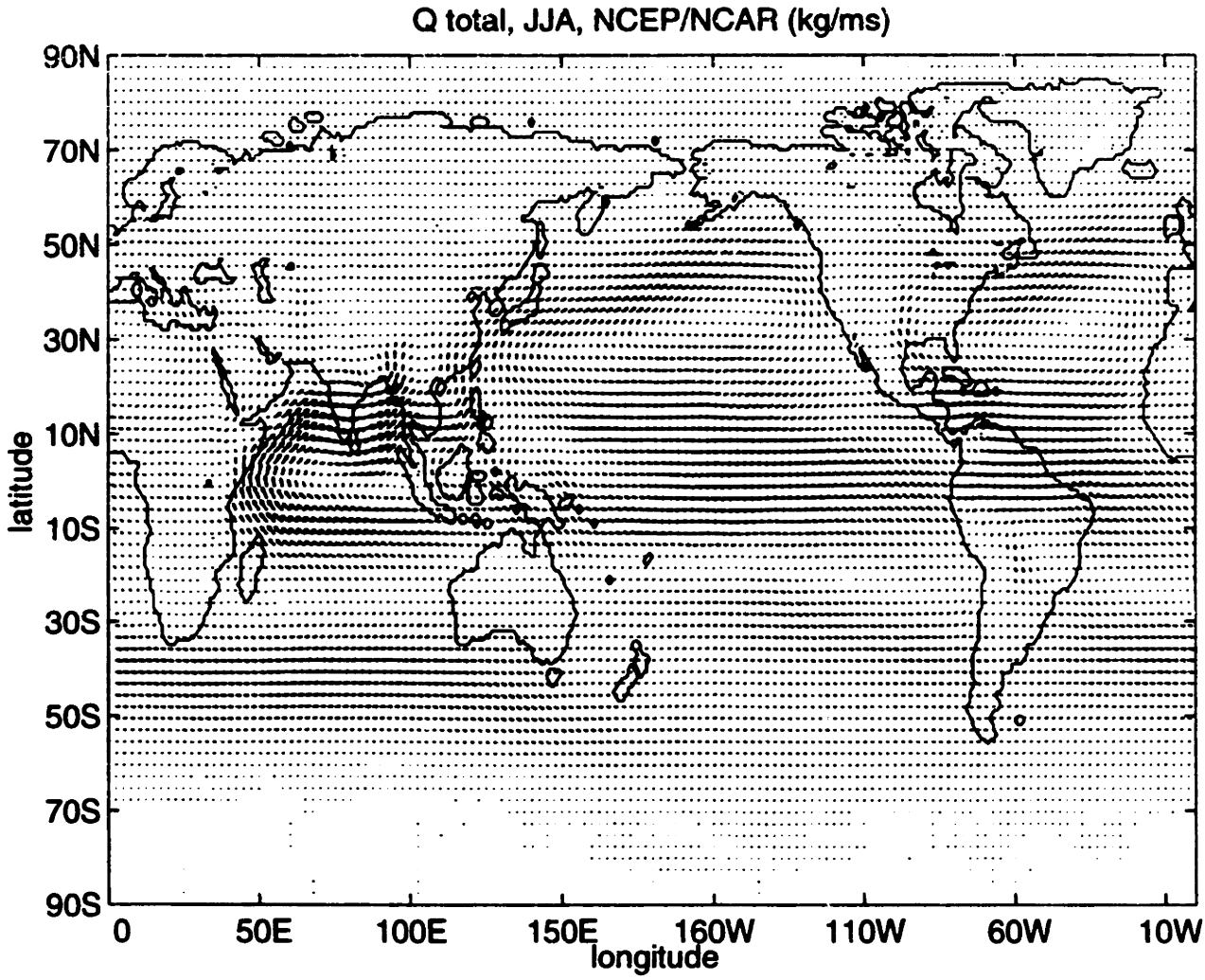

Fig 7b. The NCEP/ NCAR total vapor flux for JJA plotted as flux vectors.

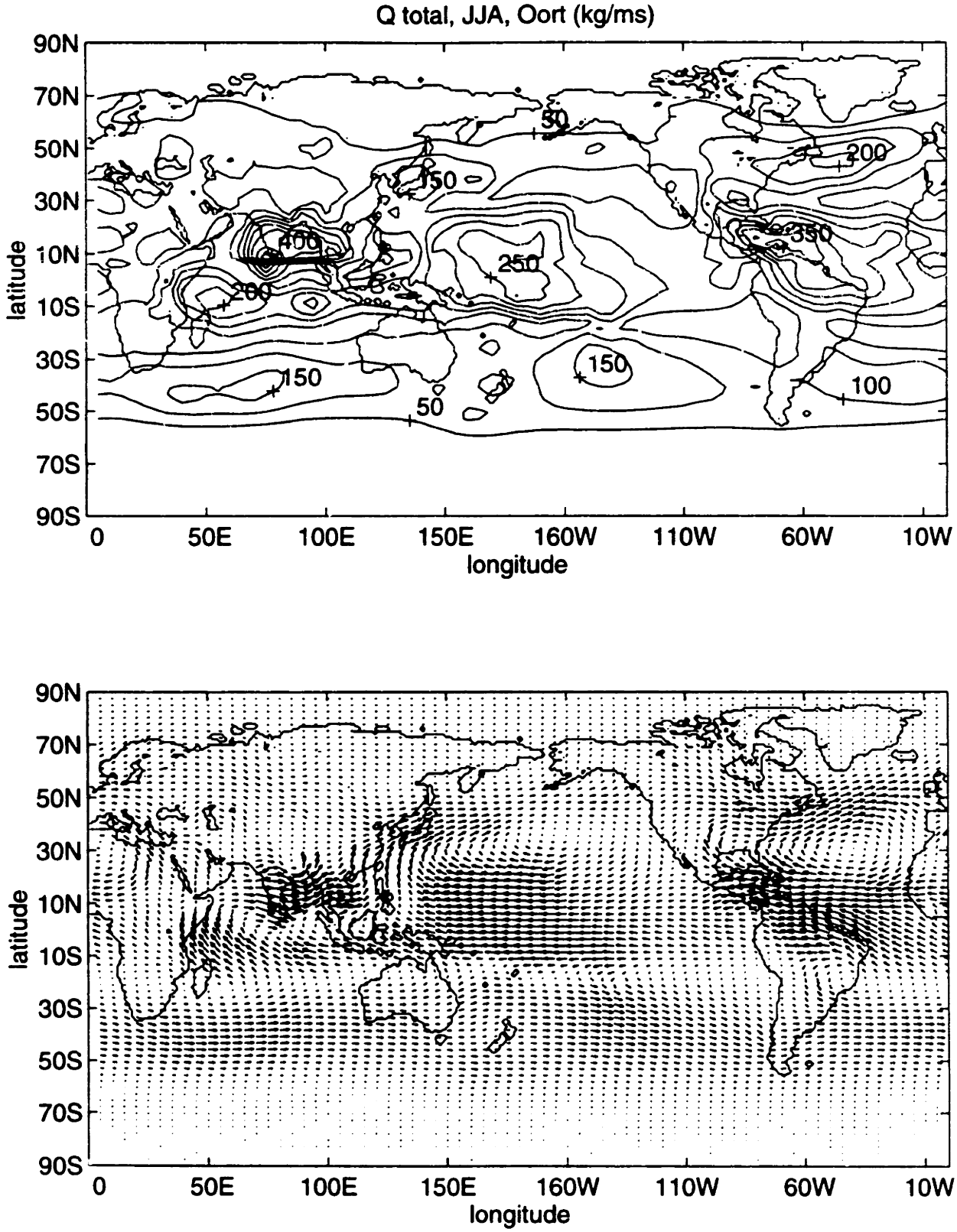

Fig 8a. (upper) The Oort total vapor flux for JJA. Contoured on 50 kg/ms intervals. 8b (lower) Above plotted as flux vectors.

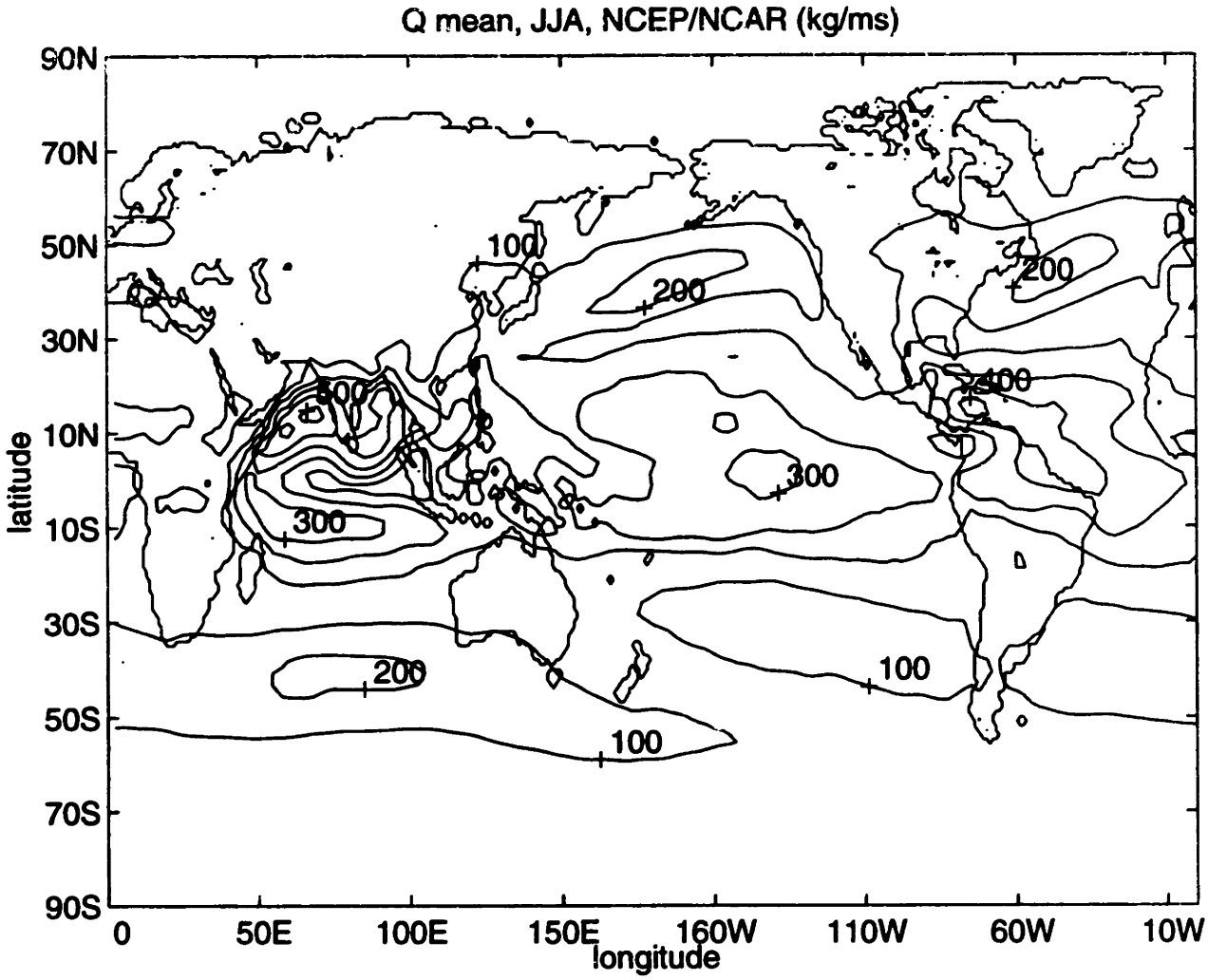

Fig 9a. The NCEP/NCAR mean vapor flux for JJA. Contoured on 100 kg/ms intervals.

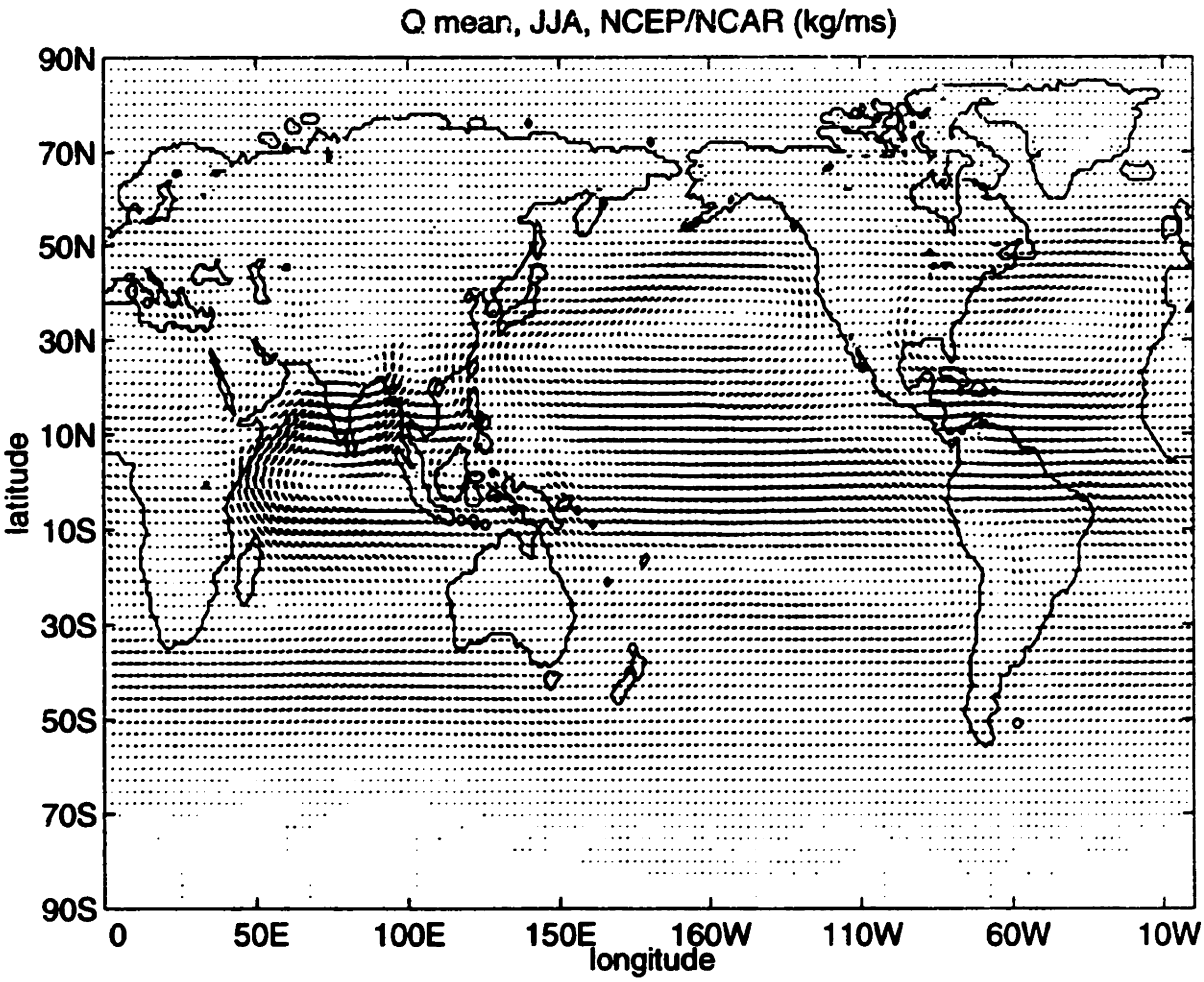

Fig 9b. The NCEP/NCAR mean vapor flux for JJA plotted as flux vectors.

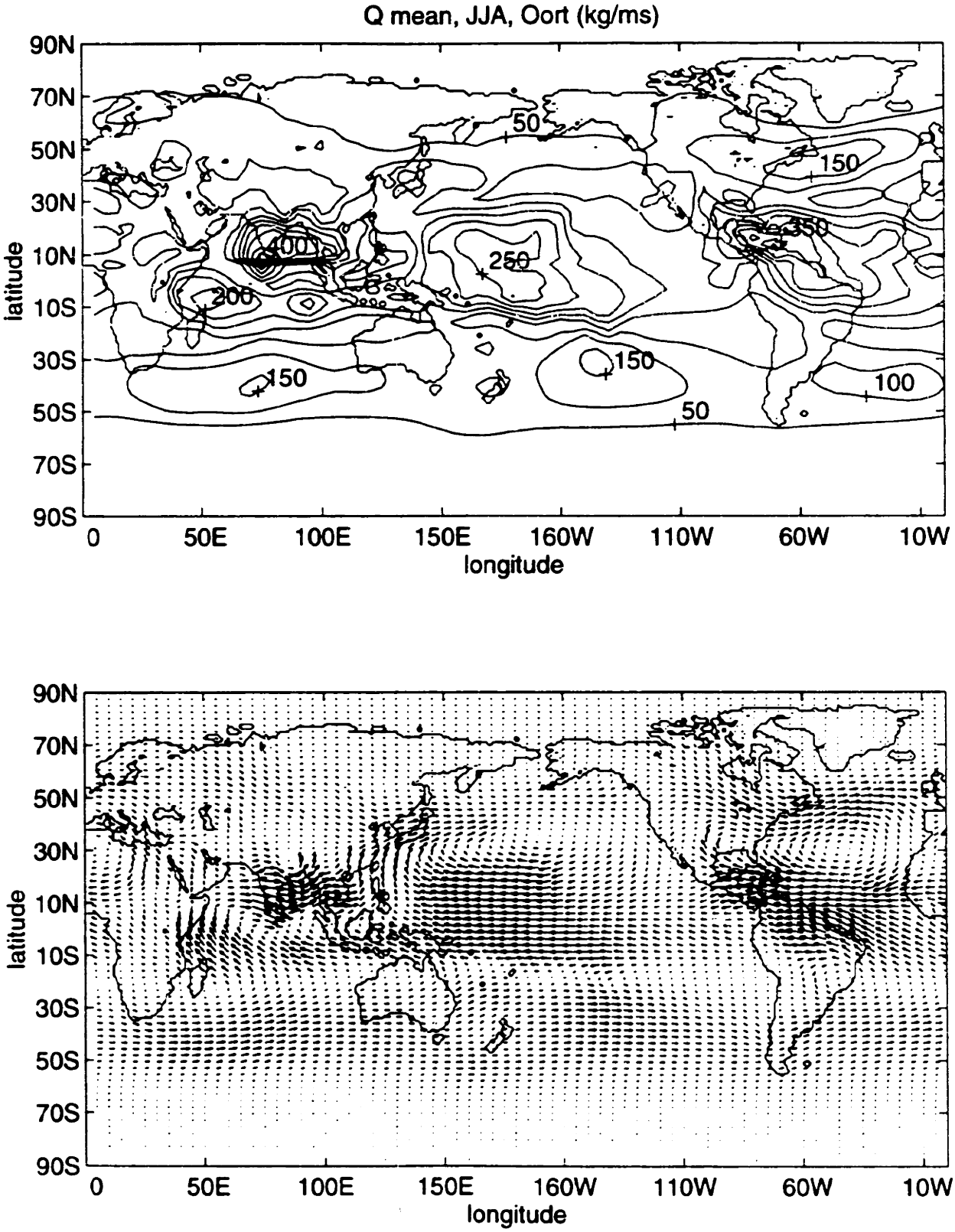

Fig 10a. (upper) The Oort mean vapor flux for JJA. Contoured on 50 kg/ms intervals. 10b (lower) Above plotted as flux vectors.

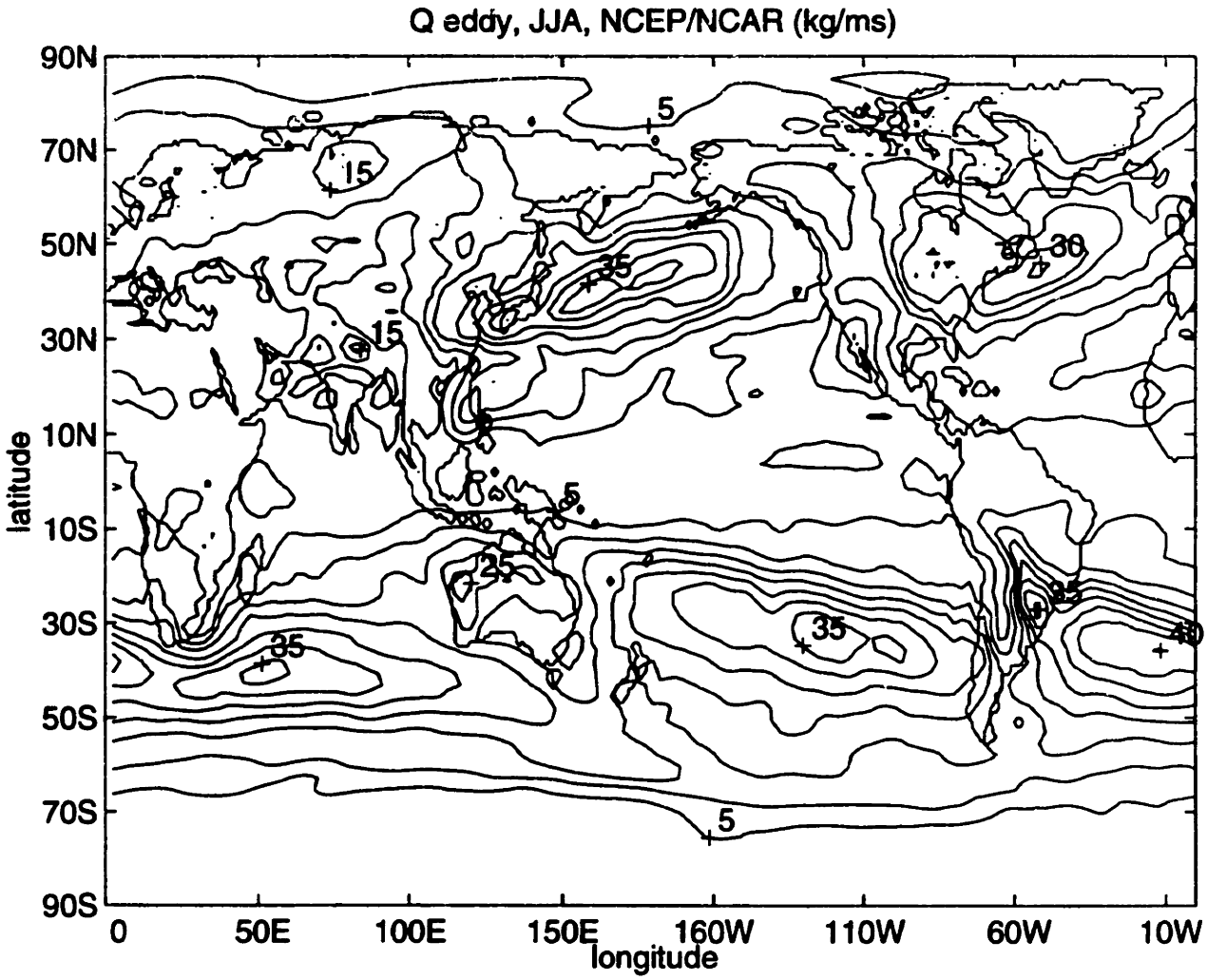

Fig 11a. The NCEP/NCAR eddy vapor flux for JJA. Contoured on 5 kg/ms intervals.

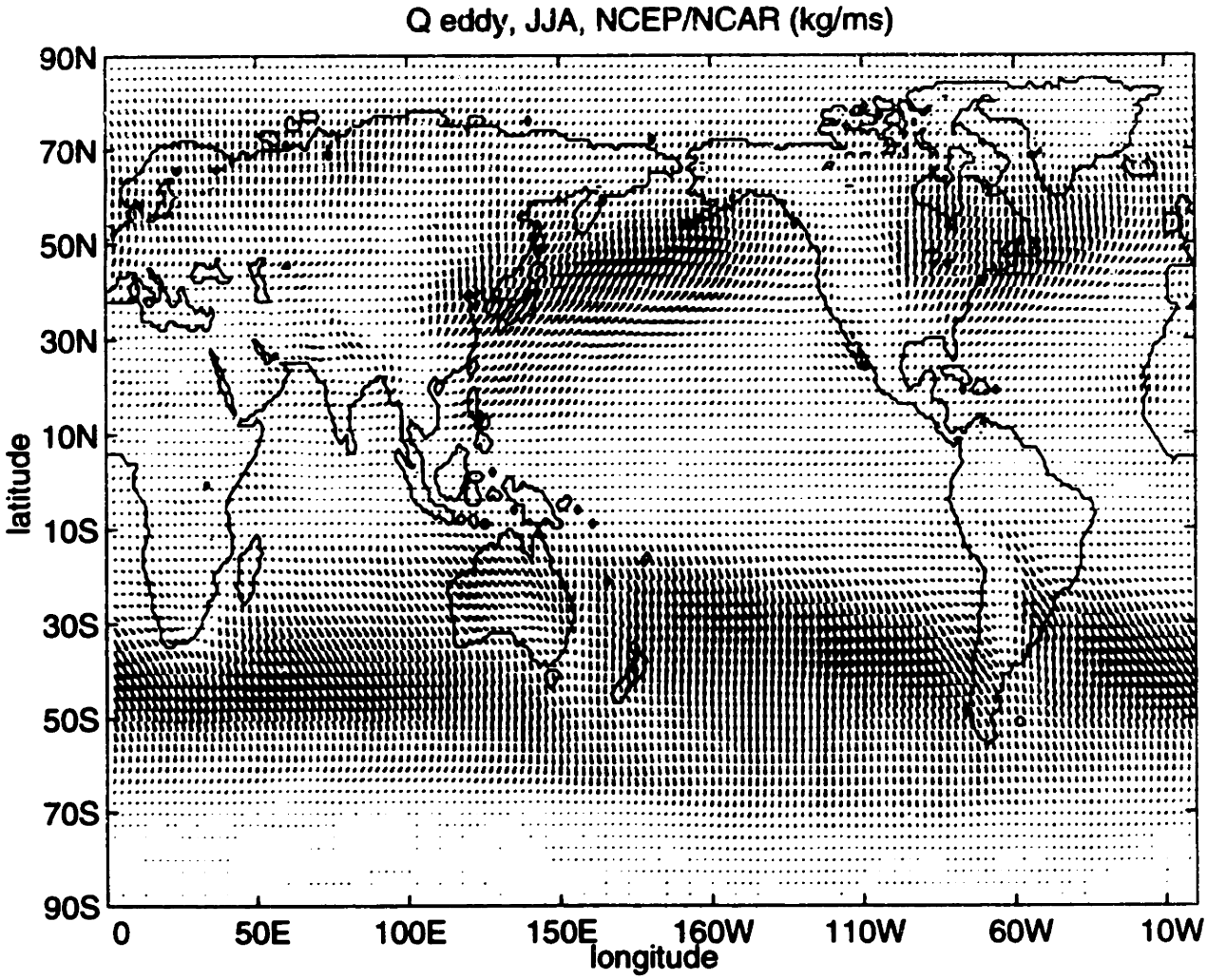

Fig 11b. The NCEP/NCAR eddy vapor flux for JJA plotted as flux vectors.

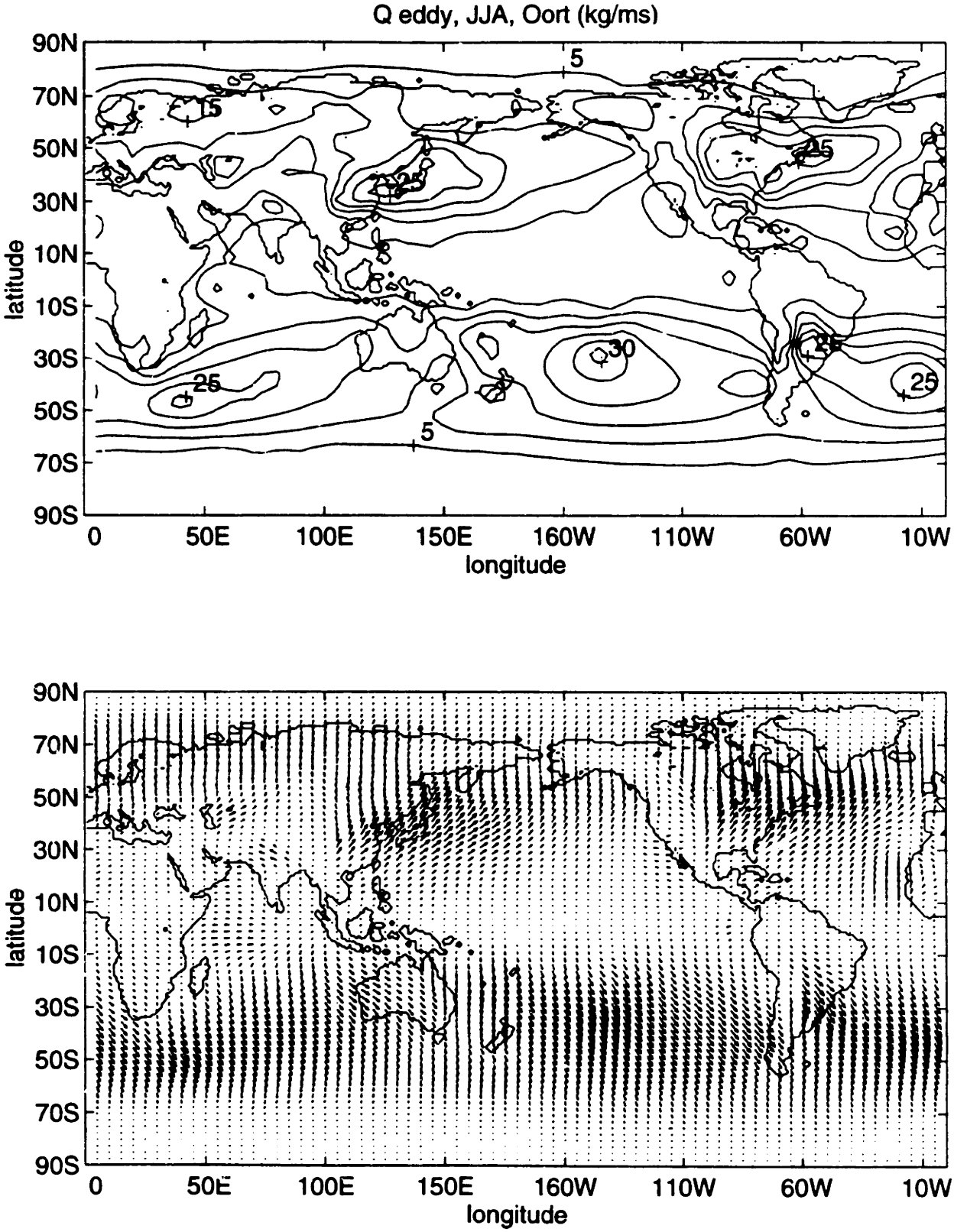

Fig 12a. (upper) The Oort eddy vapor flux for JJA. Contoured on 5 kg/ms intervals. 12b (lower) Above plotted as flux vectors.

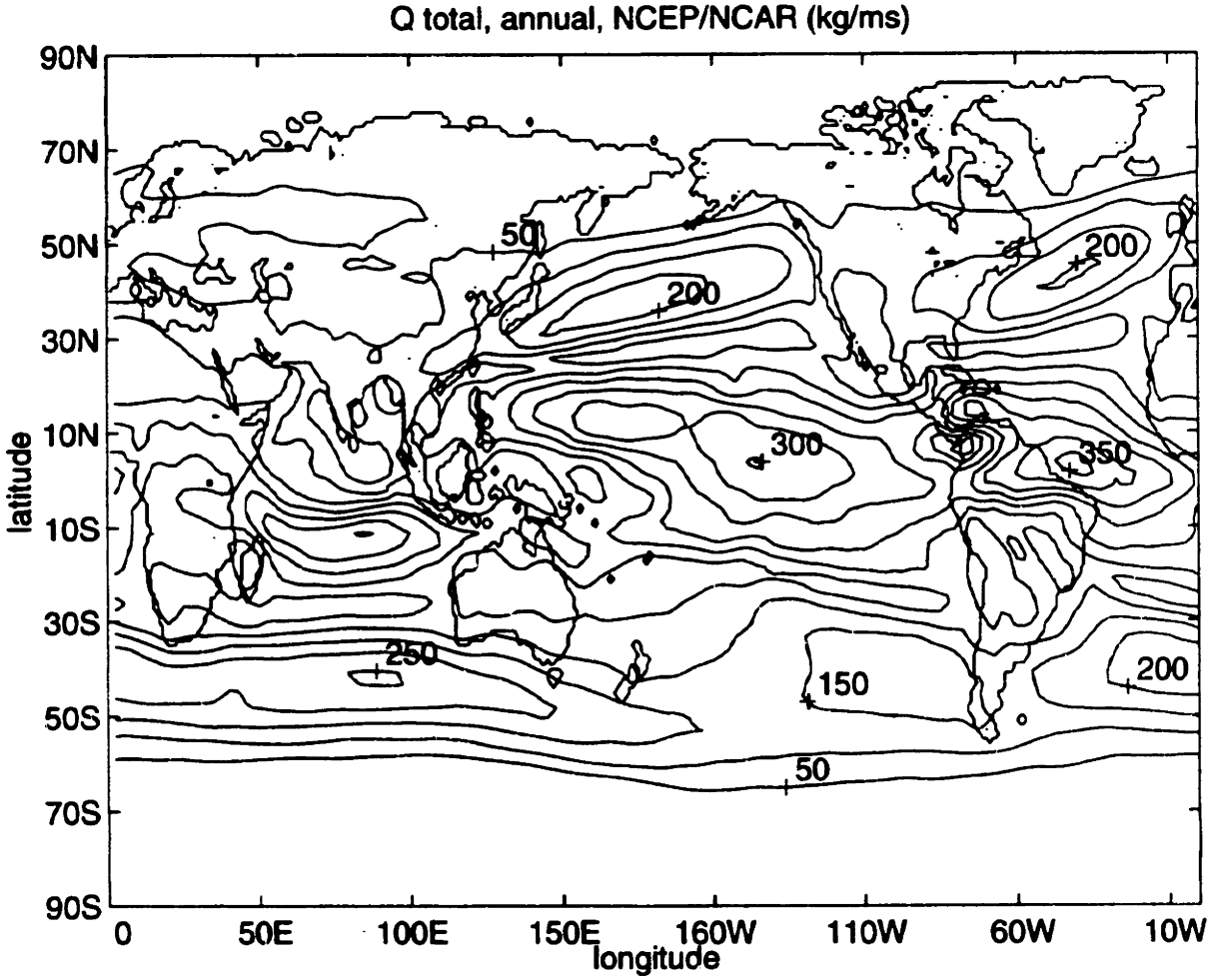

Fig 13a. The NCEP/NCAR total vapor flux for annual average. Contoured on 50 kg/ms intervals.

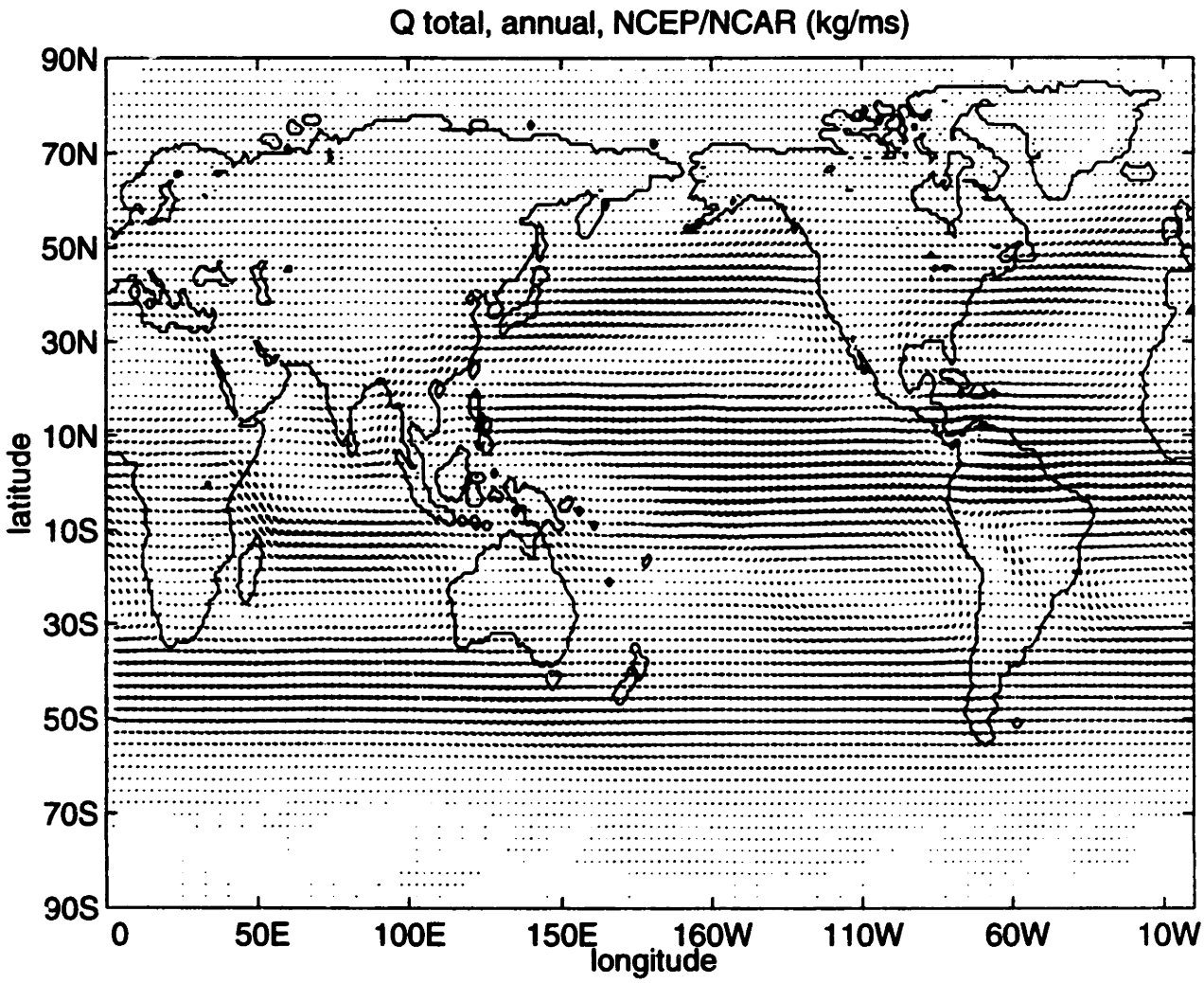

Fig 13b. The NCEP/ NCAR total vapor flux for annual average plotted as flux vectors.

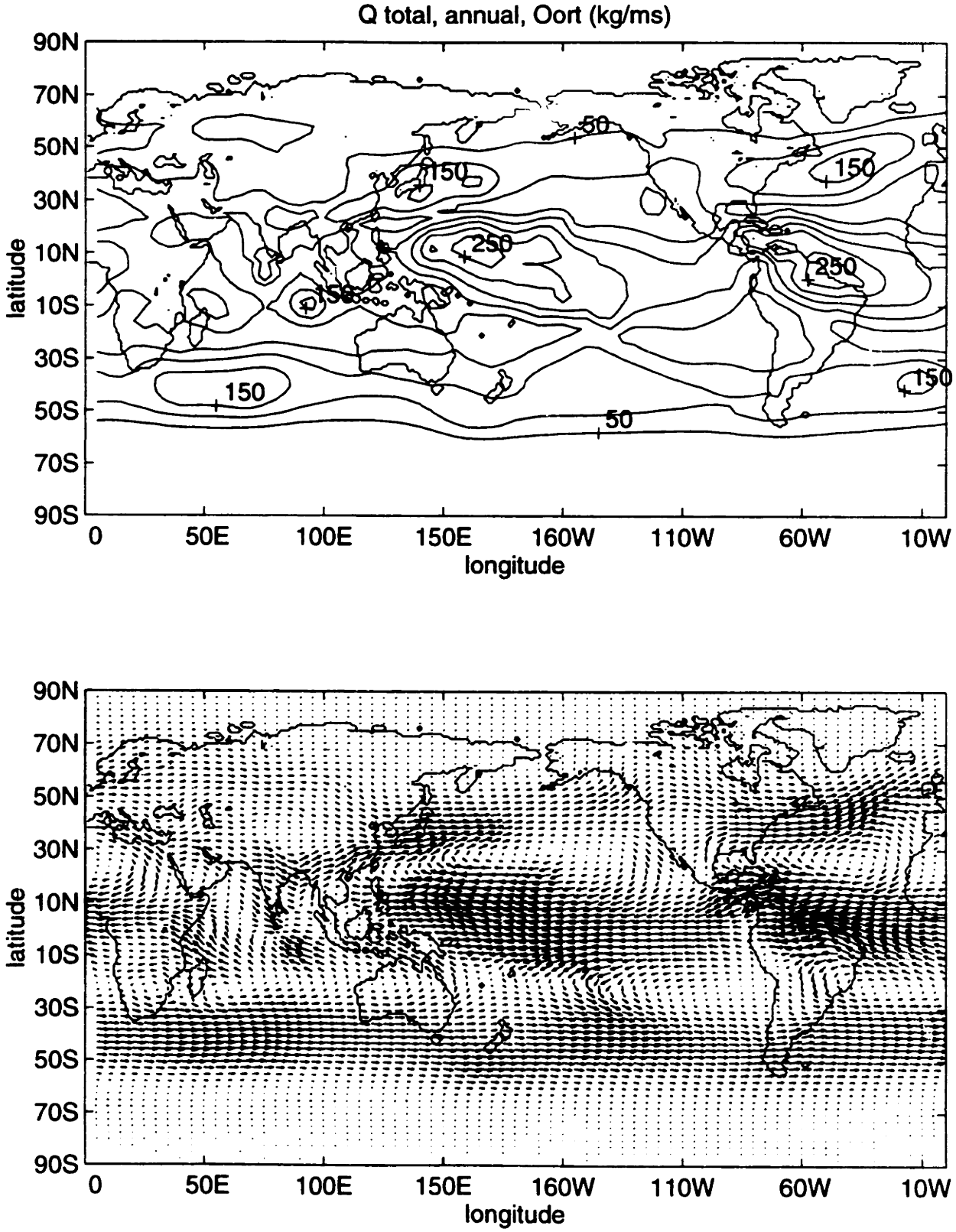

Fig 14a. (upper) The Oort total vapor flux for annual average. Contoured on 50 kg/ms intervals. 14b (lower) Above plotted as flux vectors.

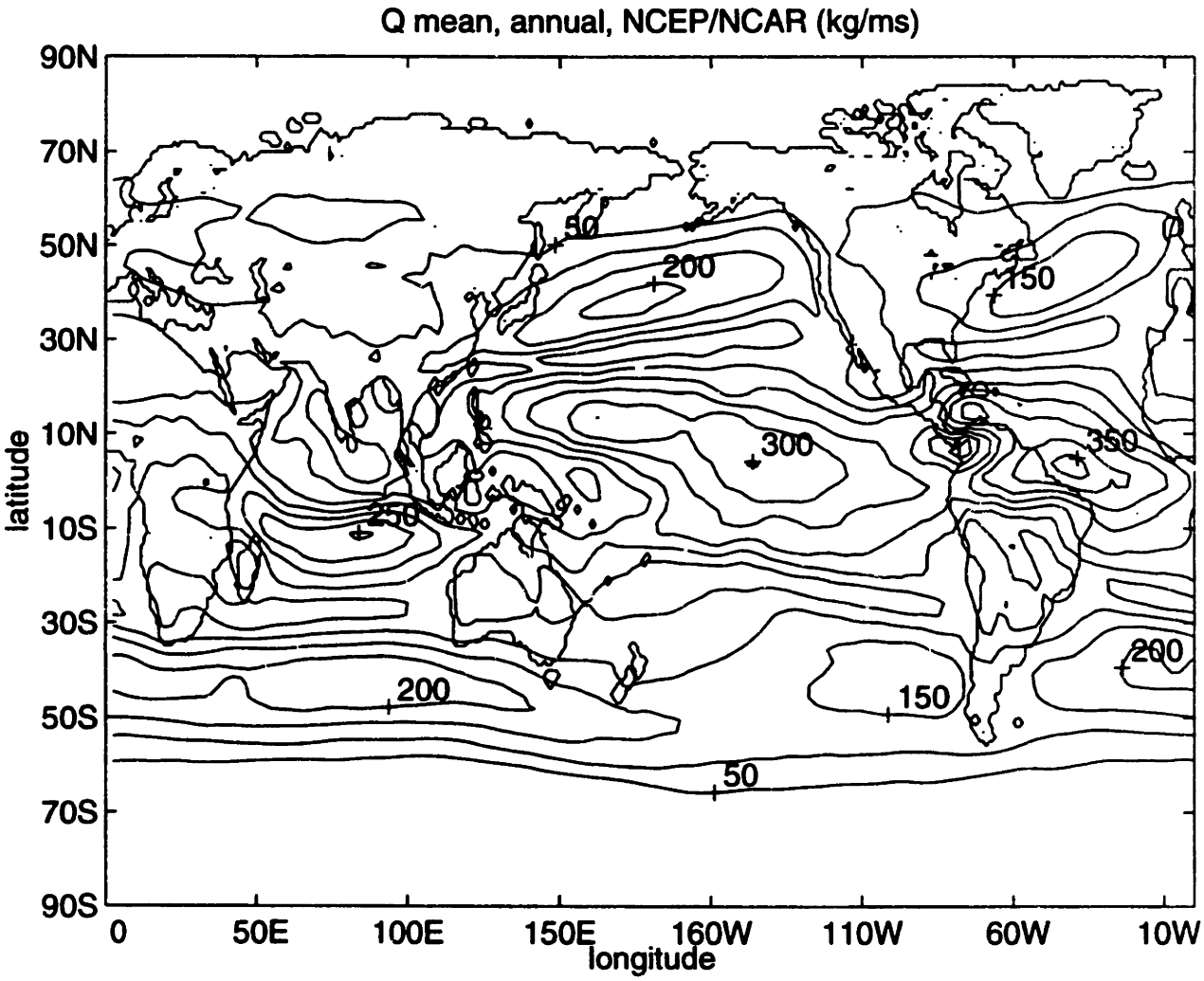

Fig. 15a. The NCEP/NCAR mean vapor flux for annual average. Contoured on 50 kg/ms intervals.

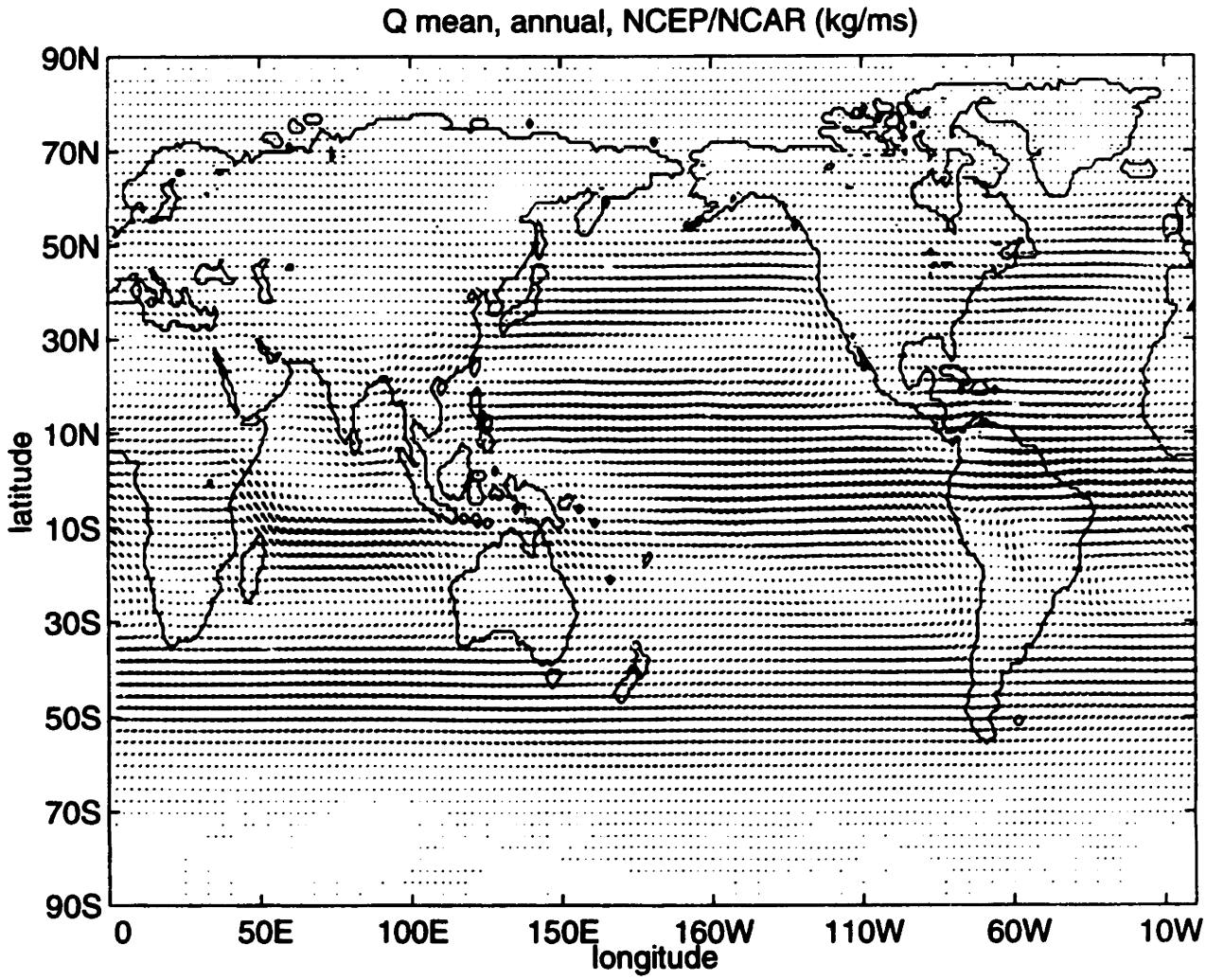

Fig 15b. The NCEP/NCAR mean vapor flux for annual average plotted as flux vectors.

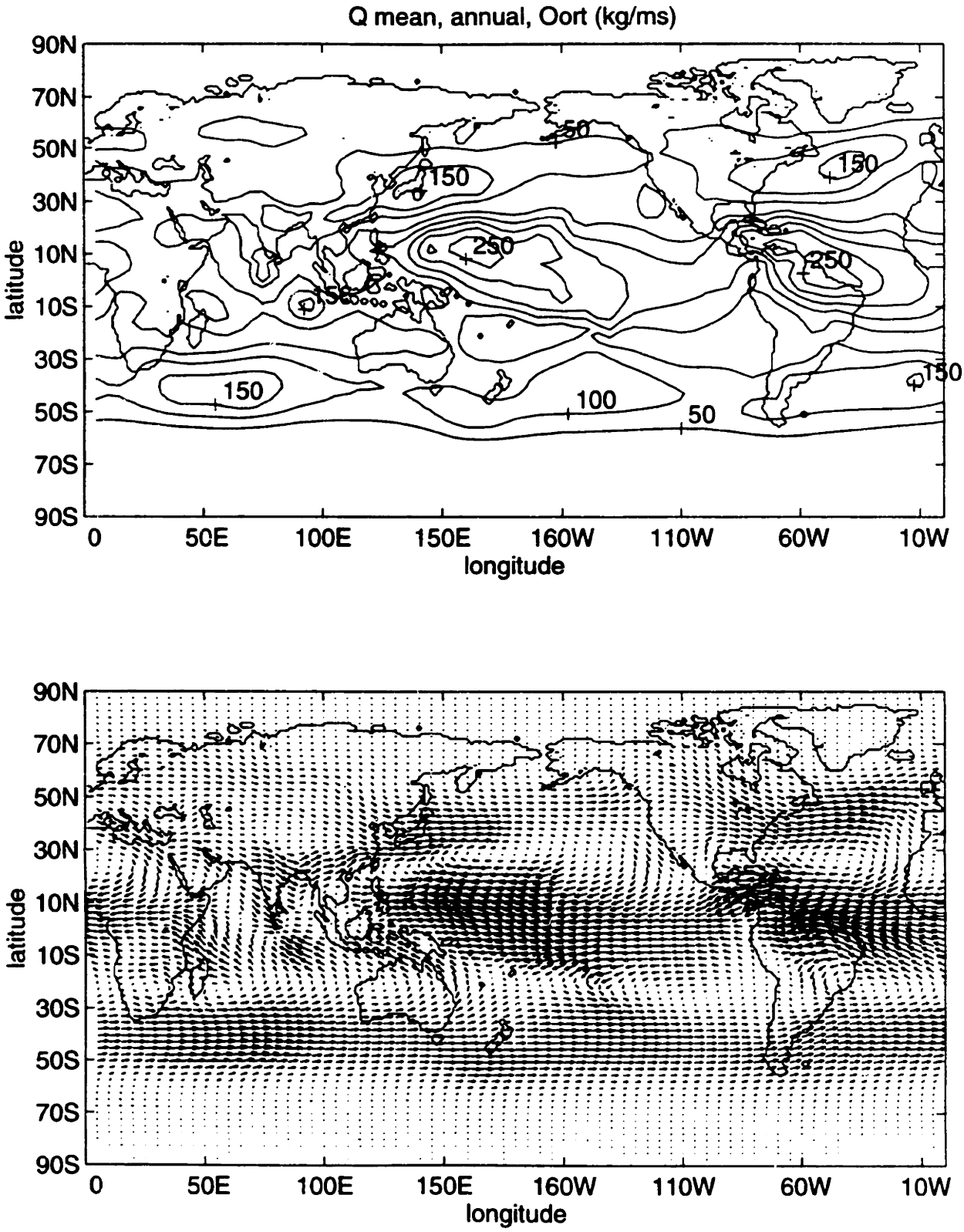

Fig 16a. (upper) The Oort mean vapor flux for annual average. Contoured on 50 kg/ms intervals. 16b (lower) Above plotted as flux vectors.

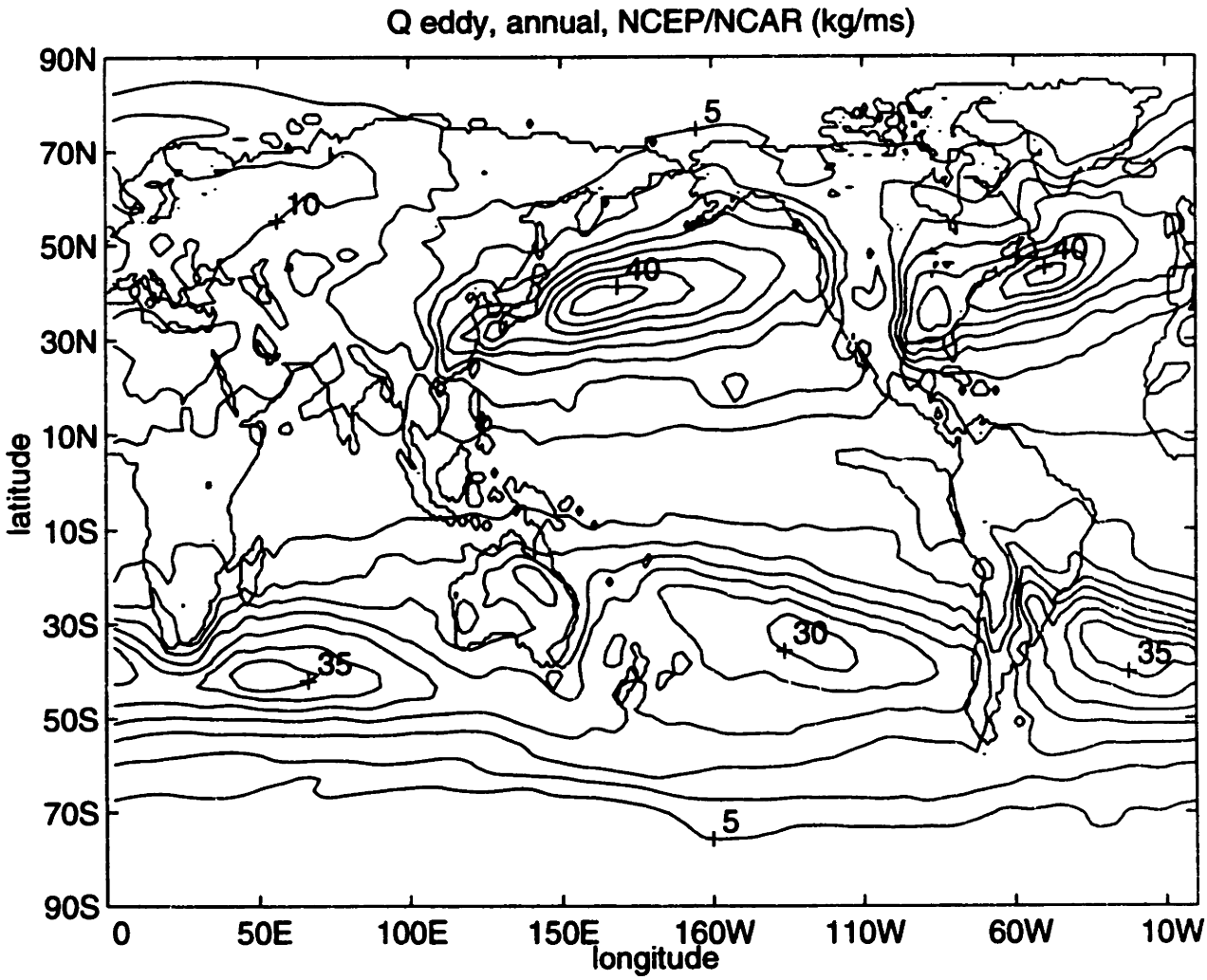

Fig 17a. The NCEP/NCAR eddy vapor flux for annual average. Contoured on 5 kg/ms intervals.

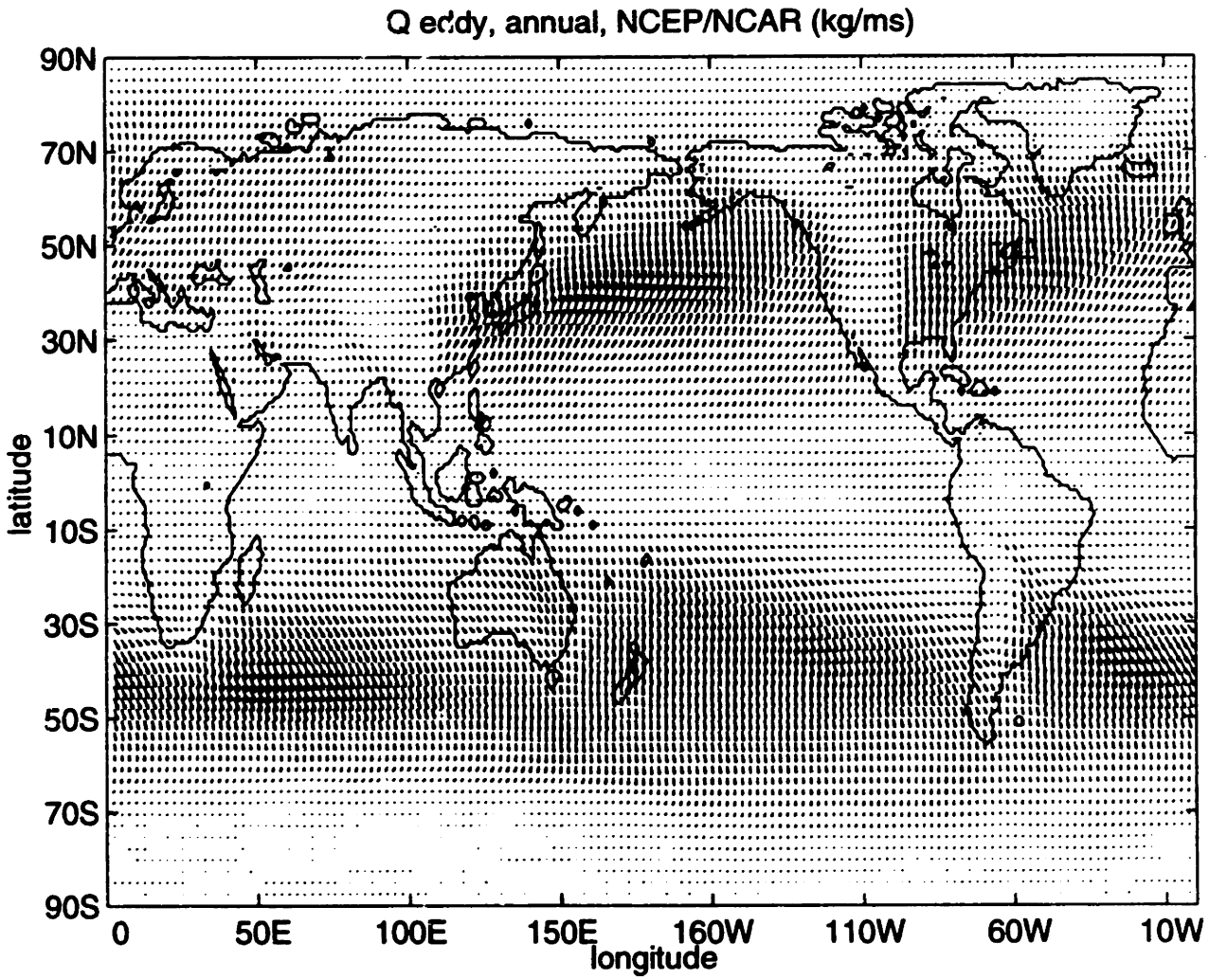

Fig 17b. The NCEP/NCAR eddy vapor flux for annual average plotted as flux vectors.

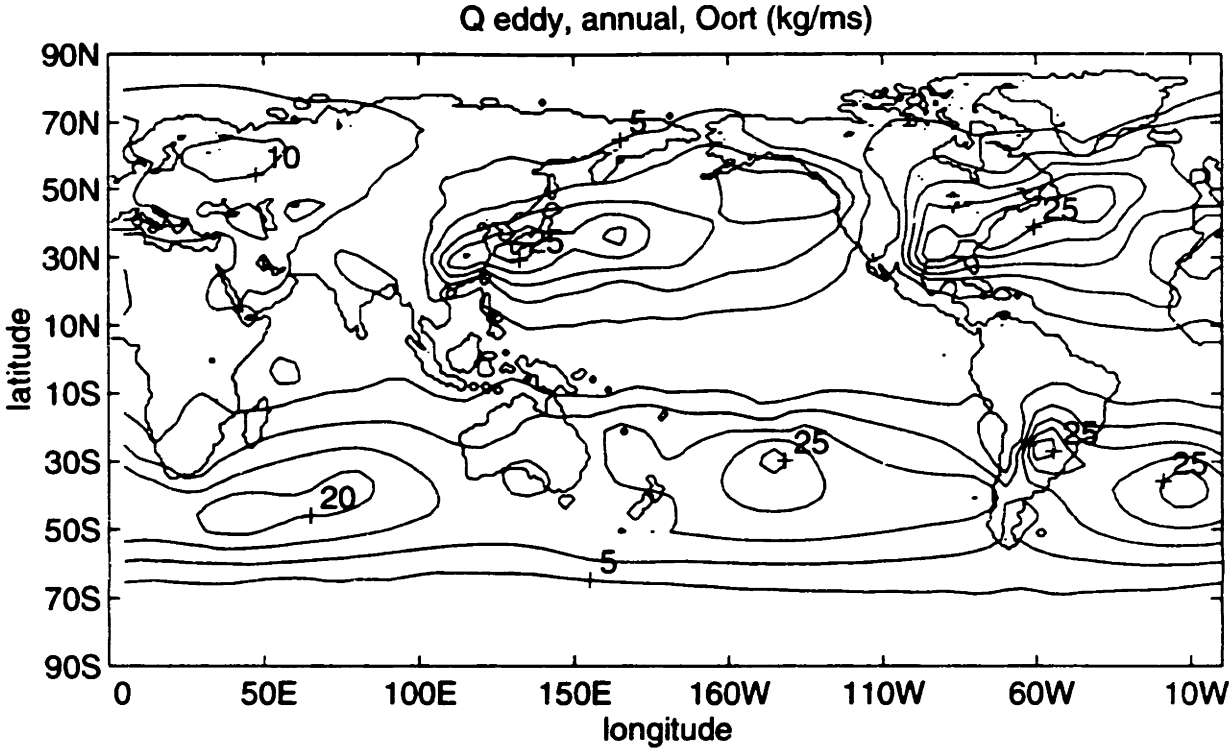

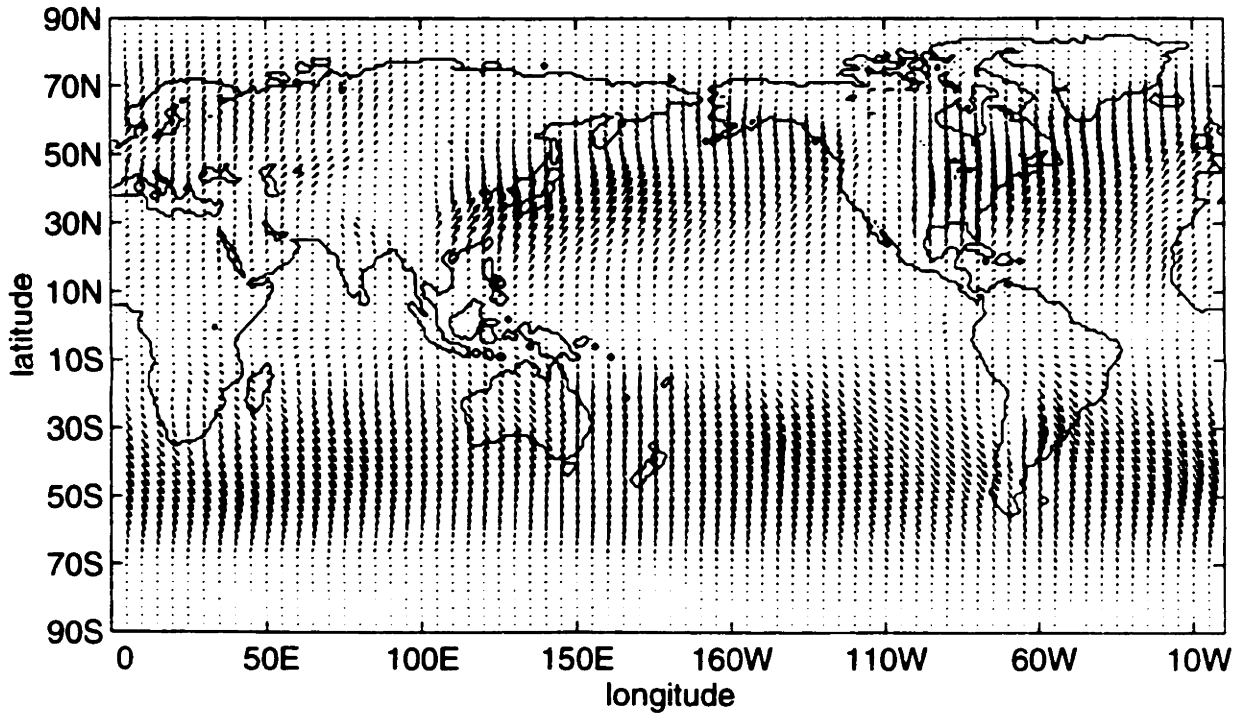

Fig 18a. (upper) The Oort eddy vapor flux for annual average. Contoured on 5 kg/ms intervals. 18b (lower) Above plotted as flux vectors.

3.2 Zonal Analysis

Figures 19a through 24b display the zonal averages of the global data presented in Figures 1 through 18. By looking at the zonal component of total flux for the NCEP/NCAR and Oort data sets in Figures 19a and 19b, respectively, a similar shape can be seen. Even zonally, the NCEP/NCAR data tends to be larger in magnitude. Two major peaks are evident, one in the mid-latitudes of each hemisphere, where the major zonal flow regimes exist. Another peak is at the Equator and it is associated with tropical easterlies. The Southern Hemisphere peak is larger. In this hemisphere, the largest difference between the two data sets is in DJF, where there is a difference between peaks of approximately 100 kg/ms. JJA has a much smaller discrepancy (30 kg/ms). Annually the difference is 50 kg/ms.

Differences of this magnitude are not seen between the data sets in the Northern Hemisphere. Both the reanalysis and Oort data sets are based on adequate sampling in the populated Northern Hemisphere. In the Southern Hemisphere the Oort interpolation scheme may fail to capture major transport features, while the reanalysis has the model estimate as a basis for its vapor transport estimates. In all three periods a discrepancy of only 30 kg/ms is seen in data-rich regions. At the equator, the annual average of both data sets differs by merely 20 kg/ms.

The data sets more closely resemble each other in Figures 20a and 20b for the meridional component of total flux. The maximum value for all three time periods differs little between the two data sets. The largest difference between the two occurs in JJA and the annual data, when the widths of the peaks are larger in the NCEP/NCAR data than in the Oort.

This disparity demonstrates that poleward transport in this region continues to a higher latitude in the NCEP/NCAR data. Also, the positive peaks for DJF are 5 to 10 kg/ms smaller in the Oort data.

The zonal components of the mean motion flux, shown in Figures 21a and 21b, are essentially the same as those of the total flux. A difference between the meridional component of the mean and total flux, can be seen by comparing Figure 20a with 22a, and 20b with 22b. While the low-latitude peaks are very similar between the mean and total flux, the values of the flux at the mid-latitudes are quite different. This is due to the significant amount of poleward flux attributable to eddies in this region. The addition of this eddy flux is sufficient to change the mean flux in the Southern Hemisphere from positive to negative. In the mid-latitude region of the Northern Hemisphere, the flux shifts toward the negative side as well. Both data sets behave similarly.

The meridional component of the eddy flux is shown in Figures 24a and 24b for each set of data. As required, the data sets show poleward flux in each hemisphere. Each has approximately equal flux between hemispheres. The NCEP data is between 5 and 10 kg/ms larger than the Oort. Each data set shows equal Southern Hemisphere flux for DJF, JJA, and the annual data. There is a difference in the flux between the time periods in the Northern Hemisphere, possibly due to an increase in seasonal variability associated with more land mass. In both data sets the DJF flux in the Northern Hemisphere is higher than that of JJA, as would be expected due to storm activity in the winter.

Figures 23a and 23b display the zonal component of the eddy flux. In the case for eddies, the values of the zonal component are less than those

of the meridional component. Again, the NCEP data has larger values than the Oort data. Small peaks in the NCEP data exist in DJF and JJA at around 15S and 15N, respectively, and are smaller or non-existent in the Oort data.

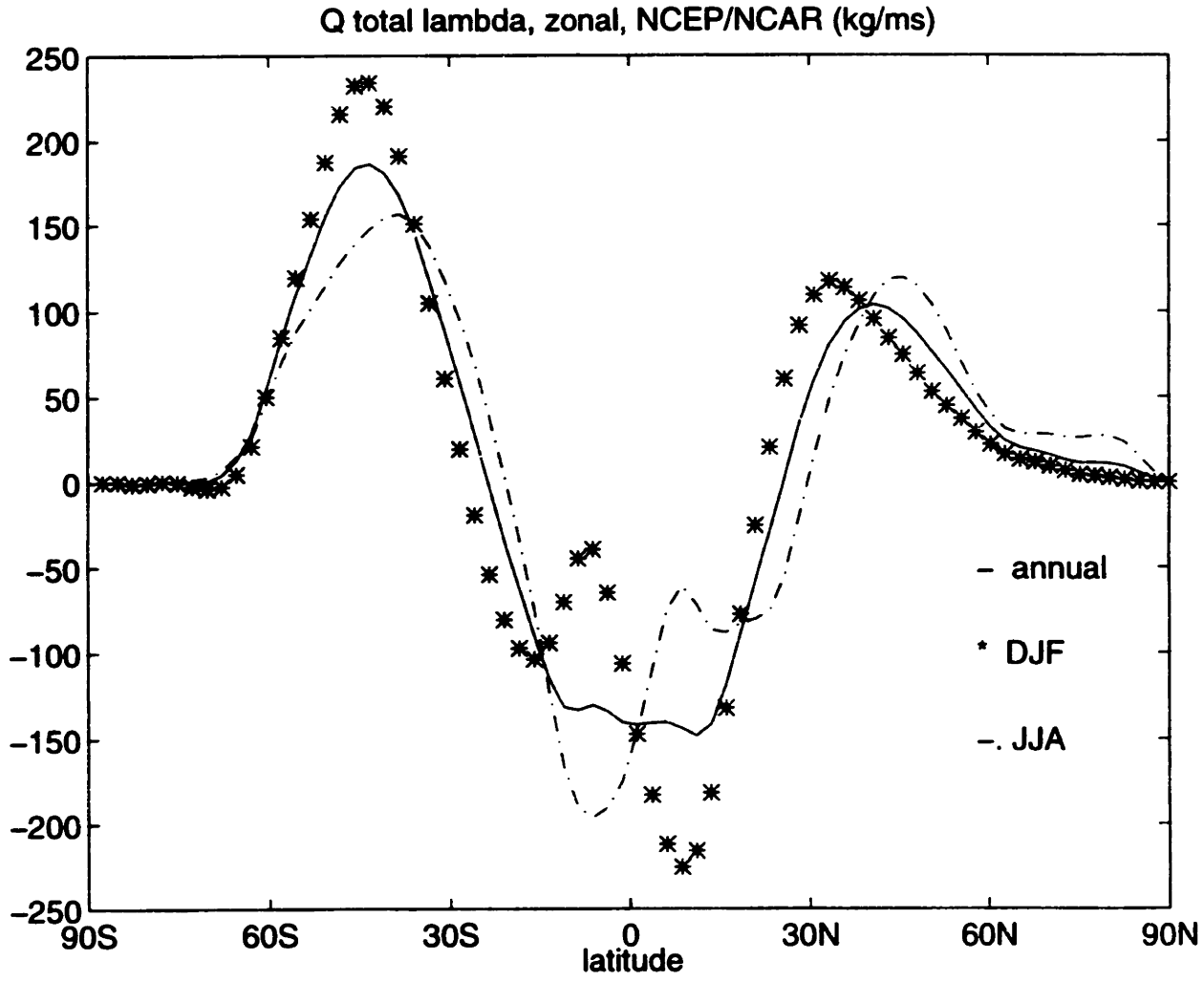

Fig. 19a. The zonally averaged total vapor flux, zonal component. For DJF, JJA, and annual averages. NCEP/NCAR data in units of (kg/ms).

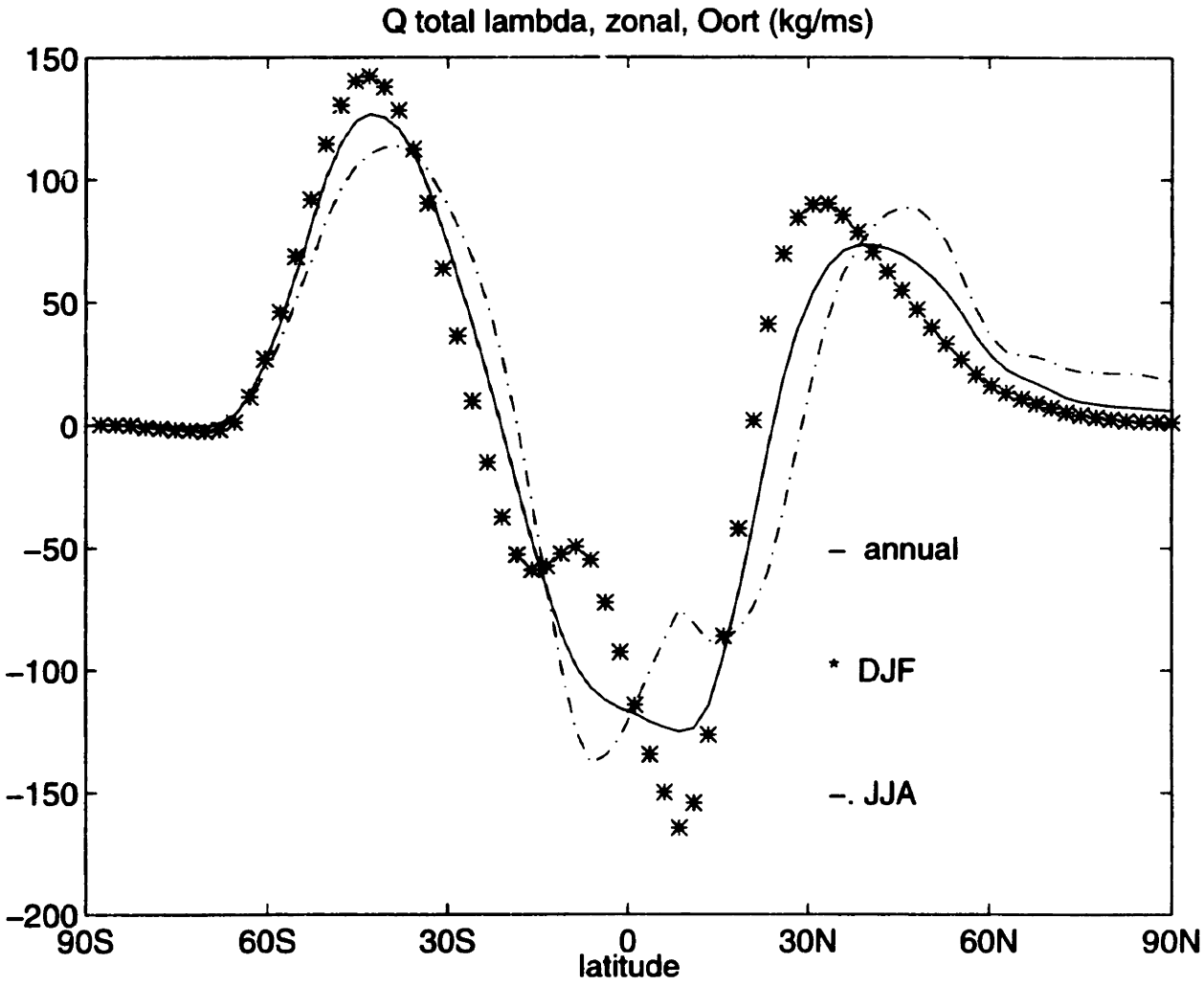

Fig. 19b. The zonally averaged total vapor flux, zonal component. For DJF, JJA, and annual averages. Oort data in units of (kg/ms).

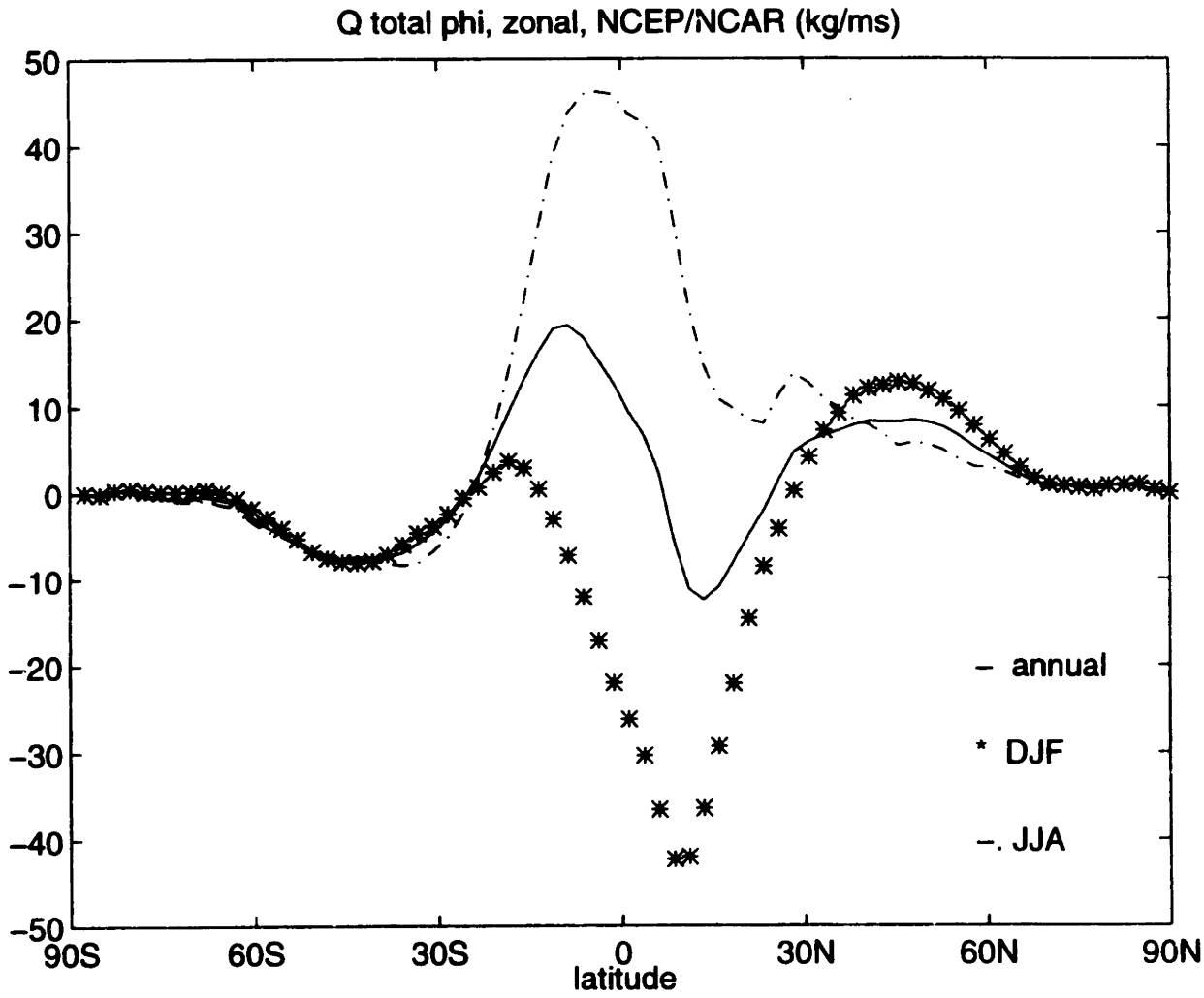

Fig. 20a. The zonally averaged total vapor flux, meridional component. For DJF, JJA, and annual averages. NCEP/NCAR data in units of (kg/ms).

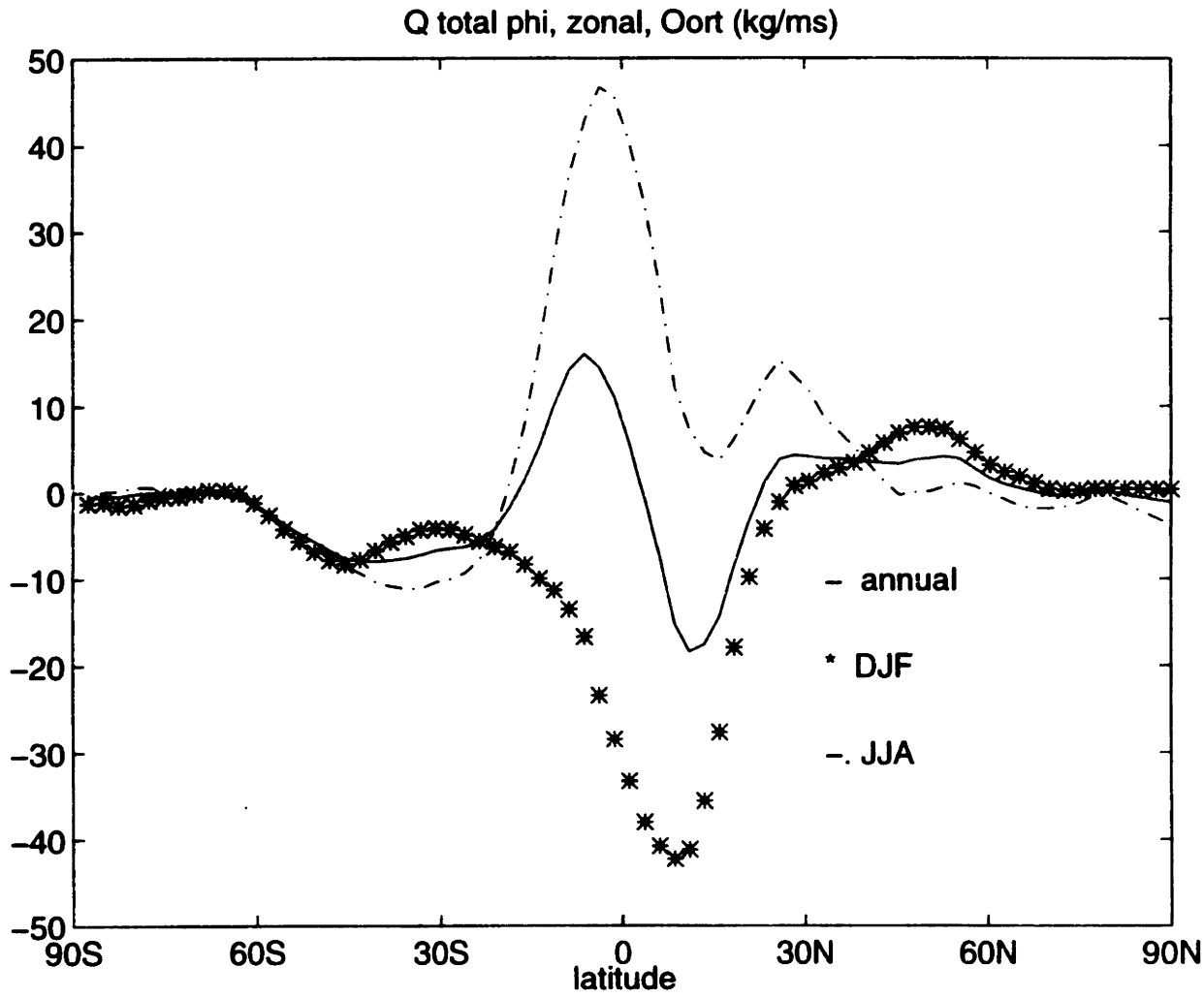

Fig. 20b. The zonally averaged total vapor flux, meridional component. For DJF, JJA, and annual averages. Oort data in units of (kg/ms).

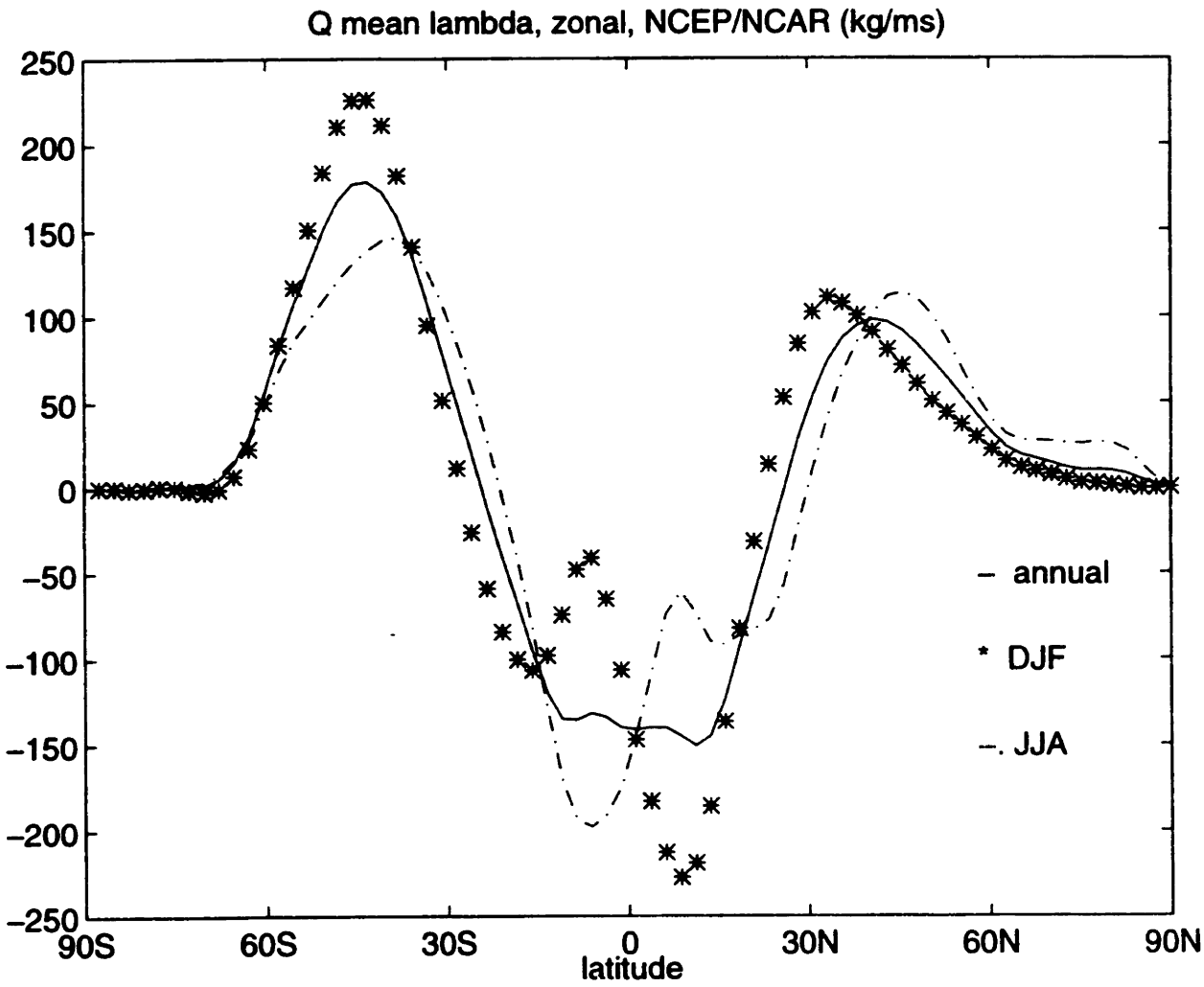

Fig. 21a. The zonally averaged mean vapor flux, zonal component. For DJF, JJA, and annual averages. NCEP/NCAR data in units of (kg/ms).

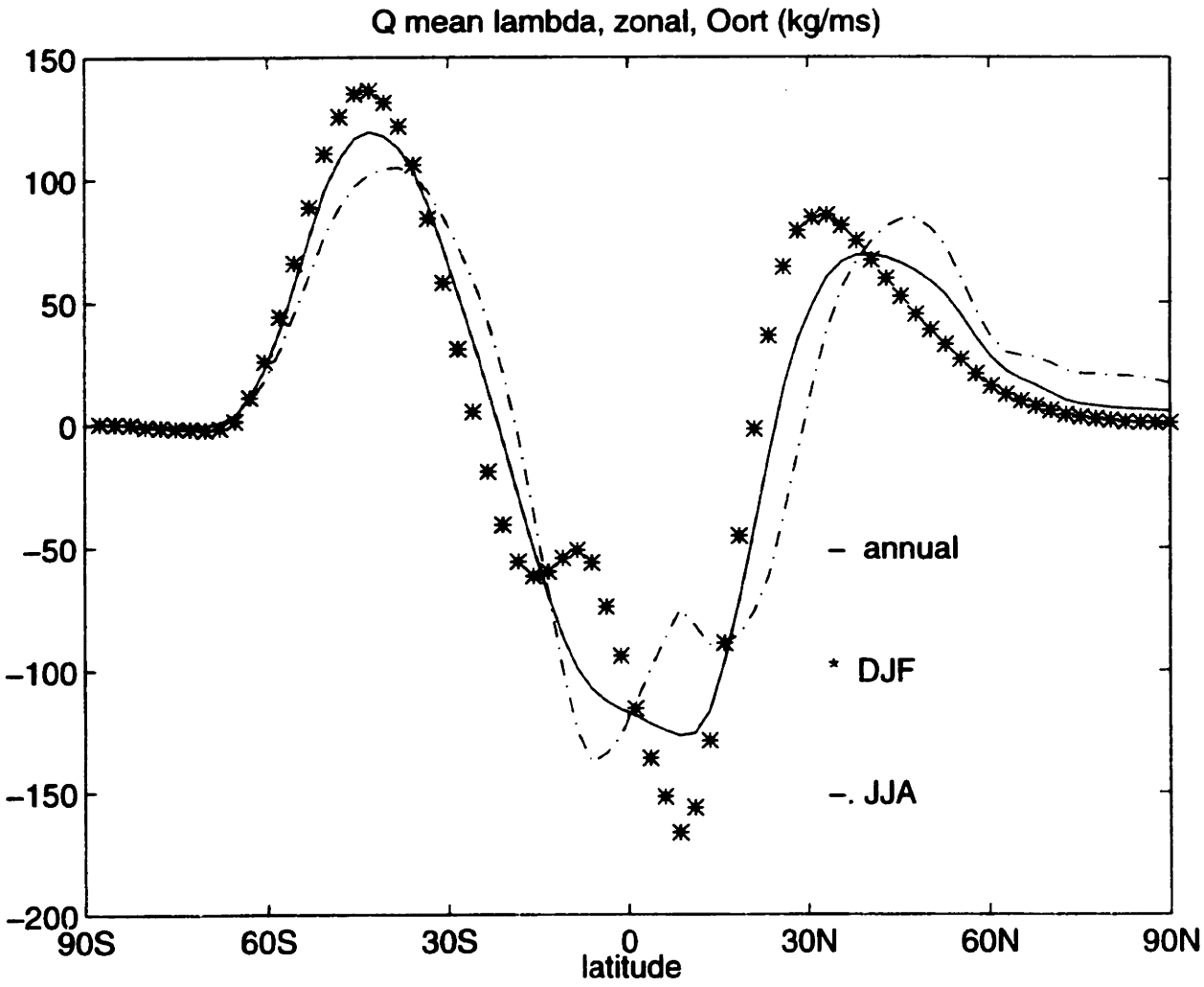

Fig. 21b. The zonally averaged mean vapor flux, zonal component. For DJF, JJA, and annual averages. Oort data in units of (kg/ms).

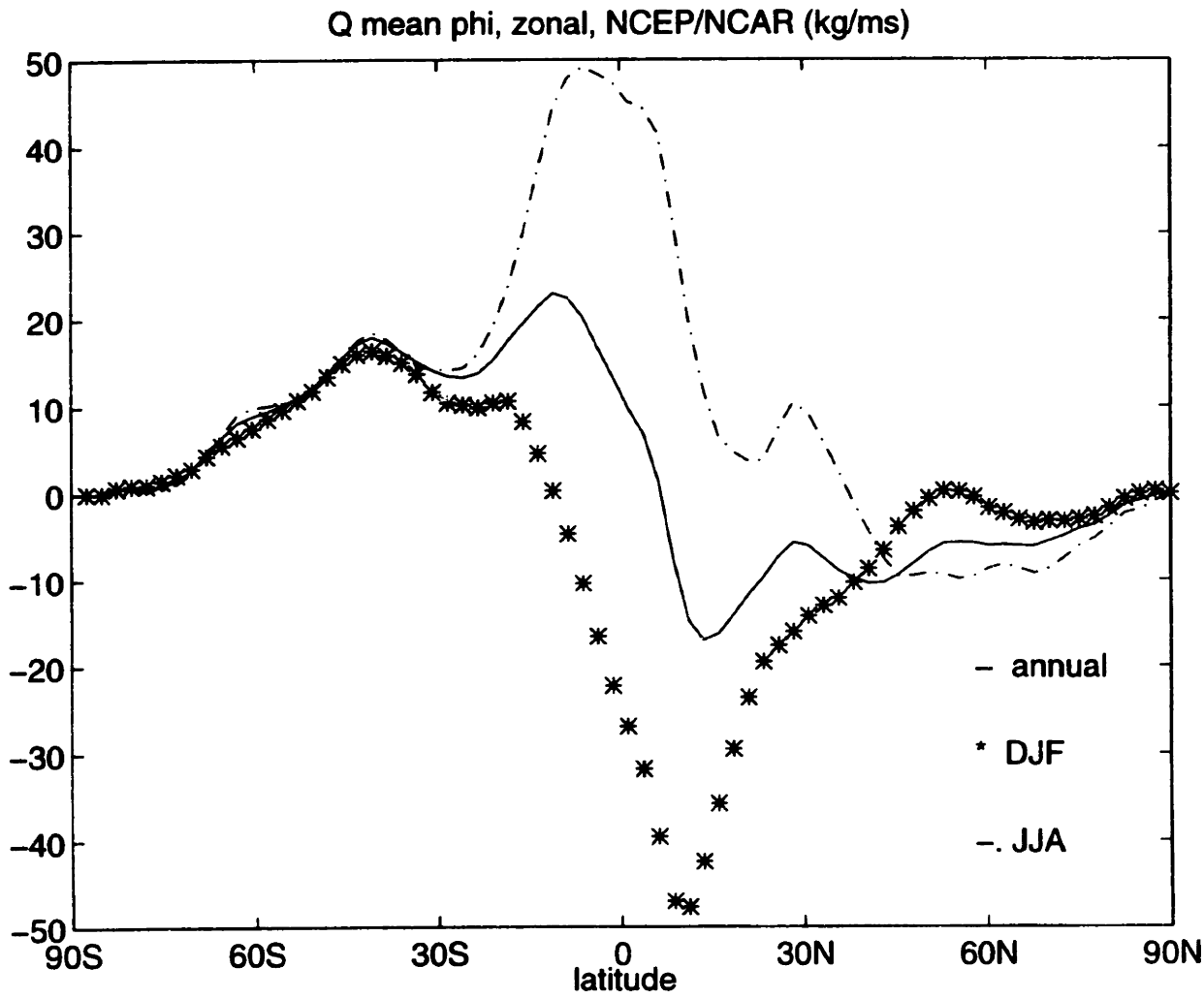

Fig. 22a. The zonally averaged mean vapor flux, meridional component. For DJF, JJA, and annual averages. NCEP/NCAR data in units of (kg/ms).

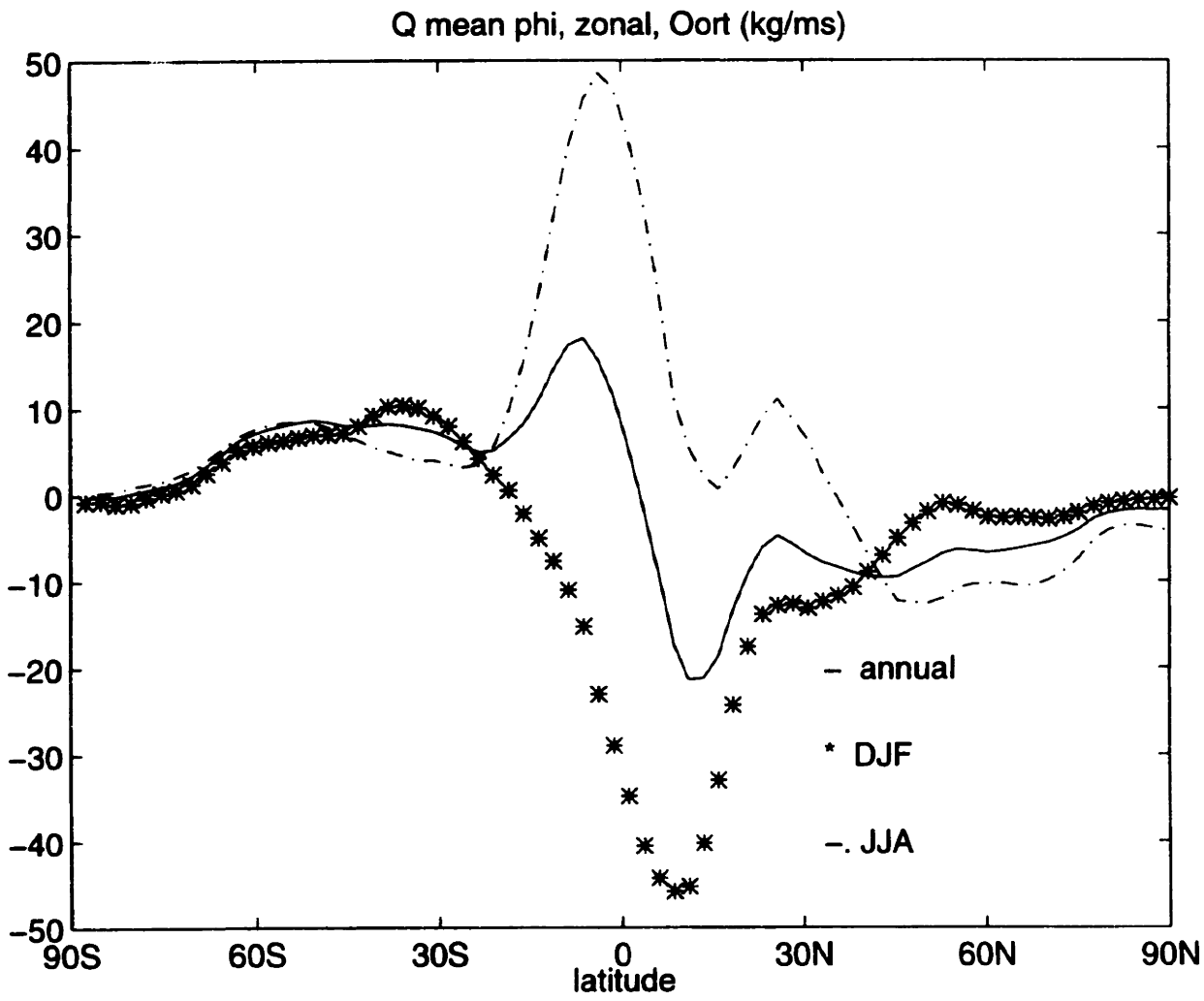

Fig. 22b. The zonally averaged mean vapor flux, meridional component. For DJF, JJA, and annual averages. Oort data in units of (kg/ms).

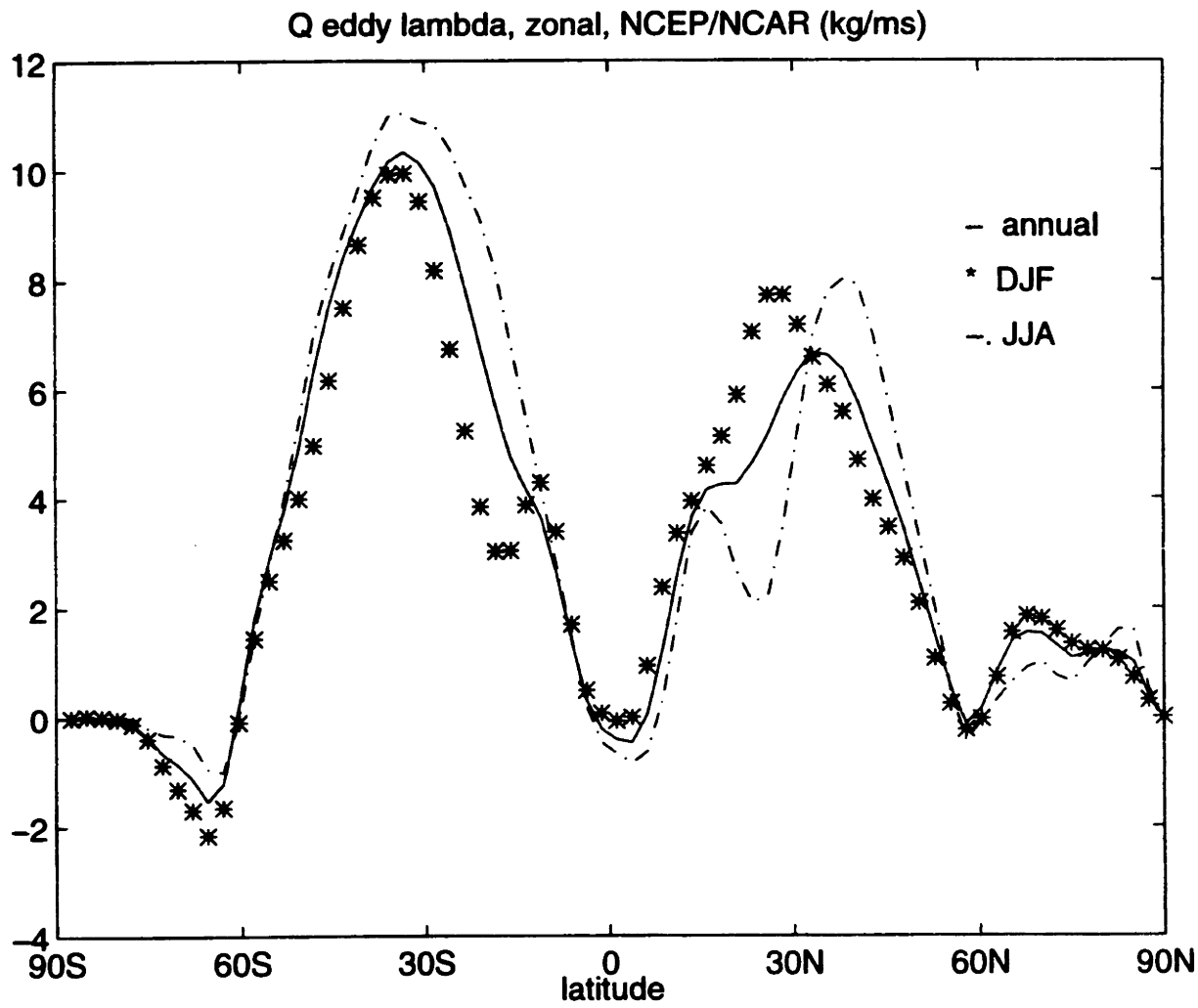

Fig. 23a. The zonally averaged eddy vapor flux, zonal component. For DJF, JJA, and annual averages. NCEP/NCAR data in units of (kg/ms).

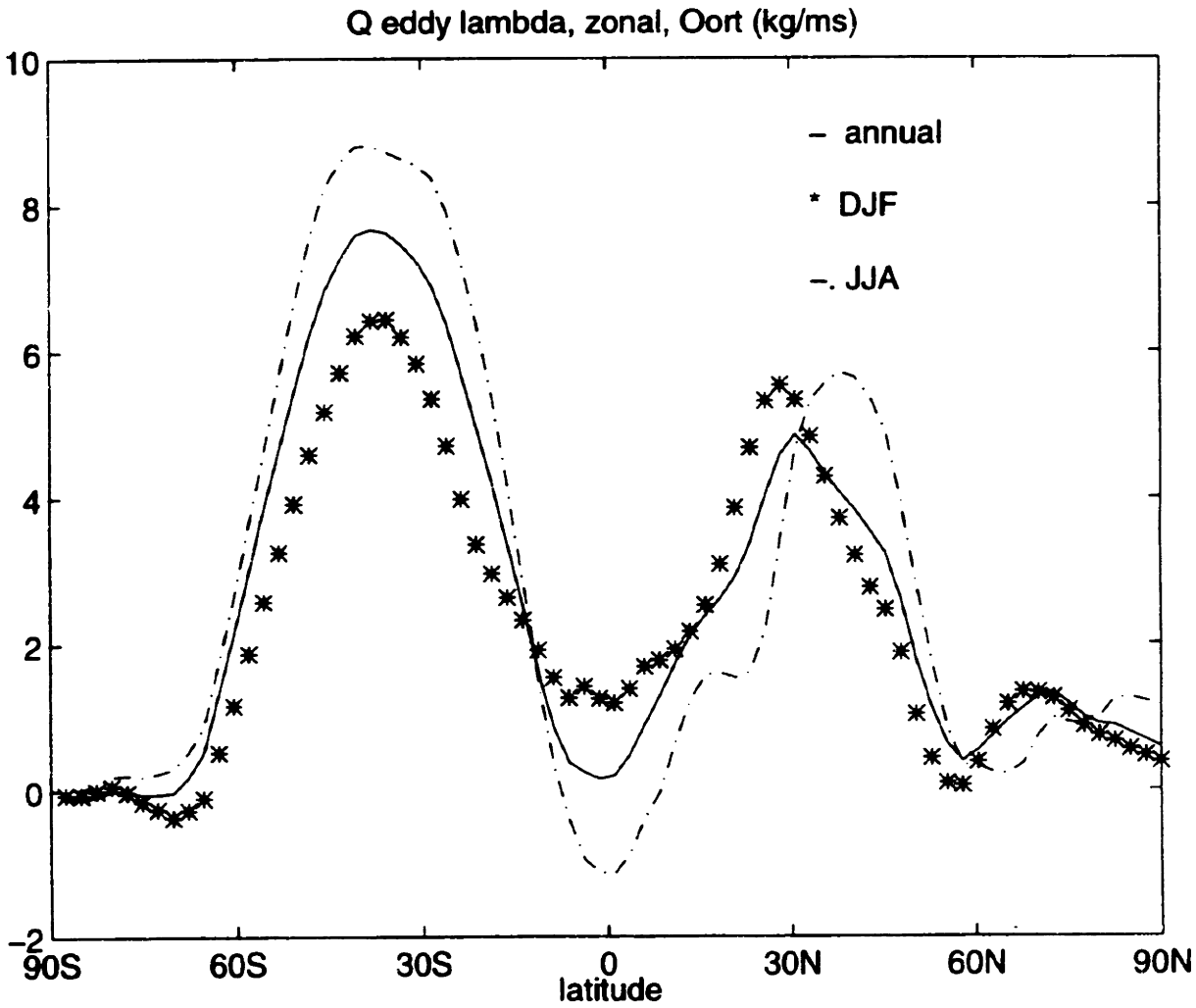

Fig. 23b. The zonally averaged eddy vapor flux, zonal component. For DJF, JJA, and annual averages. Oort data in units of (kg/ms).

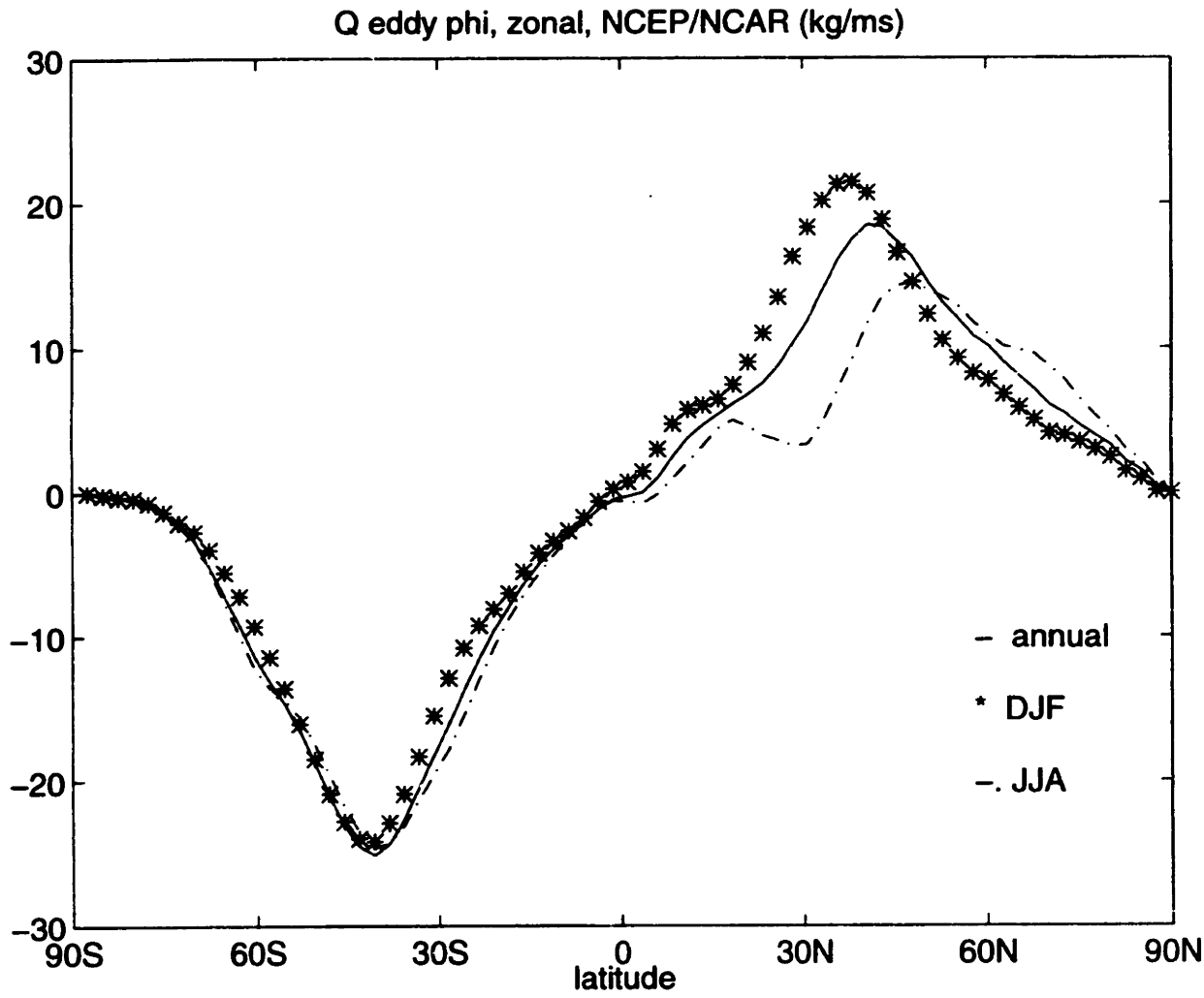

Fig. 24a. The zonally averaged eddy vapor flux, meridional component. For DJF, JJA, and annual averages. NCEP/NCAR data in units of (kg/ms).

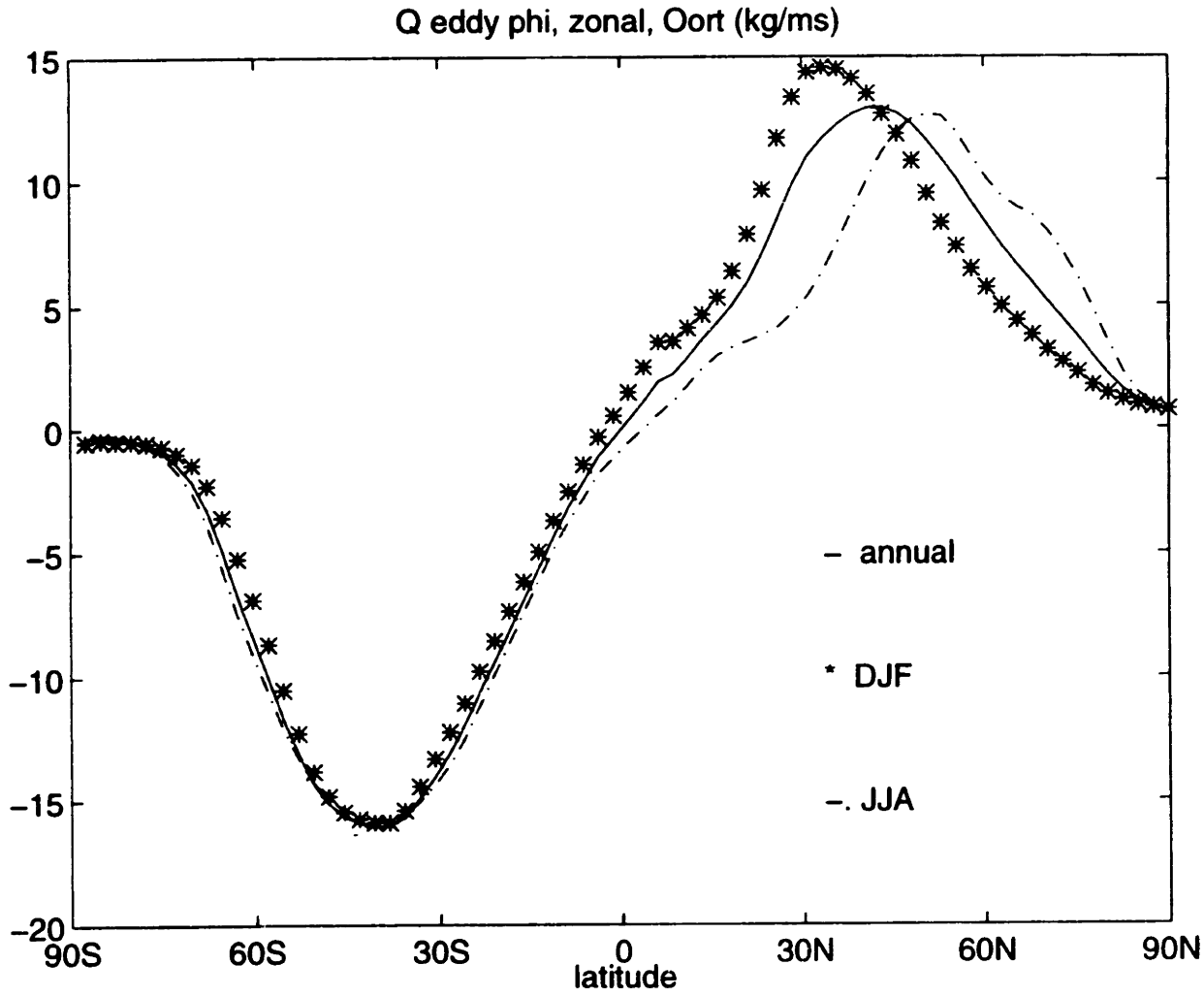

Fig. 24b. The zonally averaged eddy vapor flux, meridional component. For DJF, JJA, and annual averages. Oort data in units of (kg/ms).

3.3 Global Divergence

The divergence for the global fields of integrated water vapor flux is performed and presented in Figures 25 through 30 for both data sets. Areas of positive E-P, where convergence exists, are shaded.

Figures 25 and 26 display the divergence of total water vapor flux for NCEP/NCAR and Oort data, respectively. The most noticeable difference between the two data sets is the lack of results in the Oort set over the oceans compared to the NCEP/NCAR data. This may be due to poor data collection in these hard to reach regions for the Oort data set. The reanalysis uses model estimates of winds and humidity to resolve motions that lead to vapor divergence. But overall, they both show areas of convergence over the equatorial and mid- to high-latitude zones as expected (Pexioto and Oort, 1992 and Dodd and James, 1996). Also observed in both sets of data are regions of divergence over eastern edges of major ocean basins. These were also detected by Dodd and James (1996).

Central America, northern South America, the Thailand peninsula, and regions in the South Pacific and Indian Ocean have some of the largest values of (negative) divergence in both data sets. They also both identify an area of convergence over the Mississippi basin in the central United States, as expected over large drainage basins (Star and Pexioto, 1958). The NCEP/NCAR data shows a localized area of convergence over Brazil, possibly associated with the drainage basin of the Amazon (Star and Pexioto, 1958). The Oort data does not pick up this last zone of convergence, possibly due to poor sampling.

Figures 27 and 28 for the mean flux divergence are essentially the same as the total. But the eddy flux in Figures 29 and 30 are worth noting. The NCEP/NCAR data has higher values of eddy divergence than the Oort data. They both display couplets of convergence and divergence in the winter hemisphere storm track detected by Dodd and James (1996). Also observed by Dodd and James (1996), are the areas of divergence over South America in the region of the South American Convergence Zone (SACZ). Over the central United States, a region of eddy convergence is identified in both data sets.

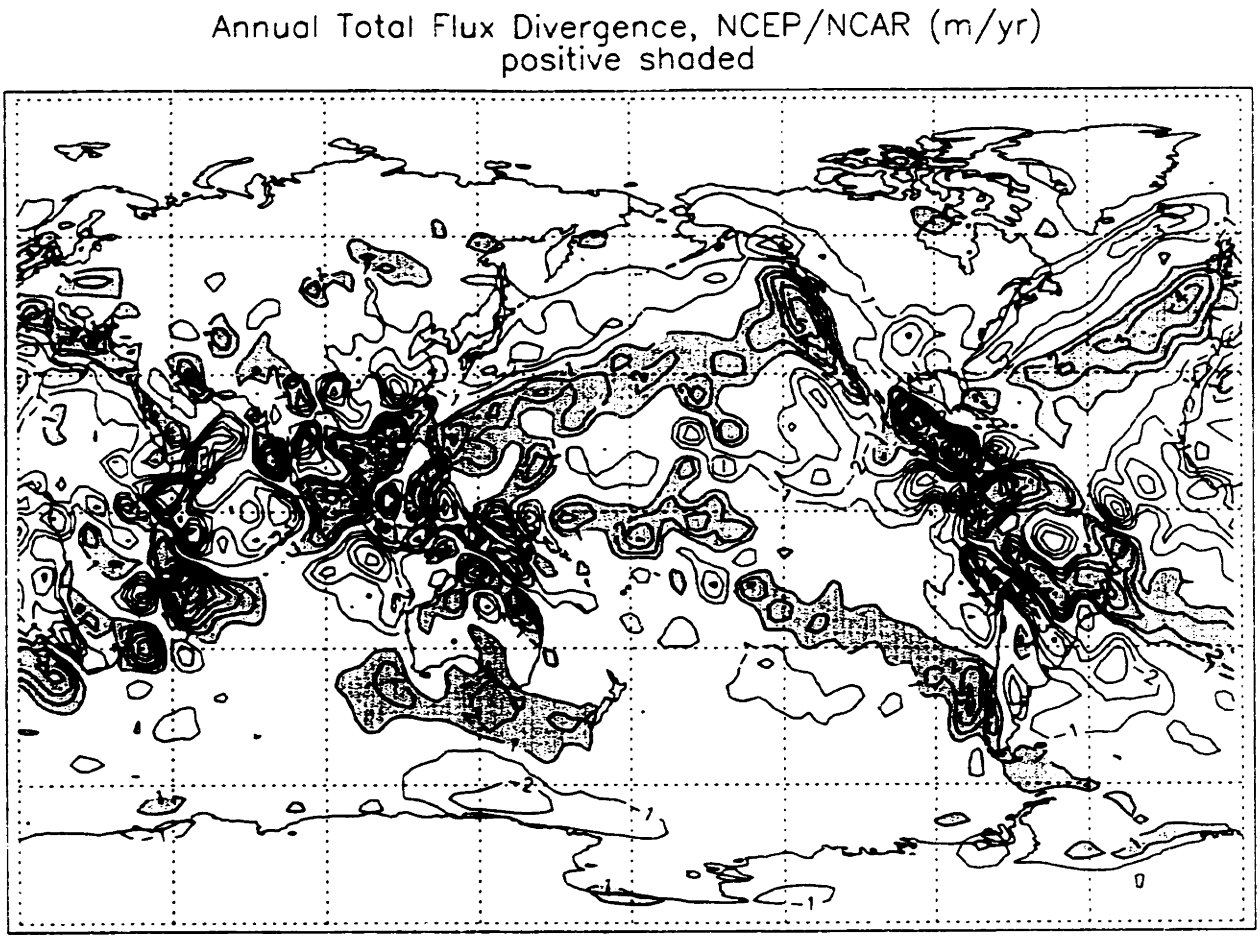

Fig. 25. The divergence of the total vapor flux. NCEP/NCAR data averaged annually. Contoured on intervals of 1 meter/year. Positive values shaded.

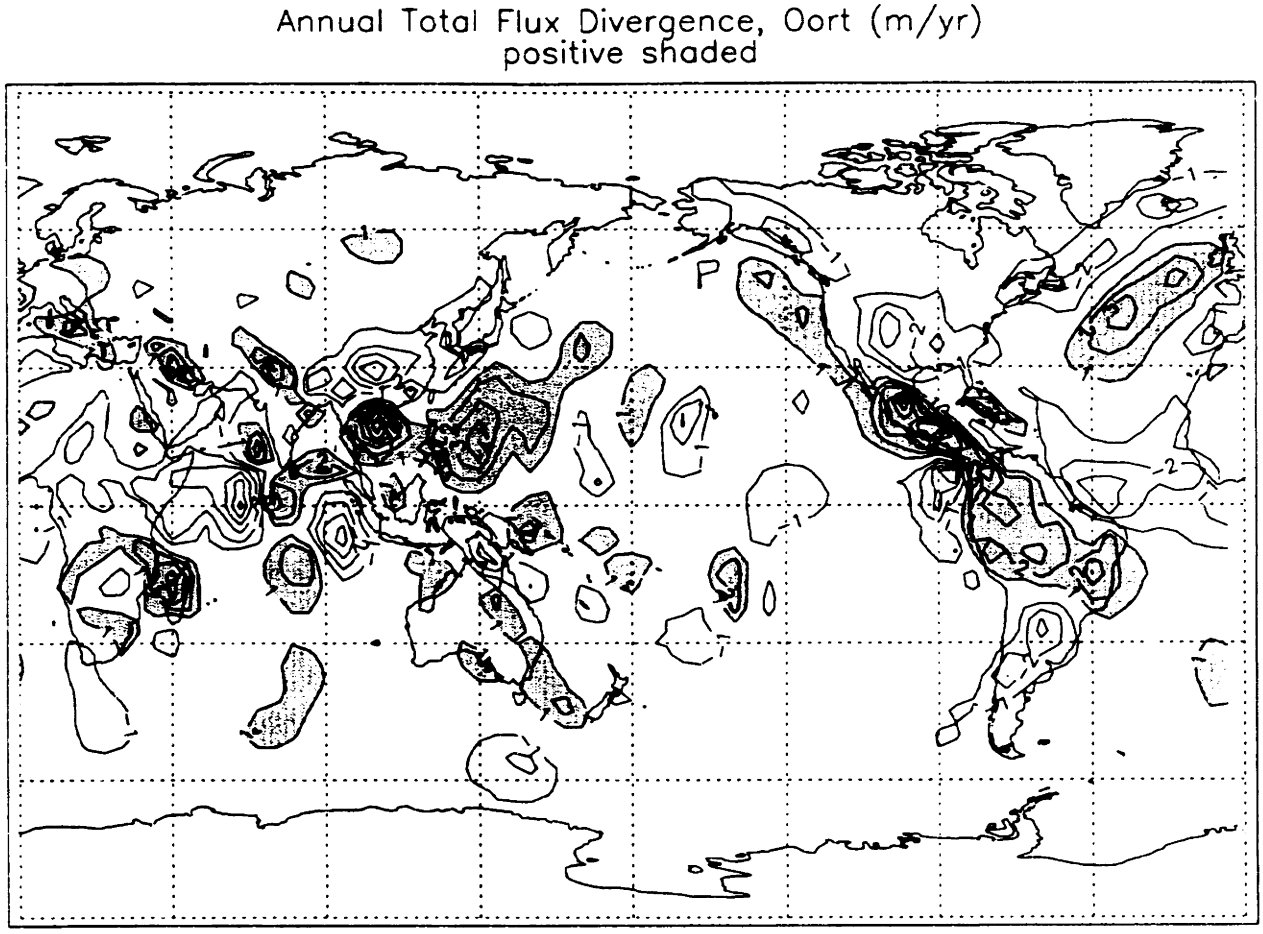

Fig. 26. The divergence of the total vapor flux. Oort data averaged annually. Contoured on intervals of 1 meter/year. Positive values shaded.

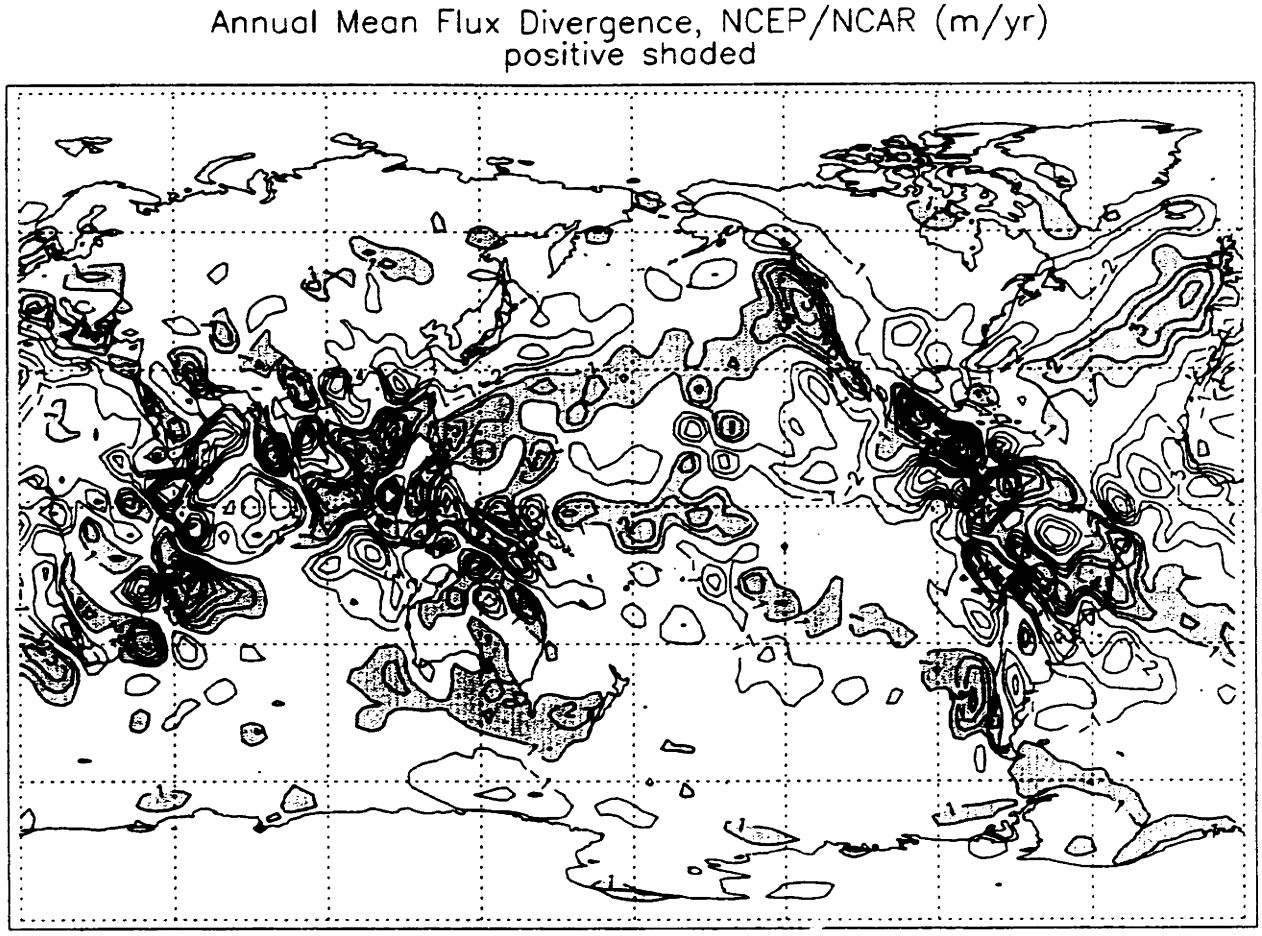

Fig. 27. The divergence of the mean vapor flux. NCEP/NCAR data averaged annually. Contoured on intervals 1 meter/year. Positive values shaded.

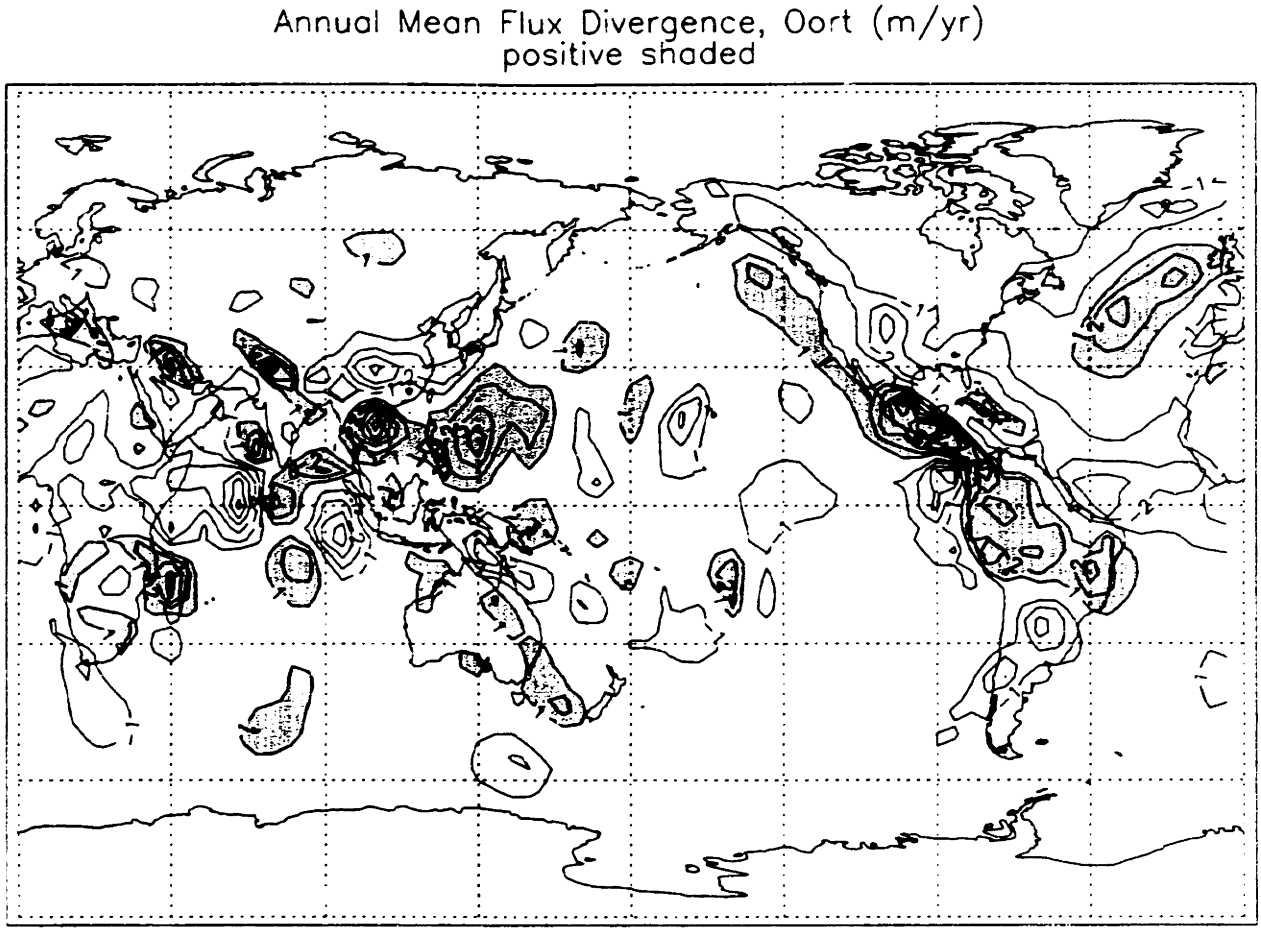

Fig. 28. The divergence of the mean vapor flux. Oort data averaged annually. Contoured on intervals of 1 meter/year. Positive values shaded.

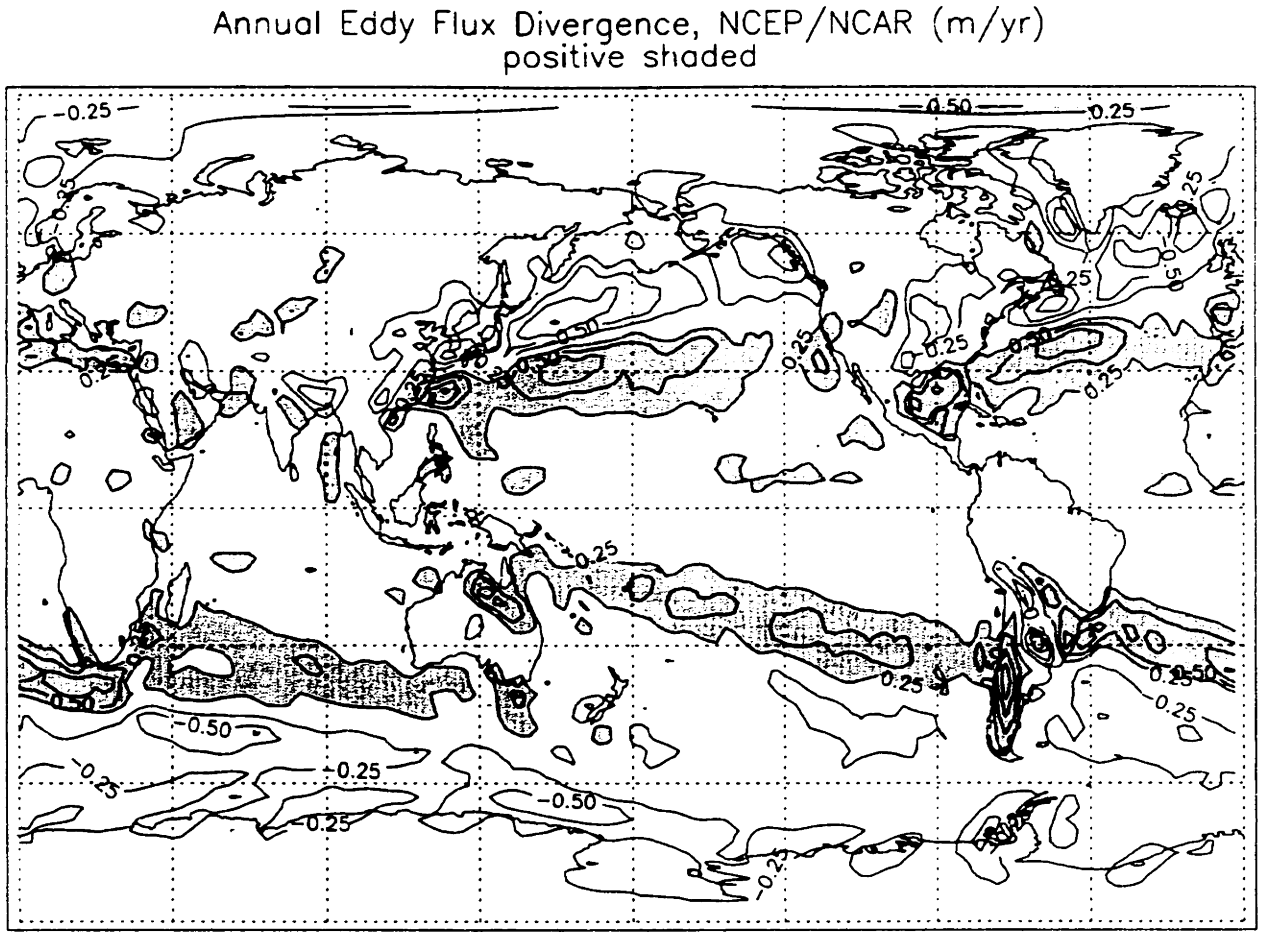

Fig. 29. The divergence of the eddy vapor flux. NCEP/NCAR data averaged annually. Contour intervals of [-1, -.75, -.5, -.25, .25, .5, .75, 1] meters/year. Positive values shaded.

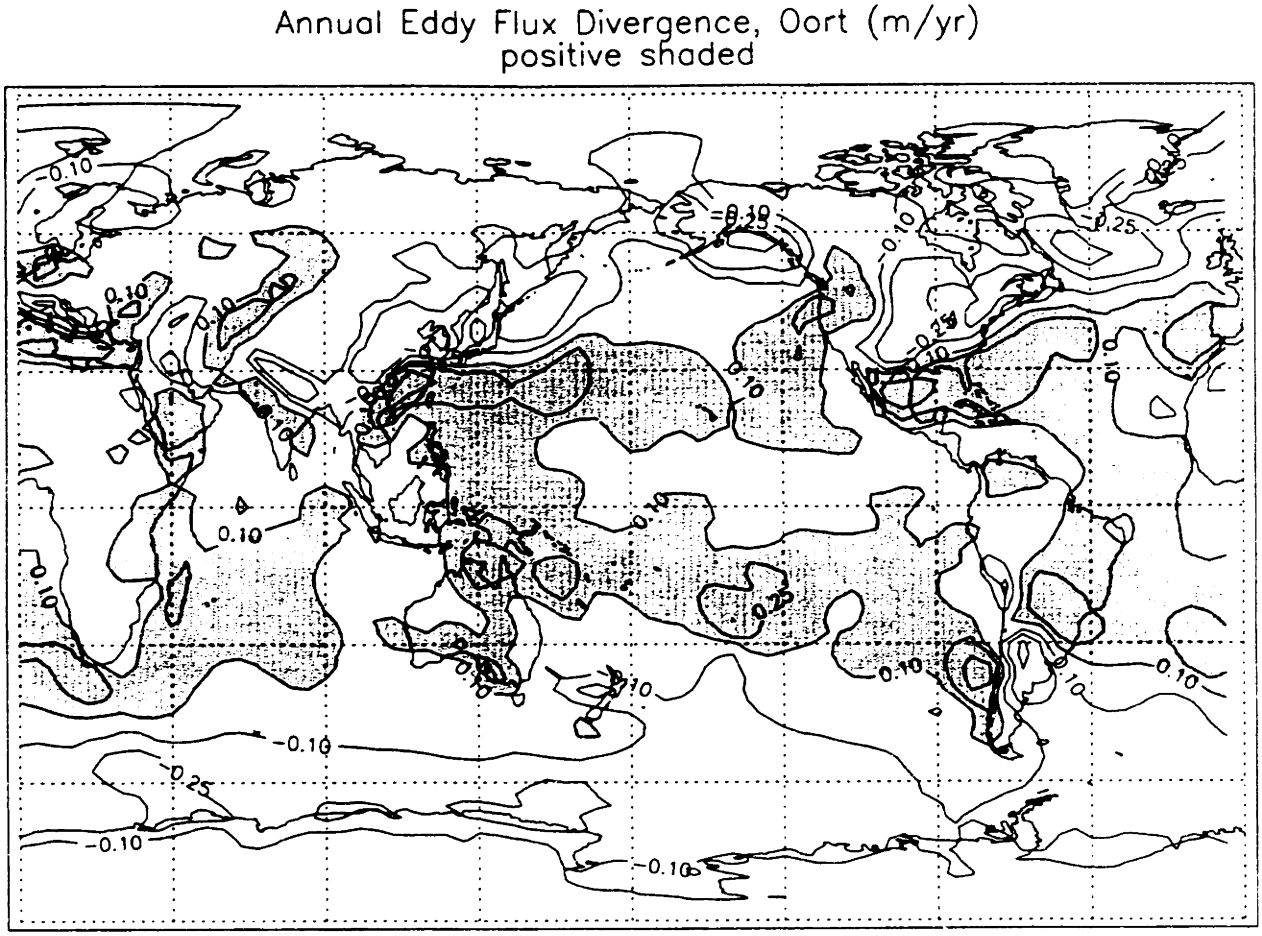

Fig. 30. The divergence of the eddy vapor flux. Oort data averaged annually. Contour intervals of [-.75, -.5, -.25, -.1, .1, .25, .5, .75] meters/year. Positive values shaded.

IV. Observations of El Nino Influence

4.1 El Nino Periods

Defining the exact life cycle of an El Nino event is difficult. Even more difficult is trying to make all El Nino's conform to one set of requirements. For this reason, it is hard to define the exact life cycle of all El Nino's during this study period. Table 1 lists the approximate starting and ending dates of the El Nino events that take place from 1964 to 1995. Also defined are the one-year blocks of data that are used for all analysis that call for "El Nino years", and the data set(s) that cover each event.

Table 1

START TIME	END TIME	1 YEAR PERIOD	DATA SET
Dec 1964	May 1966	Jan 1965-Dec 1965	Oort
Dec 1971	May 1973	Jan 1972-Dec 1972	Oort
Dec 1981	May 1983	Jan 1982-Dec 1982	Oort, NCEP/NCAR
May 1986	Dec 1987	Jan 1987-Dec 1987	Oort, NCEP/NCAR
Dec 1990	May 1992	Jan 1991-Dec 1991	NCEP/NCAR

4.2 Differences Between El Nino and Non-El Nino Periods

Taking the previously defined El Nino periods included in each data set, an average for Q_λ and Q_ϕ is made of the El Nino years and another of the non-El Nino years. These two groups of data is then differenced, and in places where the El Nino data does not fall within the 95% confidence interval of the total data mean statistic (as calculated by equation 5), the value is plotted.

$$\bar{x} - 1.96\frac{\sigma}{\sqrt{n}} < \mu < \bar{x} + 1.96\frac{\sigma}{\sqrt{n}} \qquad (5)$$

In equation 5, σ is the standard deviation of interannual variability, n is the number of points in the time series, and $\bar{x}$ is the mean of the total data. Equation (5) represents the 95% confidence interval on the estimate of the mean. The results are displayed in Figures 31 through 36 for the total, mean and eddy flux of the NCEP/NCAR and Oort data sets.

In Figures 31a and 32a, a large area of value for El Nino minus non-El Nino is seen in the western equatorial Pacific for the NCEP/NCAR and Oort data, respectively. The NCEP/NCAR data has a much larger difference than the Oort (a peak of 120 versus 80 kg/ms). This may be because each data set contains different El Nino events of varying strengths. It may therefore be best not to make comparisons of the magnitudes between the data sets. Both of these areas in the western Pacific spread east across the equator and move slightly south. Instead of slowly dropping off in magnitude to the south, the Oort data seems to drop and then rise again to form a second maxima of 30 kg/ms (along the SPCZ) that is still related to the larger maxima of 80.

Another region of large value in the NCEP/NCAR data is located off the coast of South America near Ecuador. This is the exact area where anomalously warm waters are known to form in El Nino episodes. Surprisingly, the Oort data does not show any noticeable difference here. Again, the Oort data set uses interpolation of sparse observations while reanalysis is using model estimates in addition to observations. Features in data sparse regions may not be resolved in the Oort data.

The flux vectors are displayed in Figures 31b and 32b. In both data sets it is observed that in El Nino years, water vapor diverges from the area near Indonesia east towards the Pacific, and to a lesser degree west into the Indian Ocean. During ENSO years, a weakening of the zonal and tropical Walker Circulation occurs. This results from the breakdown of the zonal sea-surface temperature difference in the equatorial Pacific Ocean. The rising branch of the Walker cell is located in the eastern equatorial Pacific, and when weakened, a reduction in precipitation and anomalous vapor divergence is evident. Eastward-moving wind anomalies have previously been observed in the western Pacific during ENSO (Barnett, 1994).

Figures 33 and 34 for the mean flux look similar to the total flux. The two data sets are most dissimilar in the eddy flux component, presented in Figures 35 and 36. In certain locations, the NCEP/NCAR data has values twice the value of the Oort data. A couple of regions where both data sets have significant values are to the south of Africa, over Australia, south of Japan, the mid-north Atlantic, and the western Atlantic. By looking at the flux vectors, the differences between the two data sets can best be observed. The Oort data shows a strongly organized divergence

from the mid-Pacific area while the NCEP/NCAR data has many seemingly uncontinuous clusters of divergence/convergence centers spread across the globe, mostly at mid-latitudes. The Oort data also has much movement parallel to latitude circles whereas NCEP/NCAR has more poleward motion.

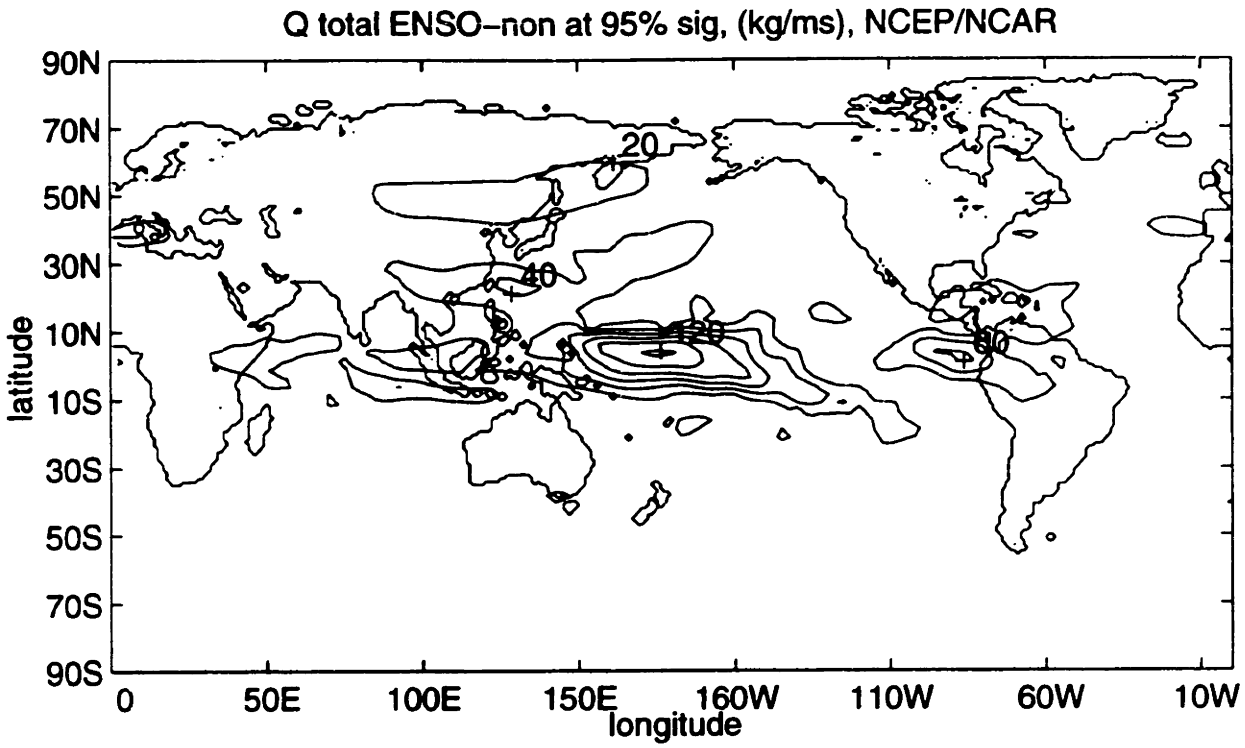

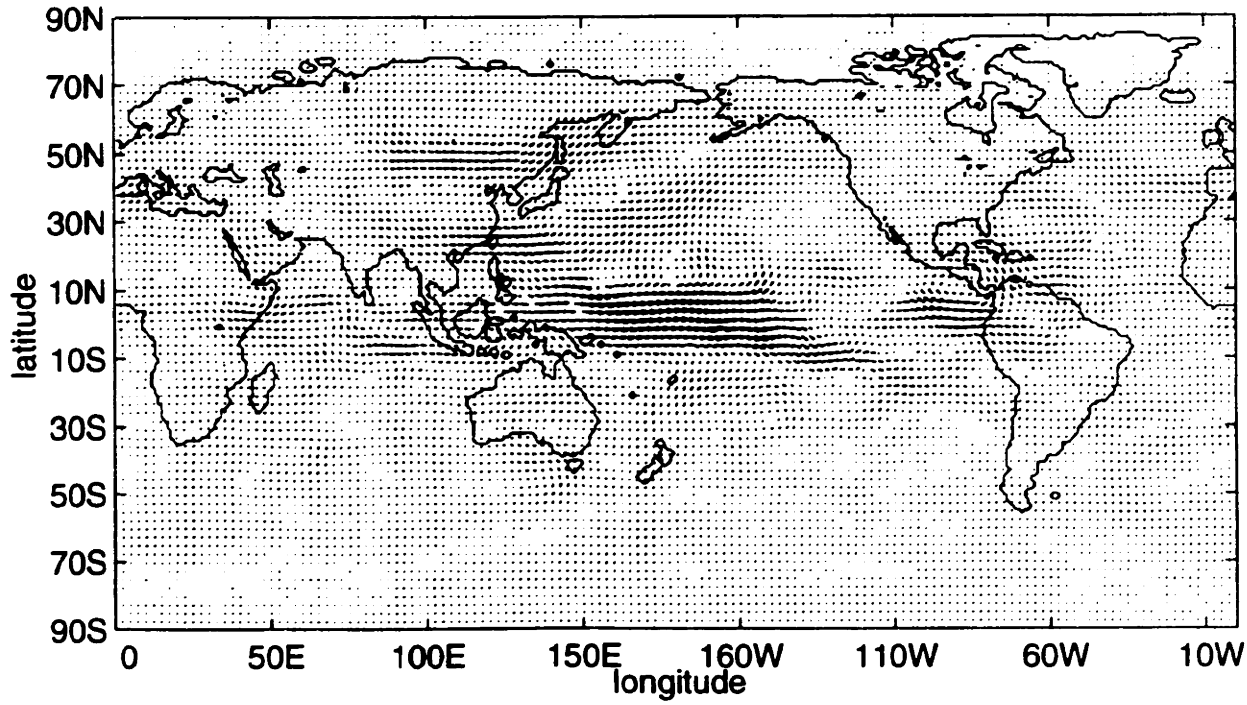

Fig. 31a (upper) Total vapor flux of 'El Nino years - non El Nino years'. Only data at 95% significance plotted. For NCEP/NCAR data, contoured on 20 kg/ms intervals. 31b (lower) Same as above plotted as flux vectors.

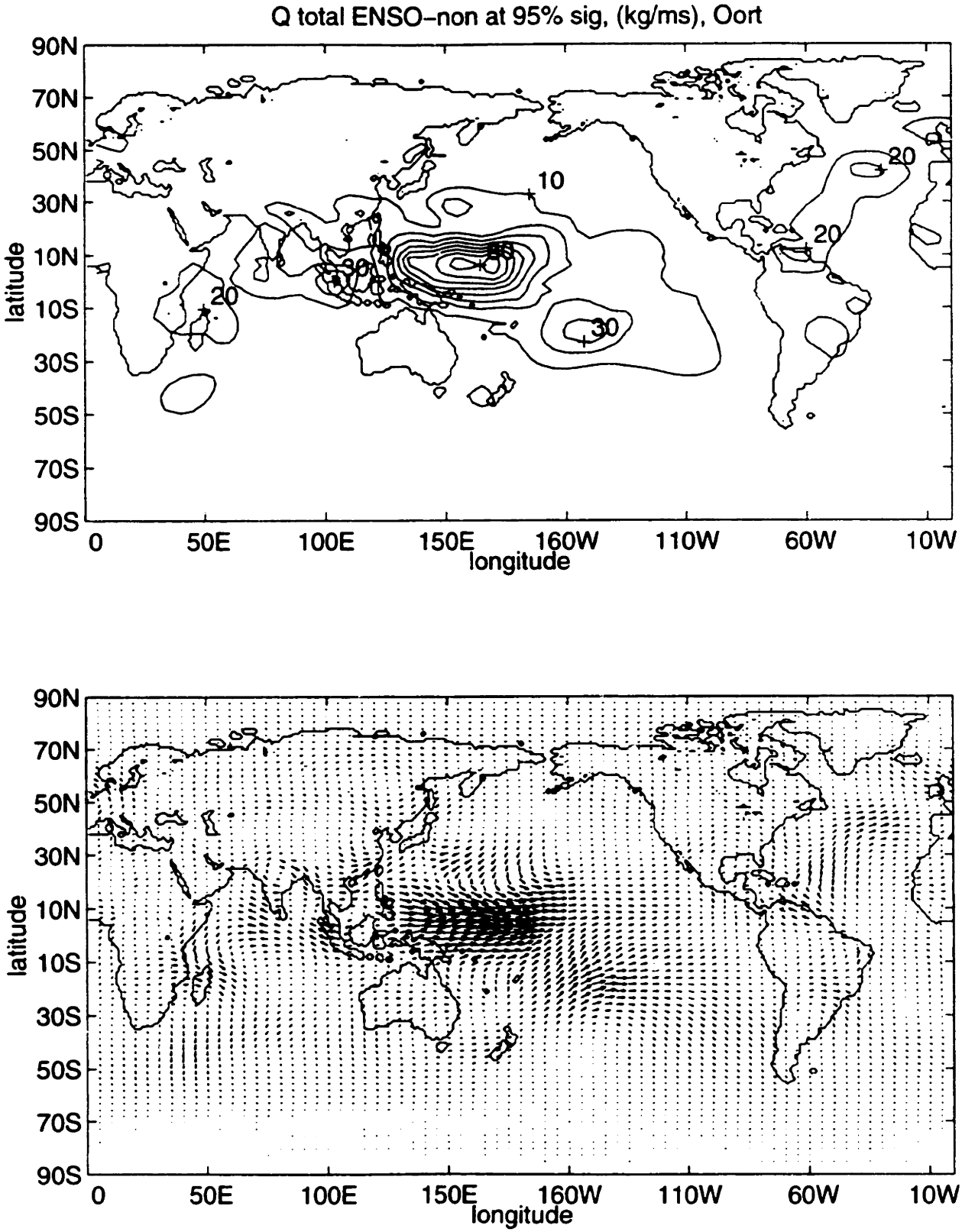

Fig. 32a (upper) Total vapor flux of 'El Nino years - non El Nino years'. Only data at 95% significance plotted. For Oort data, contoured on 10 kg/ms intervals. 32b (lower) Same as above plotted as flux vectors.

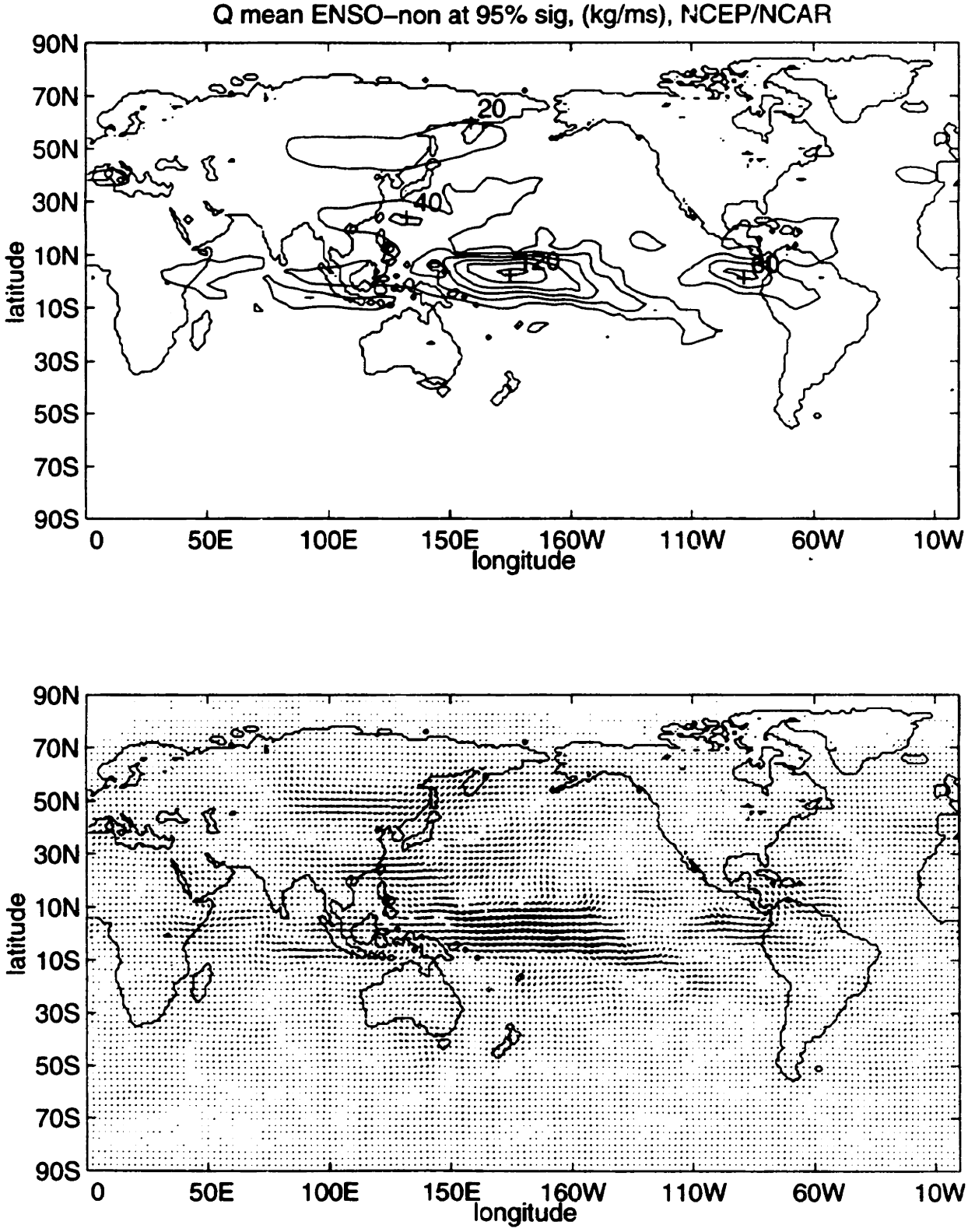

Fig. 33a (upper) Mean vapor flux of 'El Nino years - non El Nino years'. Only data at 95% significance plotted. For NCEP/NCAR data, contoured on 20 kg/ms intervals. 33b (lower) Same as above plotted as flux vectors.

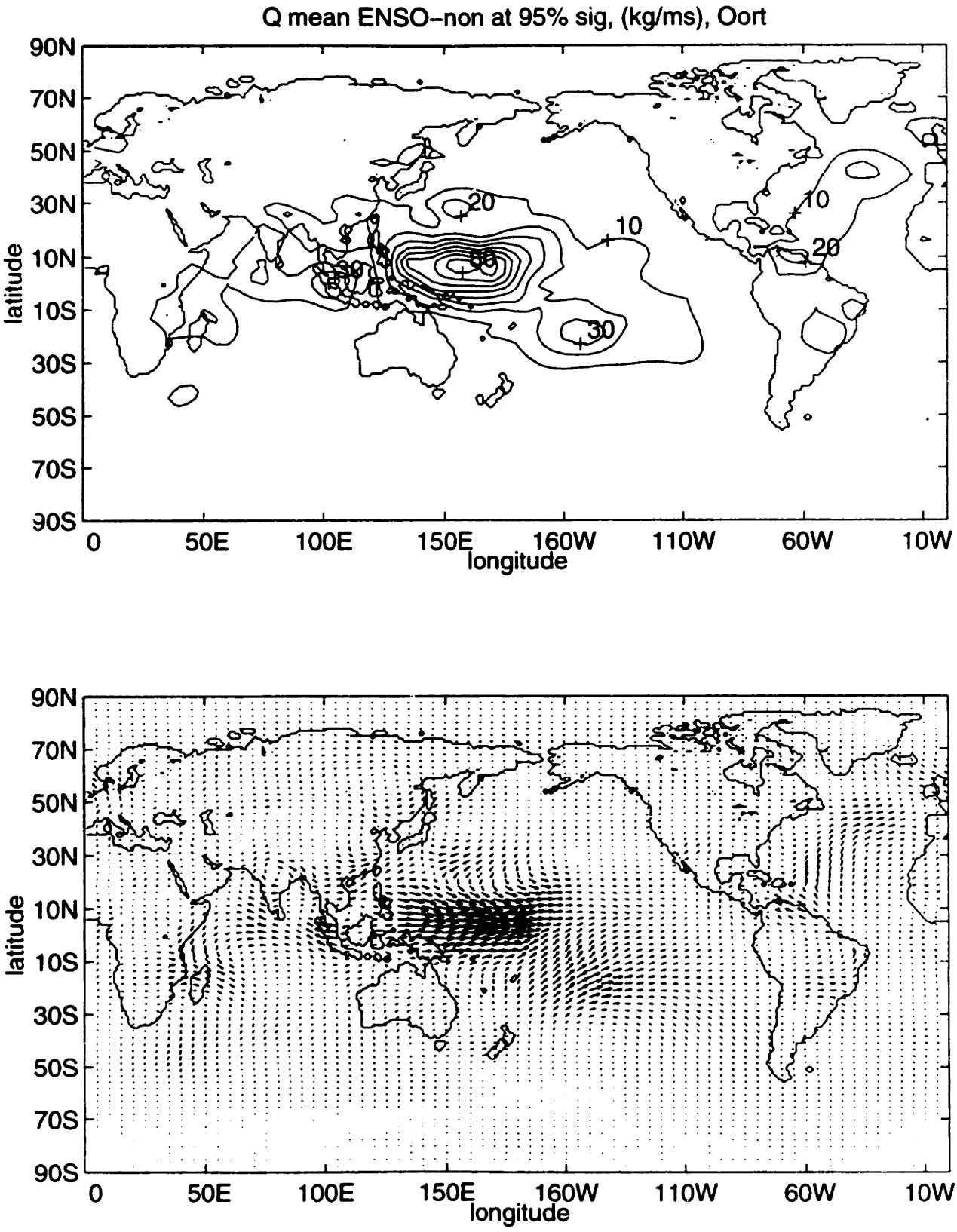

Fig. 34a (upper) Mean vapor flux of 'El Nino years - non El Nino years'. Only data at 95% significance plotted. For Oort data, contoured on 10 kg/ms intervals. 34b (lower) Same as above plotted as flux vectors.

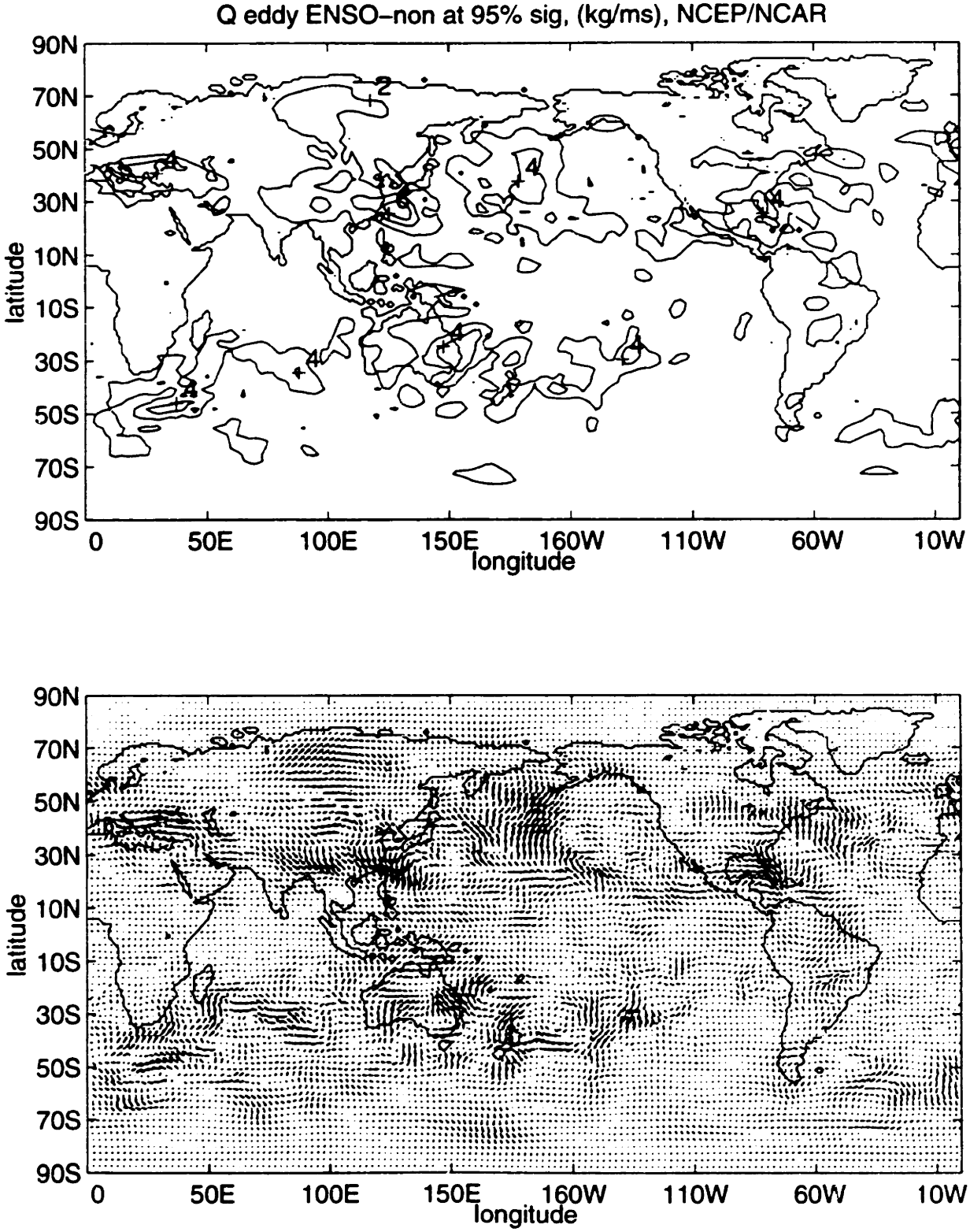

Fig. 35a (upper) Eddy vapor flux of 'El Nino years - non El Nino years'. Only data at 95% significance plotted. For NCEP/NCAR data, contoured on 2 kg/ms intervals. 35b (lower) Same as above plotted as flux vectors.

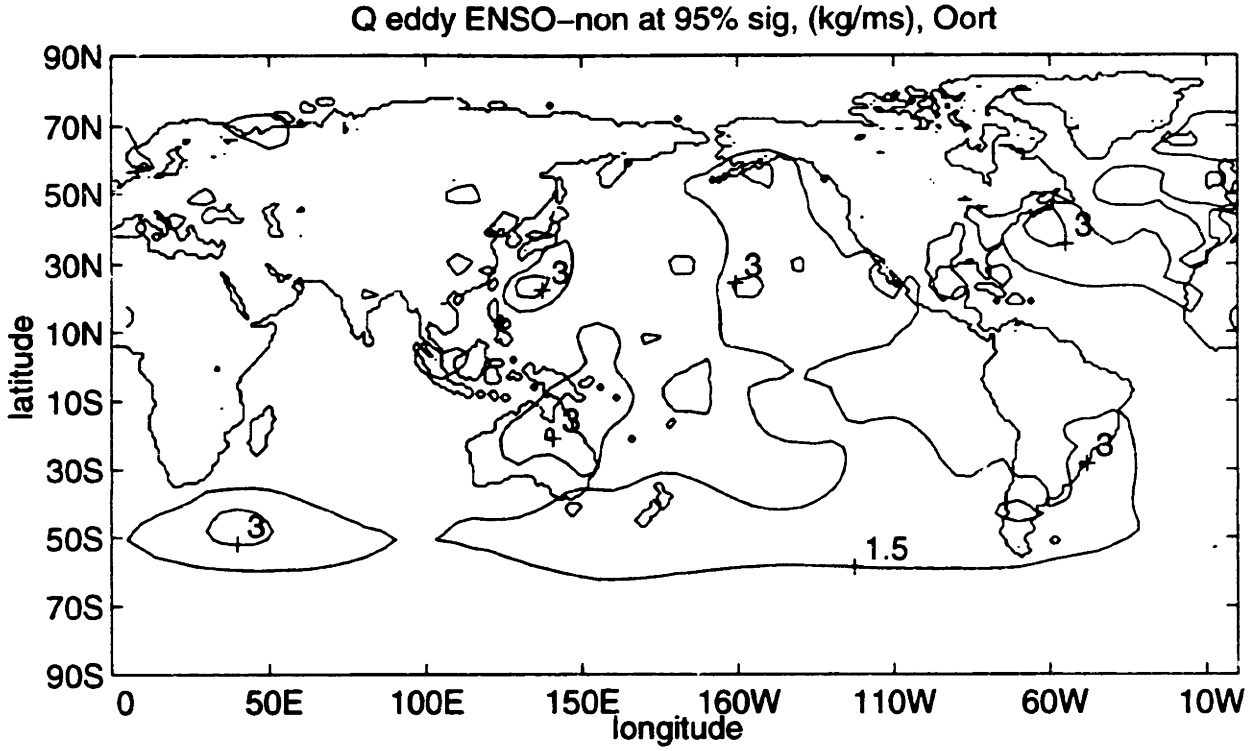

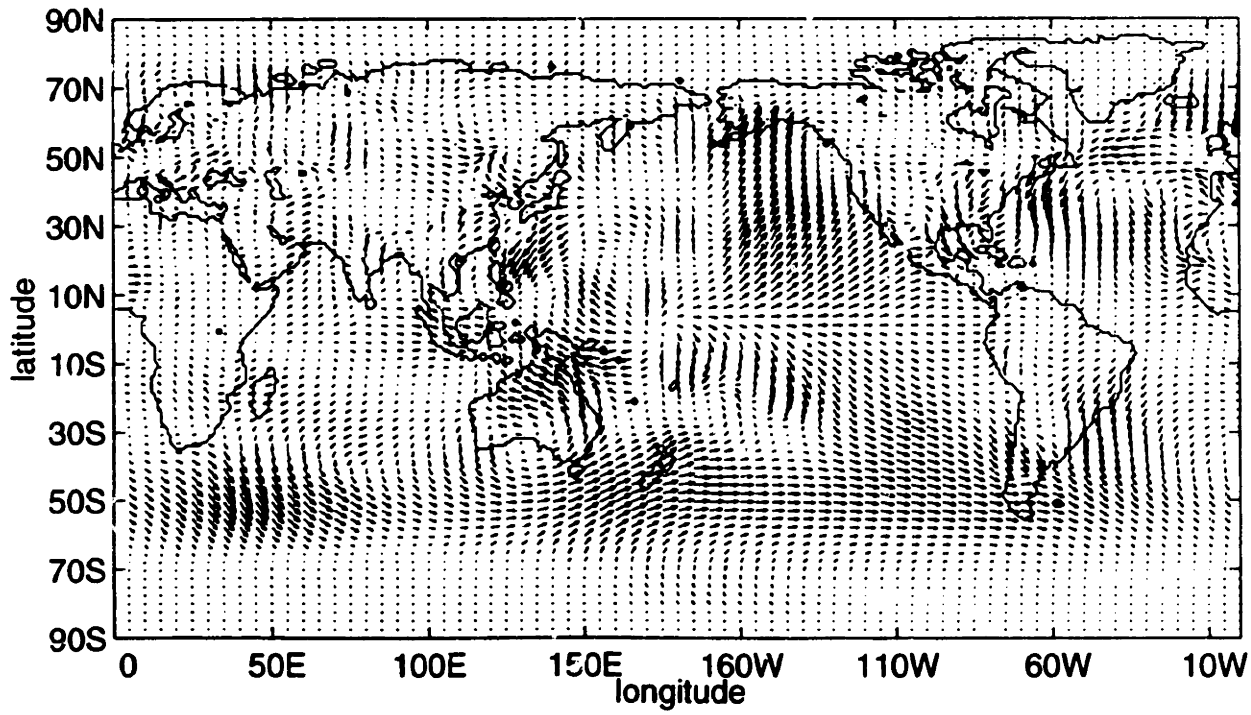

Fig. 36a (upper) Eddy vapor flux of 'El Nino years - non El Nino years'. Only data at 95% significance plotted. For Oort data, contoured on 1.5 kg/ms intervals. 36b (lower) Same as above plotted as flux vectors.

4.3 Zonal Analysis

In Figures 37 through 40, the zonal average of the El Nino years is taken, and from it the zonal average of all years is subtracted. These are then plotted against the annual average and its 95% confidence interval, both with the annual average subtracted. The El Nino years have flux values larger than the annual average from about 50S to the equator in the NCEP/NCAR data zonal component. But these differences are not statistically significant. Only small areas near the equator and 20S fall out of the 95% confidence interval making them significantly different from the rest of the years. On the other hand, the Oort data identifies the El Nino years as above average from 60S to 50N with a large area from 5S to 15N and a small area near 15N that are significant.

The meridional component of flux in Figures 39 and 40 also exhibits many differences between data sets. The NCEP/NCAR data shows slightly more than normal flux near the equator and slightly less than normal flux at 15S and 15N. Neither of these areas fall outside of the confidence interval. The Oort data in Figure 40 has a large region from 30S to the equator where it has larger than normal flux, and another from 60S to 30S where it has less than normal flux. The section from 30S to 50S is significant, some of it by a large margin. But the Oort data in the data-sparse Southern Hemisphere has limited validity.

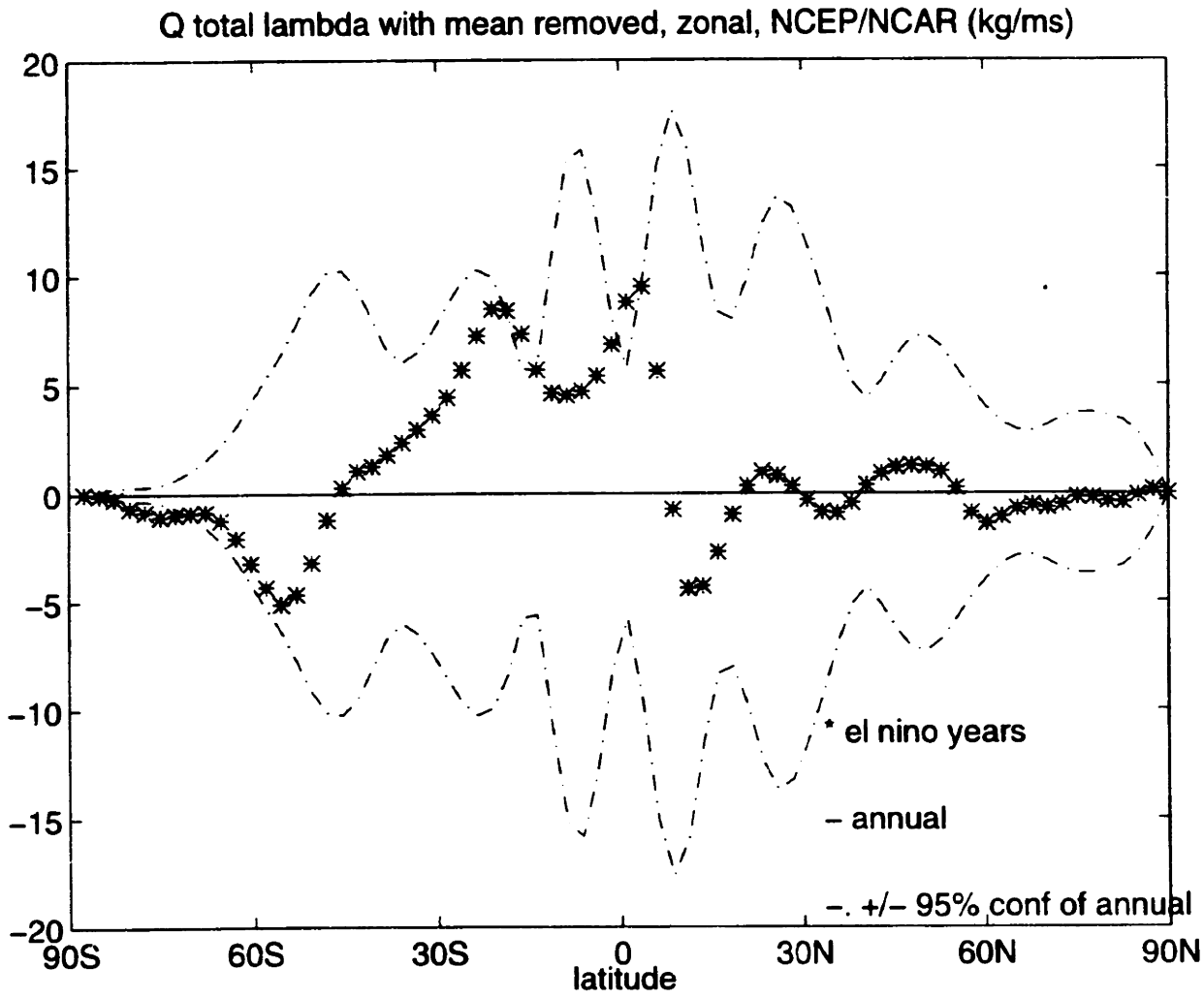

Fig. 37. Total vapor flux of 'El Nino - non El Nino years', zonal component. Zonally averaged with mean removed. For NCEP/NCAR data and plotted with 95% confidence interval of annual average. In units of (kg/ms).

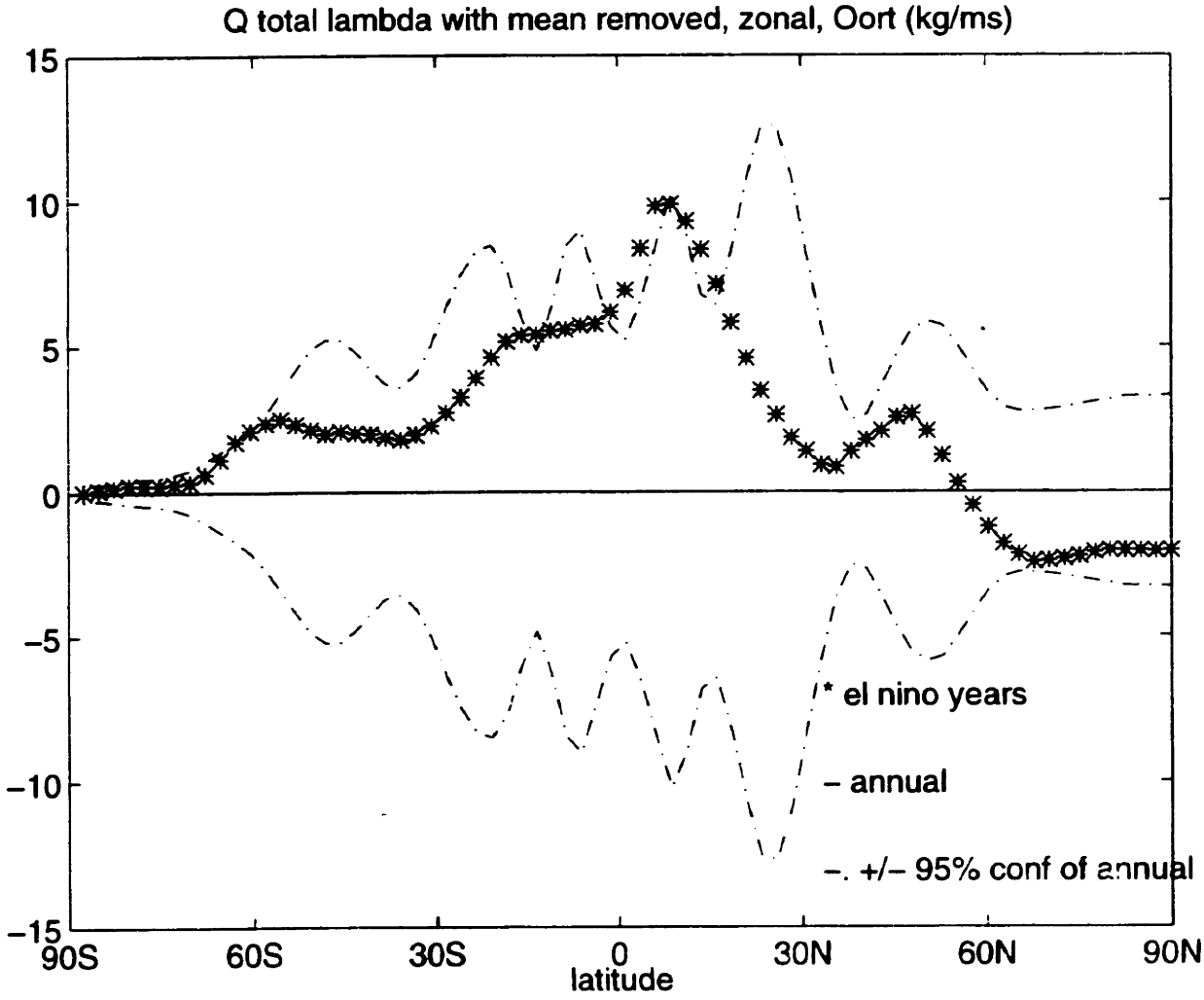

Fig. 38. Total vapor flux of 'El Nino - non El Nino years', zonal component. Zonally averaged with mean removed. For Oort data and plotted with 95% confidence interval of annual average. In units of (kg/ms).

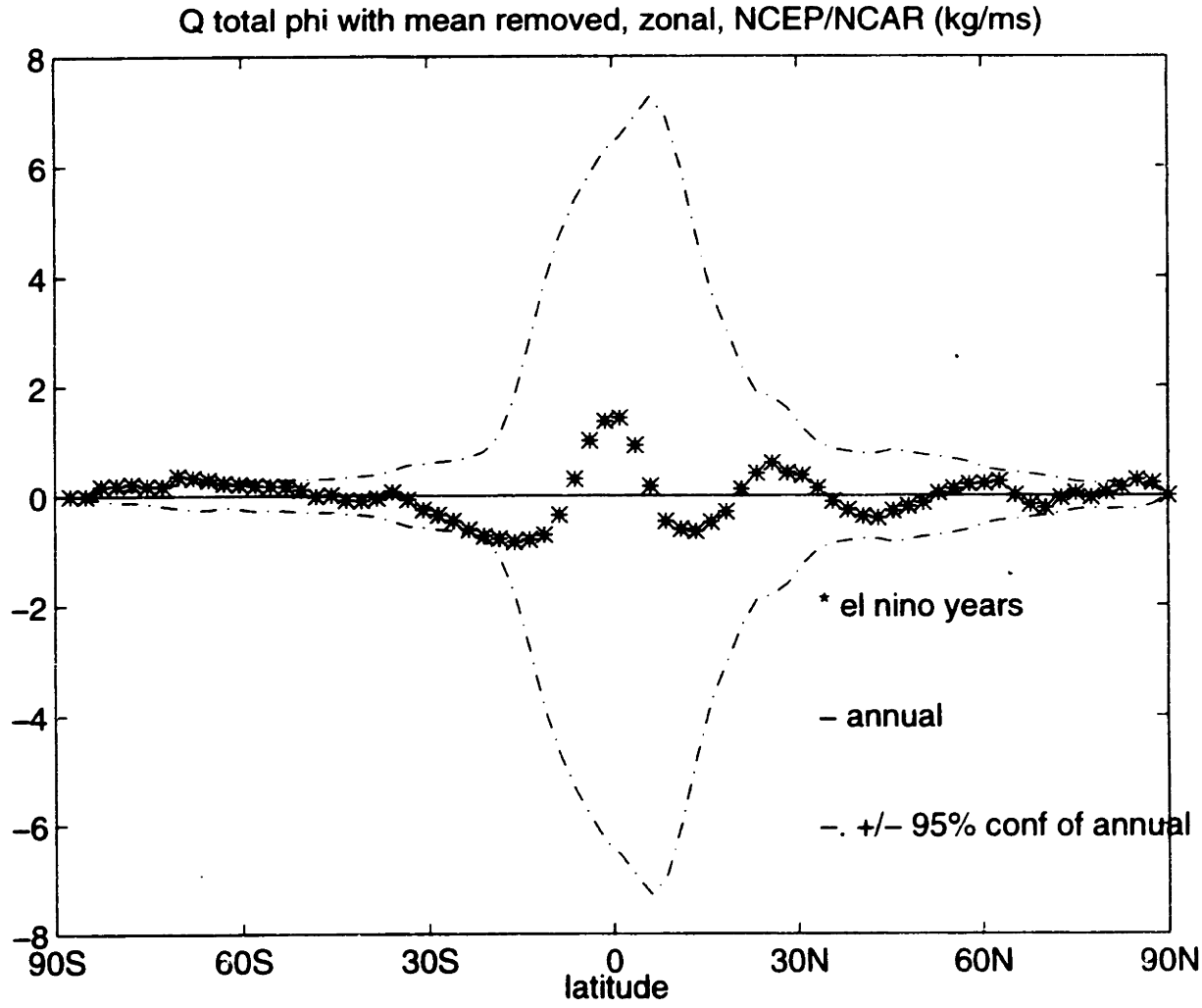

Fig. 39. Total vapor flux of 'El Nino - non El Nino years', meridional component. Zonally averaged with mean removed. For NCEP/NCAR data and plotted with 95% confidence interval of annual average. In units of (kg/ms).

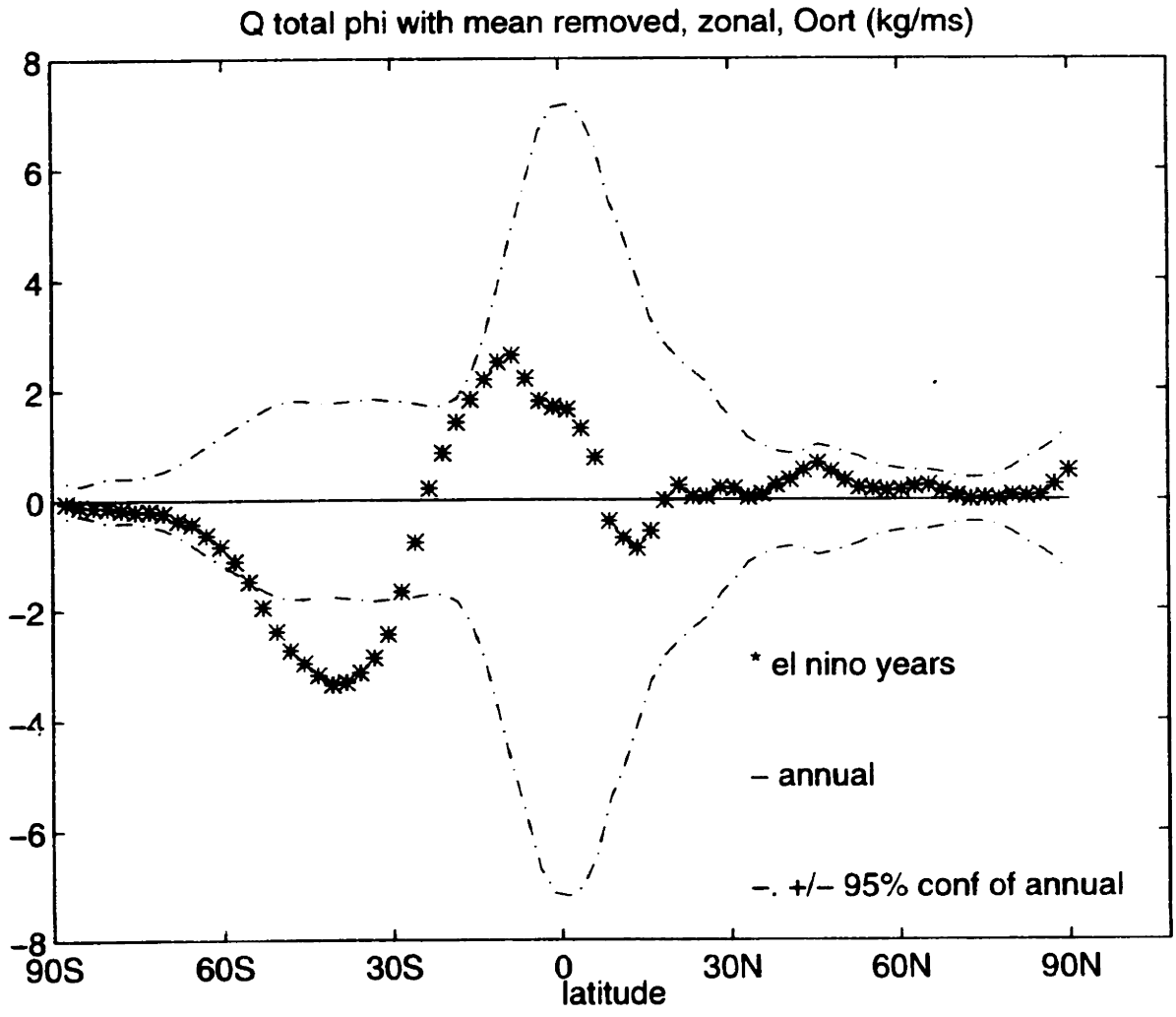

Fig. 40. Total vapor flux of 'El Nino - non El Nino years', meridional component. Zonally averaged with mean removed. For Oort data and plotted with 95% confidence interval of annual average. In units of (kg/ms).

4.4 Divergence

The flux divergence of the El Nino years minus non-El Nino years is calculated using the method of finite difference, and is presented in Figures 41 through 46 in units of m/year. The relative positive divergence and the relative negative divergence (convergence) are displayed separately for easier visibility.

During El Nino events, the relatively cold waters of the western Pacific warm up and cause a weakening of the Walker Circulation over the Pacific. This causes the usually strong area of convection over Indonesia to weaken, and the areas over central and eastern equatorial Pacific to be enhanced (Peixoto and Oort, 1992). Regions of weakened convection lead to an increase in divergence. Both data sets detect many of the same regions of significant relative divergence and are presented in Figures 41a and 42a.

The Oort and NCEP/NCAR data observe a relative divergence over northeastern and southwestern Australia, southern Africa, northern South America, very northern India, and Central America. These regions match those found to have a decrease of precipitation during ENSO (Peixoto and Oort, 1992; Kousky and Leetmaa, 1988; and Ropelewski and Halpert, 1987). Other regions where both data sets find relative divergence include the central Indian Ocean, the very southern and southeast Pacific Ocean, and the northeast Atlantic.

Figures 41b and 42b display the areas of relative convergence during El Nino years. Southern India, southern Brazil, and the eastern equatorial Pacific are known to experience increased precipitation during ENSO and

are observed in both data sets to have relative convergence (Peixoto and Oort, 1992; Kousky and Leetmaa, 1988; and Ropelewski and Halpert, 1987, 1996). Other relatively convergent regions identified by both data sets include the northwestern Atlantic, the central United States and the southeast Pacific.

In most cases the divergence values are larger in the NCEP/NCAR compared to the Oort data. This is particularly true in the case of the eddy flux in Figures 45 and 46, where the Oort data has values half that of the NCEP/NCAR and therefore was contoured with a different contour interval. Even at this interval, the Oort data is so sparse that little information can be extracted from it. The NCEP/NCAR data shows areas of positive and negative eddy divergence almost alternately in the mid-latitudes in Figure 45a and b.

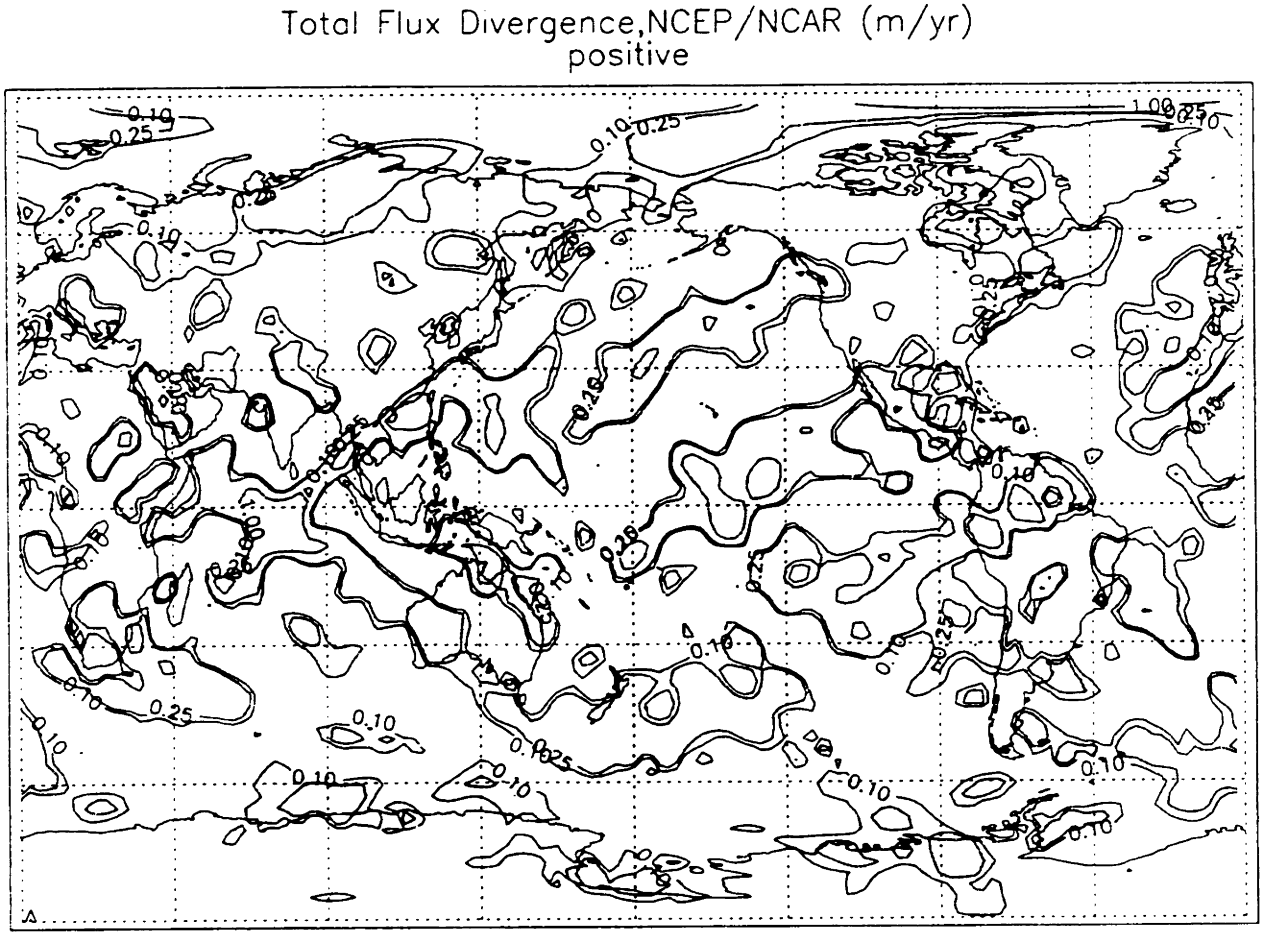

Fig. 41a. Divergence of the total vapor flux for 'El Nino - non El Nino years'. Only positive values contoured on intervals of [.1, .25, 1] meter/year. For NCEP/NCAR data.

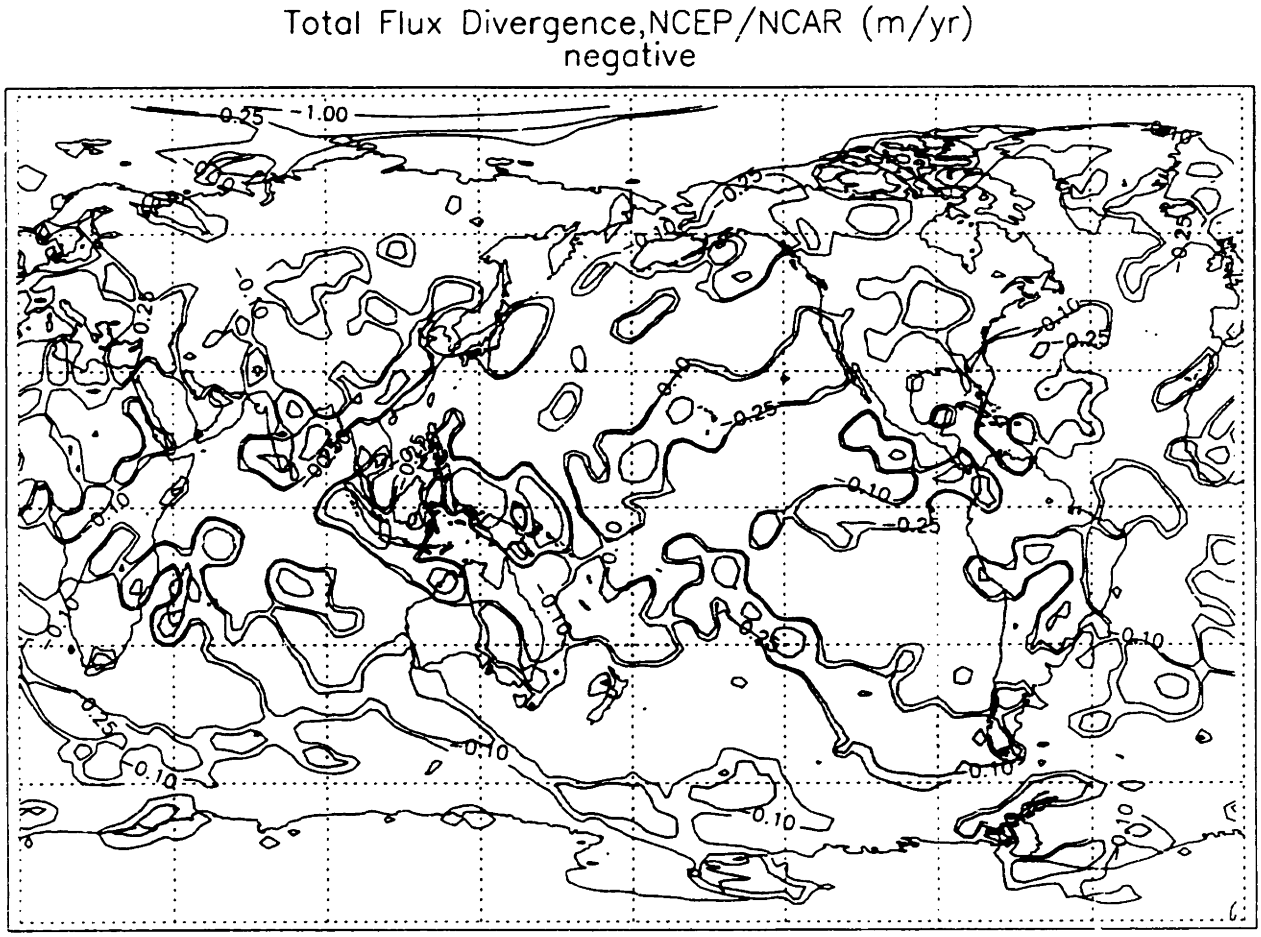

Fig. 41b. Divergence of the total vapor flux for 'El Nino - non El Nino years'. Only negative values contoured on intervals of [-1, -.25, -.1] meter/year. For NCEP/NCAR data.

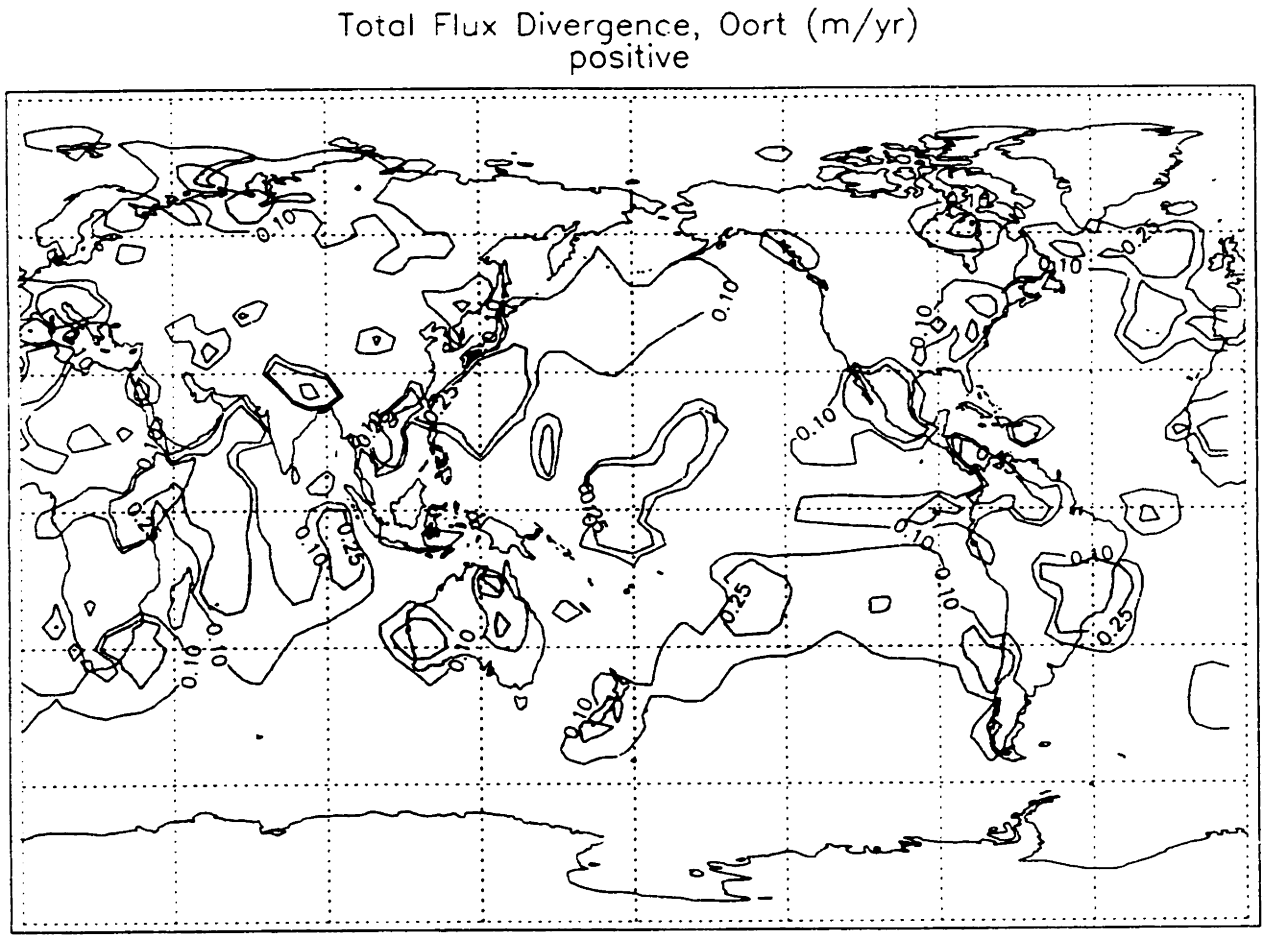

Fig. 42a. Divergence of the total vapor flux for 'El Nino - non El Nino years'. Only positive values contoured on intervals of [.1, .25, 1] meter/year. For Oort data.

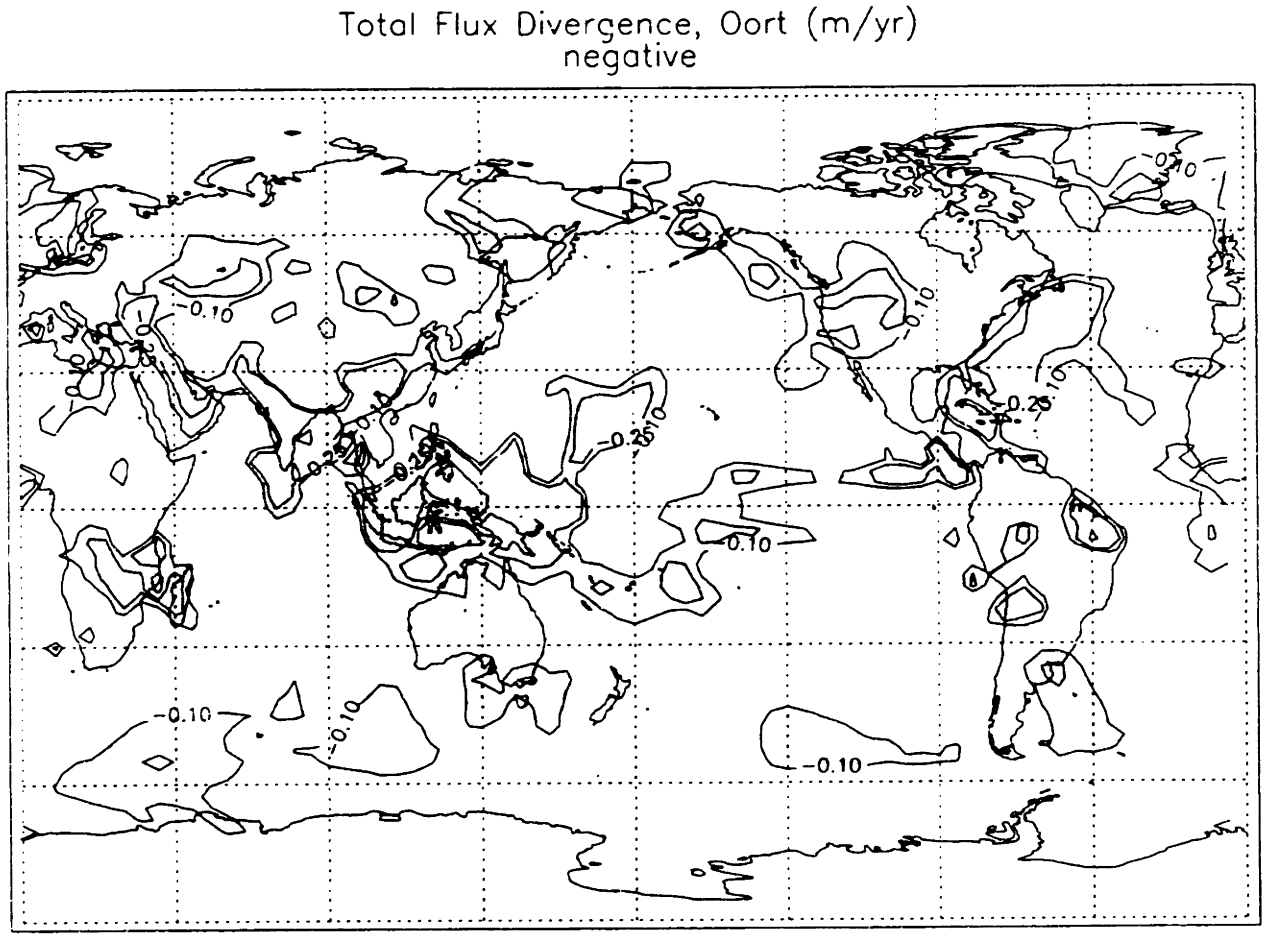

Fig. 42b. Divergence of the mean vapor flux for 'El Nino - non El Nino years'. Only negative values contoured on intervals of [-1, -.25, -.1] meter/year. For Oort data.

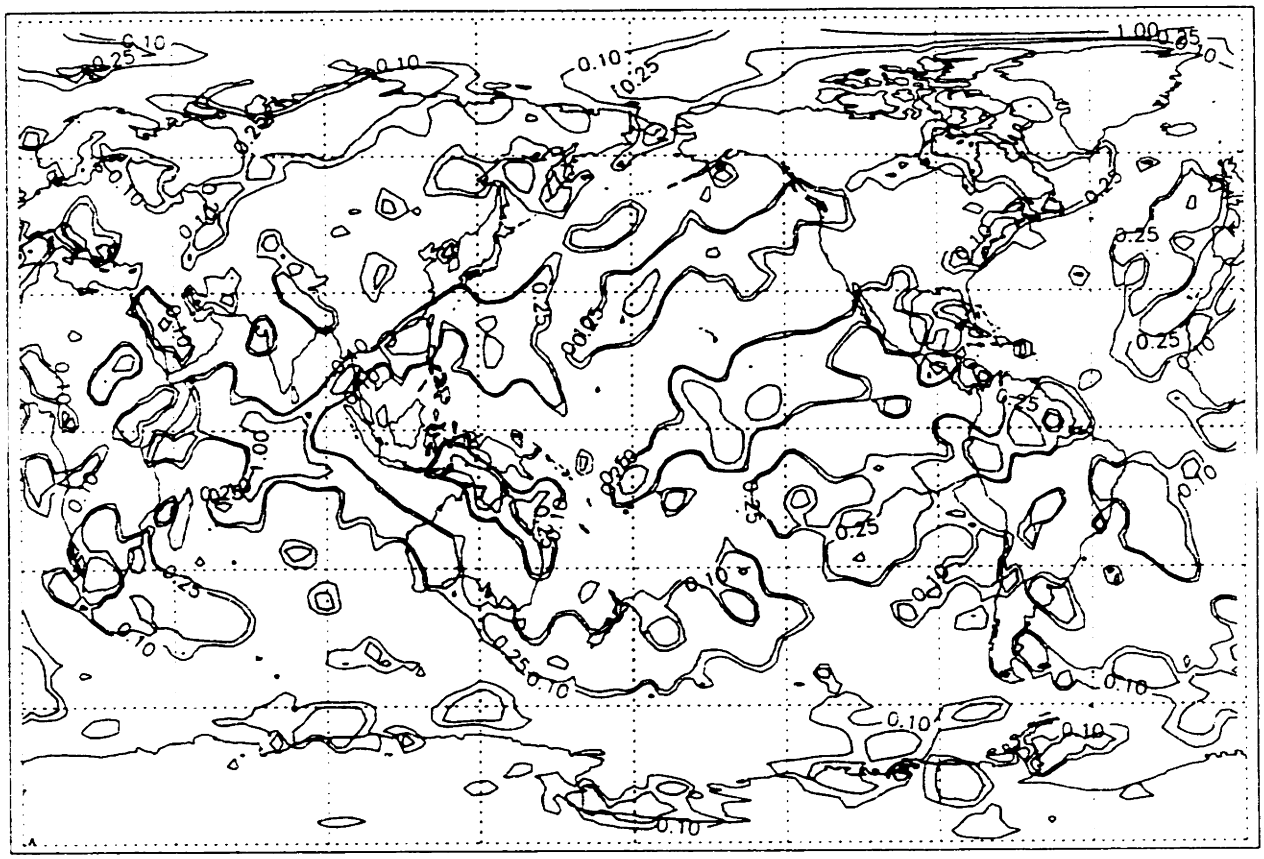

Fig. 43a. Divergence of the mean vapor flux for 'El Nino - non El Nino years'. Only positive values contoured on intervals of [.1, .25, 1] meter/year. For NCEP/NCAR data.

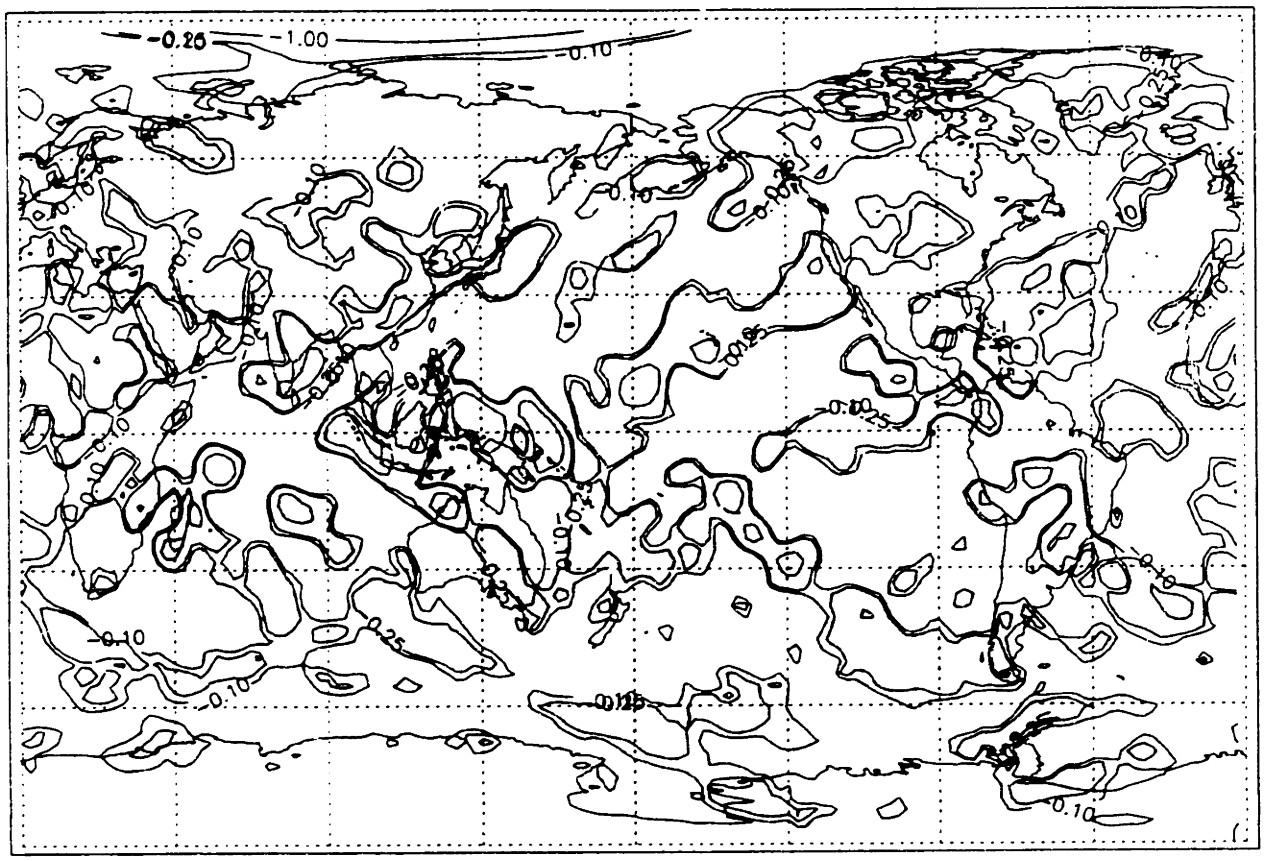

Fig 43b. Divergence of the mean vapor flux for 'El Nino - non El Nino years'. Only negative values contoured on intervals of [-1, -.25, -.1] meter/year. For NCEP/NCAR data.

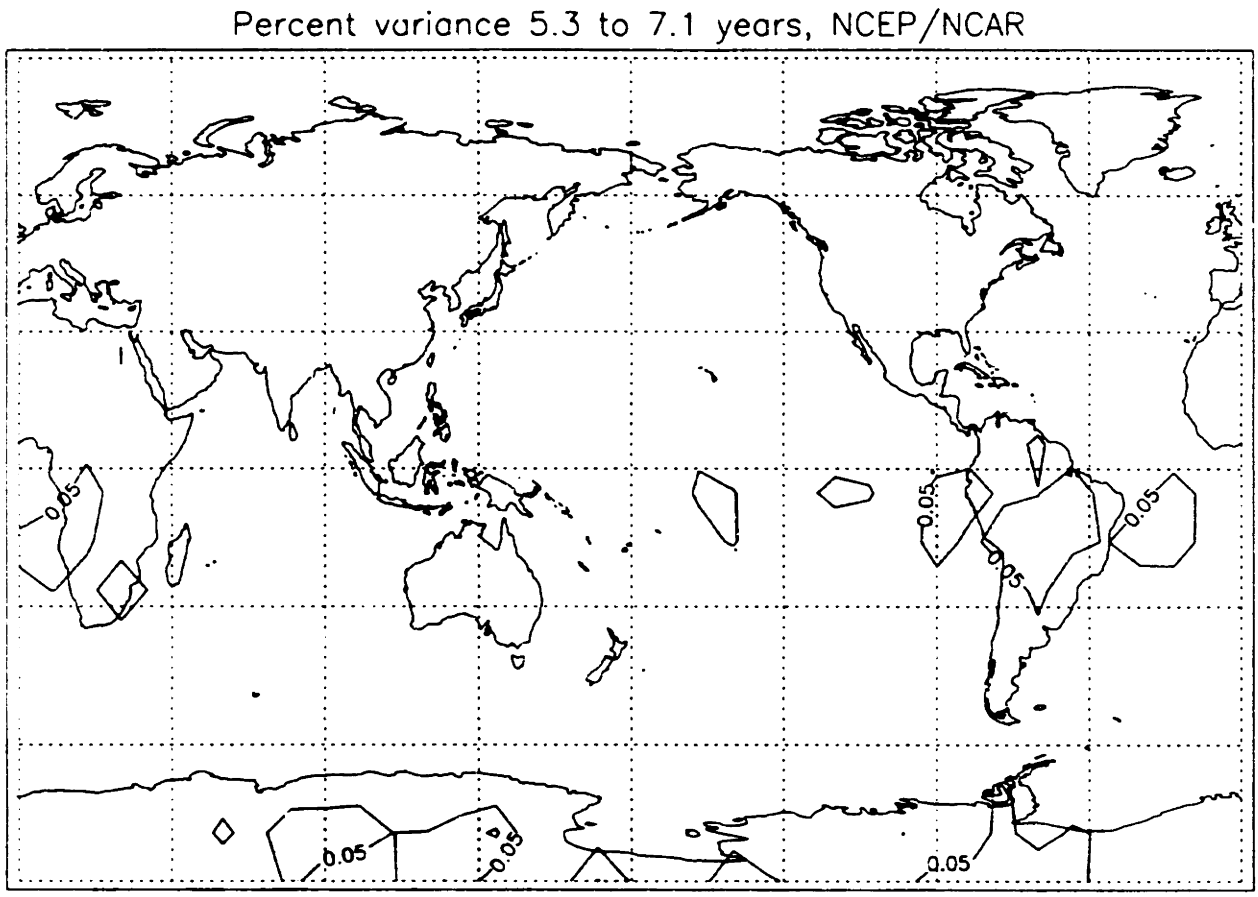

Fig 47d. Percent variance in period from 5.3 to 7.1 years of the divergence of total vapor flux for NCEP/NCAR data. Contoured on intervals of 0.05.

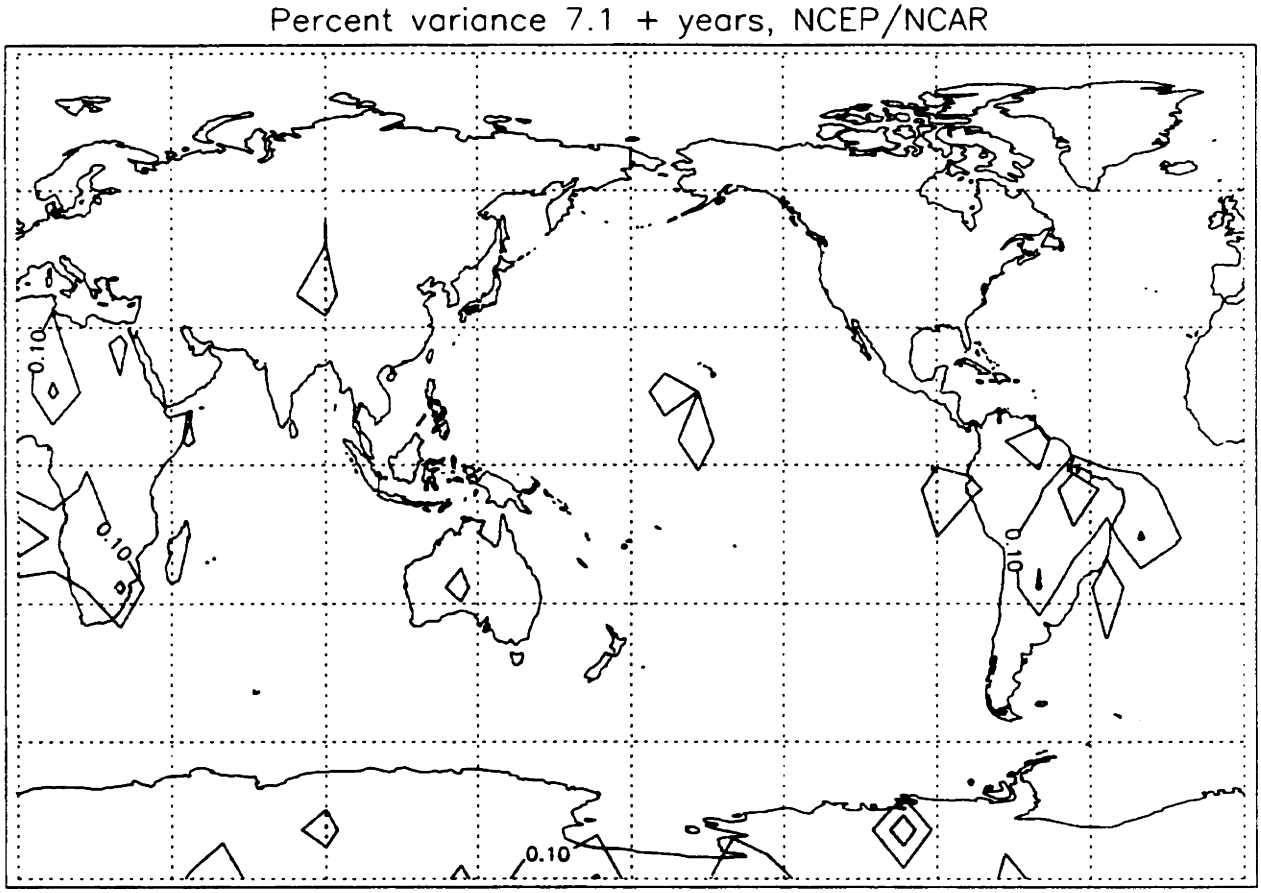

Fig 47e. Percent variance in period from 7.1 + years of the divergence of total vapor flux for NCEP/NCAR data. Contoured on intervals of 0.1.

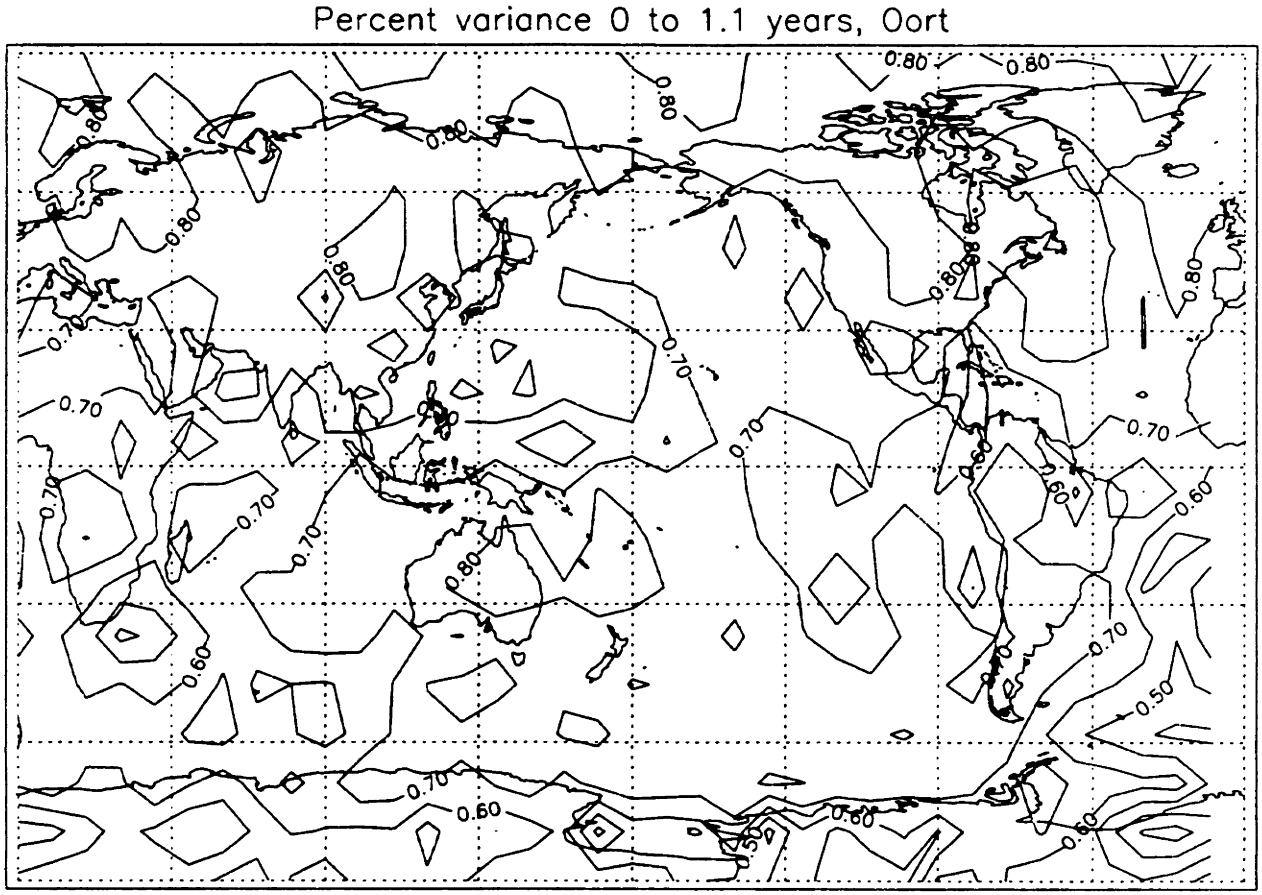

Fig 48a. Percent variance in period from 0 to 1.1 years of the divergence of total vapor flux for Oort data. Contoured on intervals of 0.1.

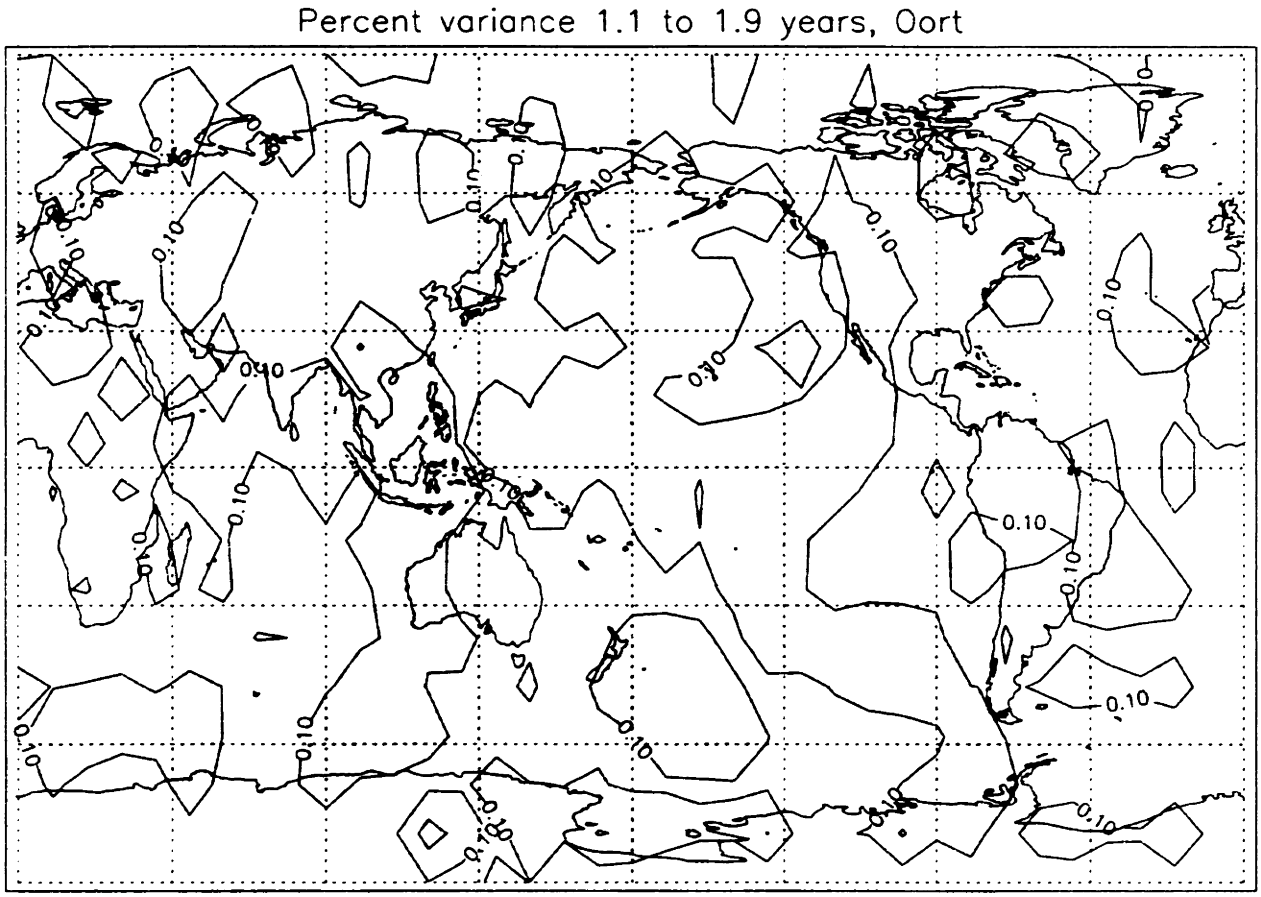

Fig 48b. Percent variance in period from 1.1 to 1.9 years of the divergence of total vapor flux for Oort data.. Contoured on intervals of 0.1.

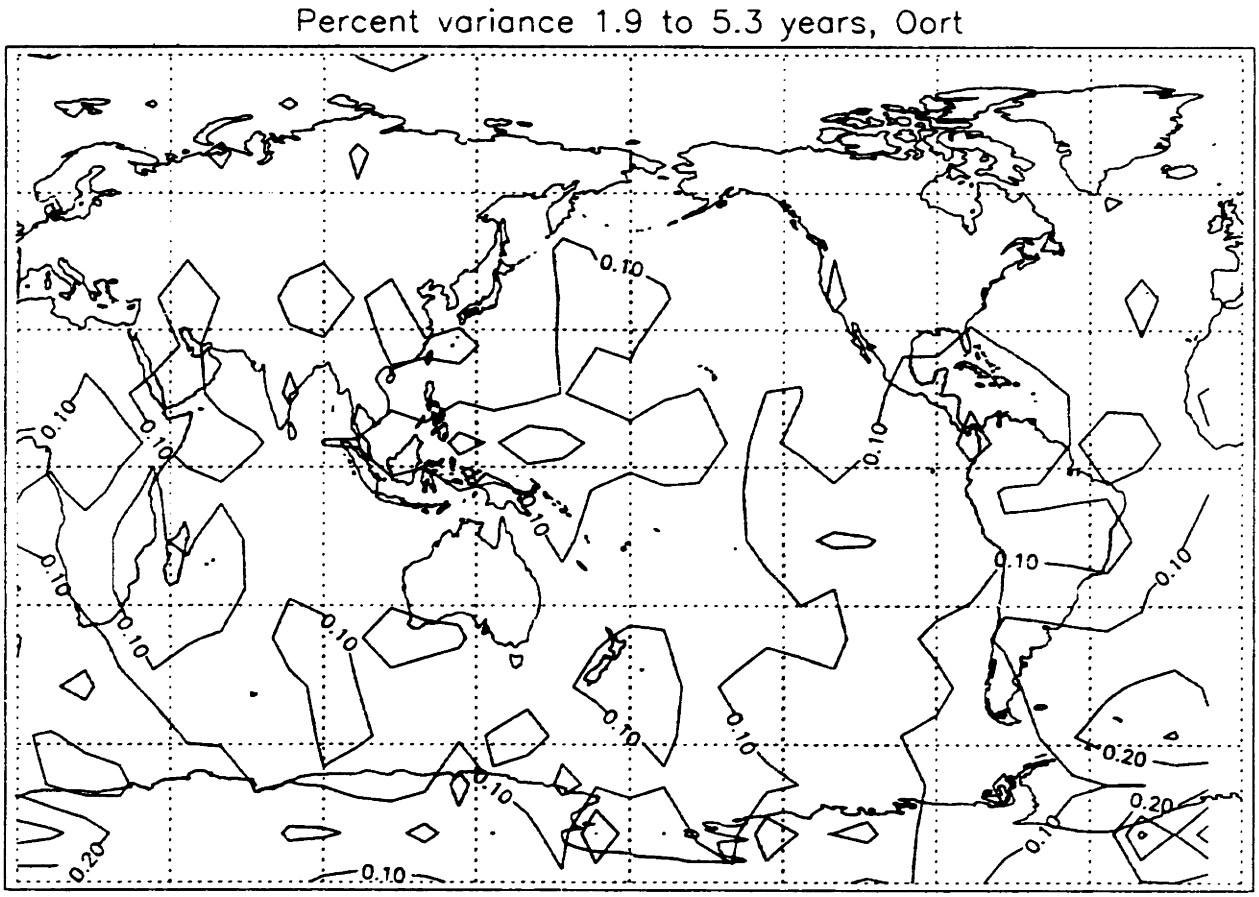

Fig 48c. Percent variance in period from 1.9 to 5.3 years of the divergence of total vapor flux for Oort data. Contoured on intervals of 0.1.

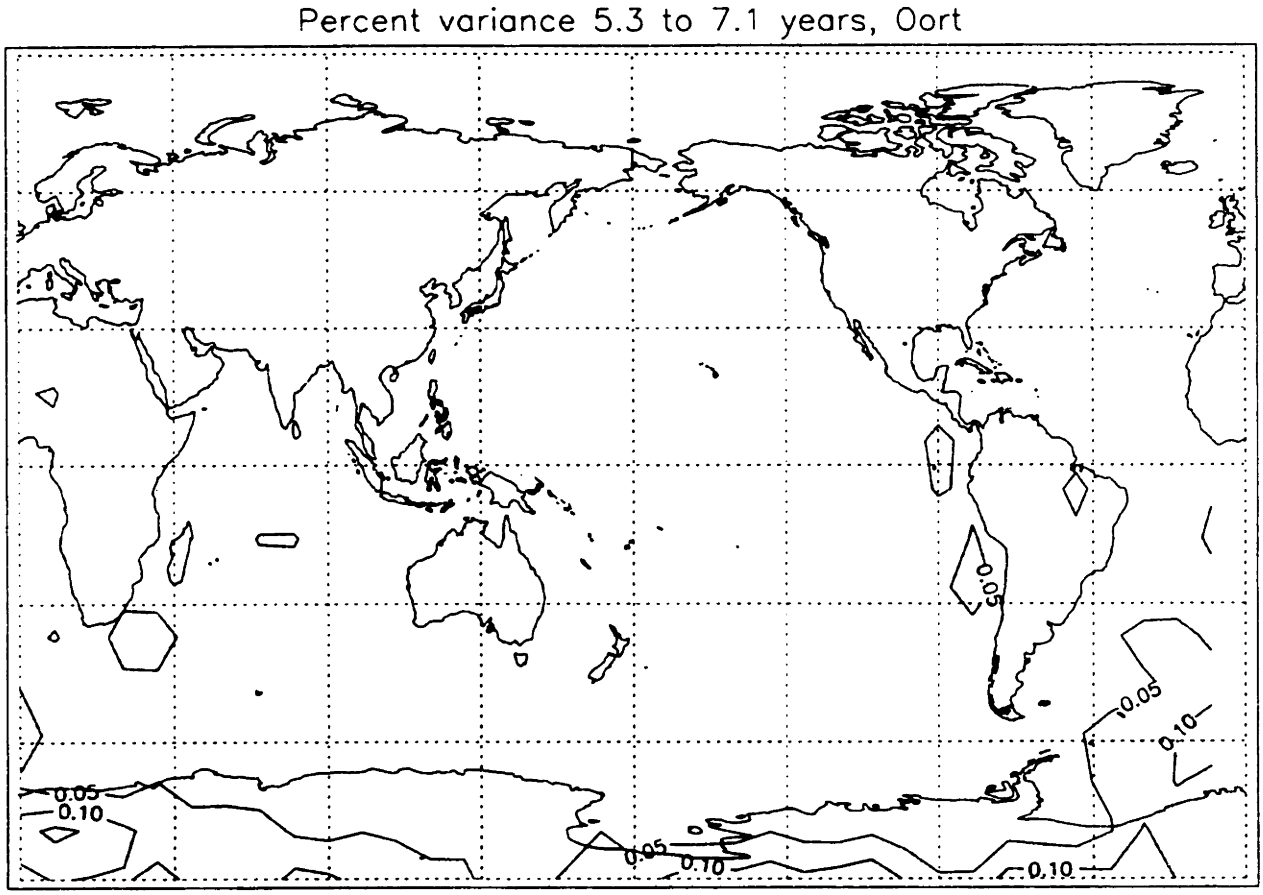

Fig 48d. Percent variance in period from 5.3 to 7.1 years of the divergence of total vapor flux for Oort data. Contoured on intervals of 0.05.

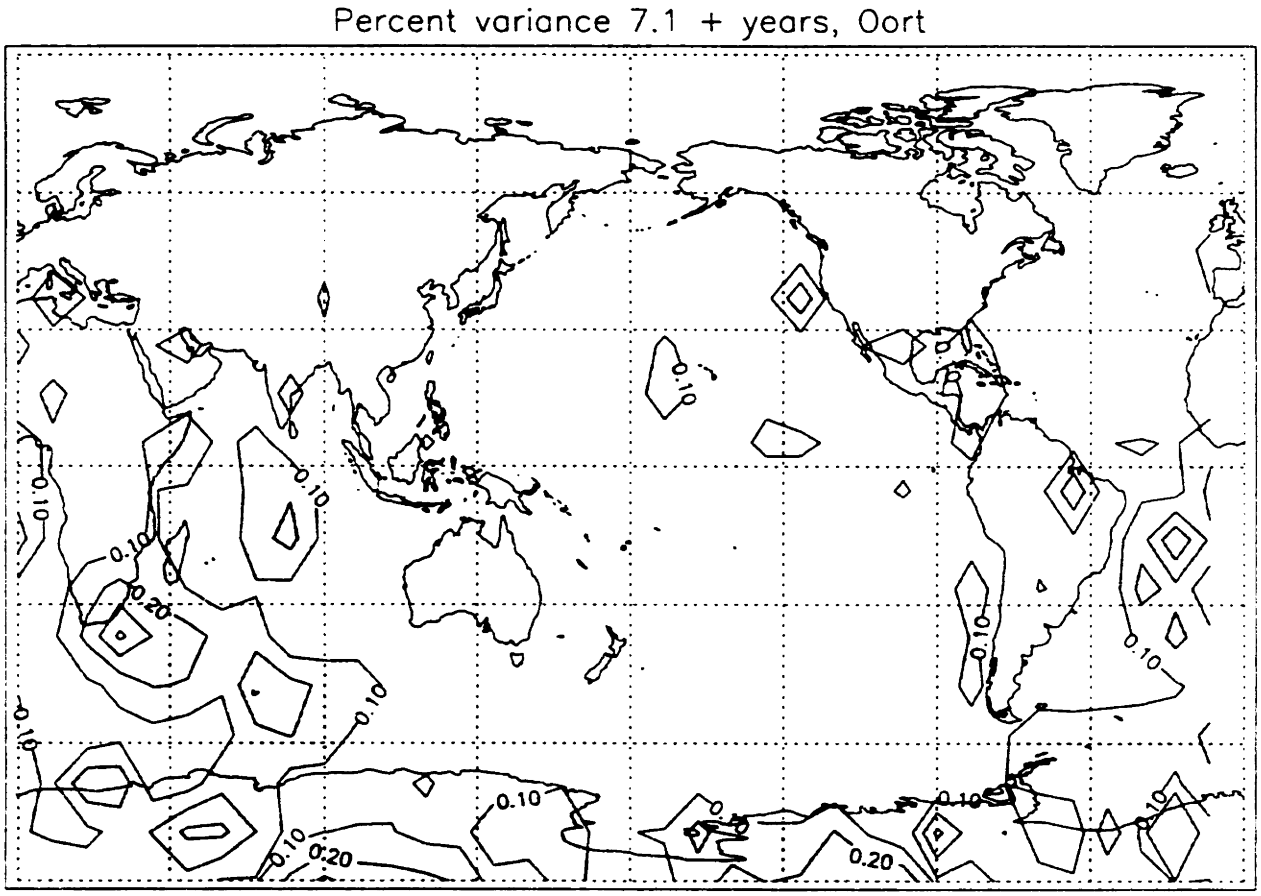

Fig 48e. Percent variance in period from 7.1 + years of the divergence of total vapor flux for Oort data. Contoured on intervals of 0.1.

VI. Conclusions and Discussion

The NCEP/NCAR reanalysis and Oort data sets both succeed in capturing the major components of the vertically integrated water vapor flux climatology. Their flow patterns match that of tropospheric flow very closely, but almost without exception, the NCEP/NCAR data records greater values of flux than the Oort. Additionally, the NCEP/NCAR data finds large flux values consistently across the oceans whereas the Oort data tends to restrict the high values close to the boundaries of these oceans. This may be a symptom of sparse data over the oceans in the Oort data. This is especially true over data sparse regions where the Oort interpolation may be less accurate than reanalysis. Reanalyses additionally include model estimates that "advect" information from other monitored regions. In addition, reanalyses models provide for important physical constraints.

The Southern Hemisphere is shown to have more transport of water vapor than the Northern, due to the lack of land mass and therefore more availability of water. It is interesting that in the Southern Hemisphere of both data sets, there is no seasonal variability seen in the zonally averaged vapor flux for the eddy zonal component. On the other hand, the Northern Hemisphere shows larger poleward eddy flux in winter as would be expected. It is possible that neither data set is picking up Southern Hemisphere eddy flux, or the eddy flux is weak due to less continent-ocean contrasts that force major high-latitude wave and storm track patterns with season.

When $\nabla \bullet Q$ is calculated for these global fields, it becomes apparent again how the Oort data may be effected by sparse data over the oceans. In comparison to the NCEP/NCAR data, it shows relatively little divergence over these oceanic regions. Both data sets do pick up many of the main convergence zones in the equatorial and mid- to high-latitude regions, and divergence zones over the eastern edges of major ocean basins (Dodd and James, 1996). Drainage basins such as the Mississippi and the Amazon are captured by the NCEP/NCAR data, but only the Mississippi is resolved by the Oort. The Amazon may be another area the Oort set does not have adequate data.

The phenomena of El Nino is resolved by both data sets. Both exhibit a large area of difference between El Nino years and non-El Nino years in the western equatorial Pacific. But other areas well known for El Nino-related abnormalities, such as the Pacific coast of Ecuador, only show anomalous flux in the NCEP/NCAR data. While any comparison of data sets covering different time ranges must allow for a great deal of unexplained variation, El Nino likely causes a difference of flux over the anomalously warm waters off of Ecuador. The Oort data does not register this effect.

It is significant that both data sets show a relative divergence away from the Indonesian area during the El Nino years. While a shift in circulation and moisture in this region is well documented (Ropelewski and Halpert, 1987), each data set handles the eddy flux differently. They both have most of their differences in the mid-latitudes due to the existence of eddies in this region. But the flux vectors in the NCEP/NCAR data are

contained within large eddy fields, whereas the Oort data has a more organized pattern.

This pattern can be investigated further by looking at the zonal averages of the El Nino period. NCEP/NCAR exhibits very little difference in the total meridional component from El Nino years compared with the annual average. Oort displays significant differences, though mostly in the Southern Hemisphere. With the total zonal flux, the NCEP/NCAR data exhibits significant differences only in the Southern Hemisphere while in the Oort data, differences exist evenly in both.

When looking at the actual divergence ($\nabla \bullet Q$) of the El Nino minus non-El Nino data, the NCEP/NCAR data has consistently larger values than the Oort data. The larger range of flux values, noted above, may contribute to this. But the two data sets generally agree on the regions of significant divergence, and with known regions of anomalous precipitation.

Another approach for validating the occurrence of El Nino in each data set is power spectra analysis. The results from this were quite significant. The NCEP/NCAR data picks up 50% variance over the Amazon for the period of time from 1.9 to 5.3 years. This region has been documented to have a very large ENSO-related precipitation anomaly (Ropelewski and Halpert, 1987, 1996). The Oort data does not pick up as much percent variation here, again possibly pointing to poor data in this region. The two sets do agree on other documented areas affected by ENSO such as the western equatorial Pacific and the entire equatorial region in general.

Overall, both data sets resolve global water vapor flux quite well. In remote locations, the Oort data is inferior to the NCEP/NCAR data. While

a great deal of variation is to be expected between data sets that cover different time periods, certain anomalies and fluxes that should be picked up at any time period are not present in the Oort data. In the future, further comparisons of the two data sets with other data sets (e.g. satellite) should be made over regional domains. Only then may the sources of the differences between the two data sets be identified.

References

Barnett, T. P., 1994: Interaction of the Monsoon and Pacific Trade Wind System at Interannual Time Scales. Part III: A Partial Anatomy of the Southern Oscillation. *Monthly Weather Review*, **112**, 2388-2400.

Benton, G. S. and M. A. Estoque, 1954: Water-Vapor Transfer over the North American Continent. *Journal of Meteorology*, **11**,462-477.

Brubaker, K. L., D. Entekhabi, and P. S. Eagleson, 1994: Atmospheric Water Vapor Transport and Continental Hydrology over the Americas. *Journal of Hydrology*, **155**, 407-428.

Dodd, J. P. and I. N. James, 1996: Diagnosing the Global Hydrologic Cycle from Routine Atmospheric Analysis. *Q.J.R. Meteorol. Soc.*, **122**, 1475-1499.

Hefland, H. M. and S.D. Schubert, 1995: Climatology of the Simulated Great Plains Low-Level Jet and Its Contribution to the Continental Moisture Budget of the United States. *Journal of Climate*, **8**, 784-806.

Higgins, R. W., K. C. Mo, and S. D. Schubert, 1996: The Moisture Budget of the Central United States in Spring as Evaluated in the NCEP/NCAR and the NASA/DAO Reanalyses. *Monthly Weather Review*, **124**, 939-963.

Gill, A. E. and E. M. Rasmusson, 1983: The 1982-83 Climate Anomaly in the Equatorial Pacific. *Nature*, **306**, 229-234.

Kalnay, E. et al, 1996: The NCEP/NCAR 40-Year Reanalysis Project. *Bulletin of the American Meteorological Society*, **77**, 437-471.

Kousky, V. E. and A. Leetmaa, 1988: The 1986-87 Pacific Warm Episode: Evolution of Oceanic and Atmospheric Anomaly Fields. *Journal of Climate*, **2**, 254-267.

Mo, K. C. and W. Higgins, 1996: Large-Scale Atmospheric Moisture Transport as Evaluated in the NCEP/NCAR and NASA/DAO Reanalysis. *Journal of Climate*, **9**, 1531-1545.

Oort, A. H., 1983: Global Atmospheric Circulation Statistics, 1958-1973. NOAA Professional Paper 14. 180 pp.

Peixoto, J. P. and A. H. Oort, 1992: *Physics of Climate*. American Institute of Physics, New York, 520 pp.

Rasmusson, E. M., 1966: Diurnal Variations in the Summer Water Vapor Transport over North America. *Water Resources Research*, **2**, 469-477.

-------, 1967: Atmospheric Water Vapor Transport and the Water Balance of North America: Part I. Characteristics of the Water Vapor Flux Field. *Monthly Weather Review*, **95**, 403-426.

-------,1968: Atmospheric Water Vapor Transport and the Water Balance of North America II. Large-Scale Water Balance Investigations. *Monthly Weather Review*, **96**, 720-734.

-------, and T. H. Carpenter, 1982: Variations in Tropical Sea Surface Temperature and Surface Wind Fields Associated with the Southern Oscillation/ El Nino. *Monthly Weather Review*, **110**, 354-384.

-------, and K. C. Mo, 1996: Large-Scale Atmospheric Moisture Cycling as Evaluated from NMC Global Analysis and Forecast Products. *Journal of Climate*, **9**, 3276-3297.

Ropelewski, C. F. and M. S. Halpert, 1987: Global and Regional Scale Precipitation Patterns Associated with the El Nino/Southern Oscillation. *Monthly Weather Review*, **115**, 1606-1626.

-------, 1996: Quantifying Southern Oscillation-Precipitation Relationships. *Journal of Climate*, **9**, 1043-1059.

Salstein, D. A., R. D. Rosen, and J. P. Peixoto, 1980: Hemispheric Water Vapor Flux Variability--Streamfunction and Potential Fields. *Atmospheric Water Vapor*, 555-573.

Star, V. P. and J. P. Pexioto, 1958: On the Global Balance of Water Vapor and the Hydrology of Deserts. *Tellus*, **II**, 188-194.

Trenberth, K. E. and C. J. Guillemot, 1995: Evaluation of the Global Atmospheric Moisture Budget as Seen From Analyses. *Journal of Climate*, **8**, 2255-2272.

Wang, B., 1995: Interdecadal Changes in El Nino Onset in the Last Four Decades. *Journal of Climate*, **8**, 267-285.

Wyrtki, K., 1975: El Nino-The Dynamic Response of the Equatorial Pacific Ocean to Atmospheric Forcing. *Journal of Physical Oceanography*, **5**, 572-584.